TRIBOLOGICAL BEHAVIOUR OF SiC-WC COMPOSITES

Ph.D. THESIS

by

SANDAN KUMAR SHARMA

DEPARTMENT OF METALLURGICAL AND MATERIALS ENGINEERING
INDIAN INSTITUTE OF TECHNOLOGY ROORKEE
ROORKEE – 247667, INDIA
JULY, 2017

TRIBOLOGICAL BEHAVIOUR OF SiC-WC COMPOSITES

A THESIS

Submitted in partial fulfilment of the requirements for the award of the degree

of

DOCTOR OF PHILOSOPHY

in

METALLURGICAL AND MATERIALS ENGINEERING

by

SANDAN KUMAR SHARMA

DEPARTMENT OF METALLURGICAL AND MATERIALS ENGINEERING
INDIAN INSTITUTE OF TECHNOLOGY ROORKEE
ROORKEE – 247667, INDIA
JULY, 2017

INDIAN INSTITUTE OF TECHNOLOGY ROORKEE
ROORKEE

CANDIDATE'S DECLARATION

I hereby certify that the work which is being presented in the thesis entitled **"TRIBOLOGICAL BEHAVIOUR OF SiC-WC COMPOSITES"** in partial fulfilment of the requirements for the award of the degree of Doctor of Philosophy and submitted in the Department of Metallurgical and Materials Engineering, Indian Institute of Technology Roorkee, Roorkee is an authentic record of my own work carried out during the period from January, 2013 to July, 2017 under the supervision of Dr. B. V. Manoj Kumar, Associate Professor, Department of Metallurgical and Materials Engineering, Indian Institute of Technology Roorkee, Roorkee.

The matter presented in this thesis has not been submitted by me for the award of any other degree of this or any other Institution.

(SANDAN KUMAR SHARMA)

This is to certify that the above statement made by the candidate is correct to the best of my knowledge.

Date:

(B. V. Manoj Kumar)
Supervisor

ABSTRACT

Silicon carbide (SiC) ceramics are considered as suitable materials for various structural applications such as nozzles, heat exchanger tubes, mechanical seals, bearings, cutting tools or cylinder liners because of their superior properties of high hardness, high temperature strength and excellent resistance to wear and corrosion. Accordingly, extensive research has been carried out towards estimating the tribological potential of these ceramics in various wear conditions. One promising approach for improving wear performance is to combine the properties of different materials. Examples are SiC–TiC composites for improved fracture toughness and Si_3N_4–SiC composites for improved strength. A new approach that has received much less attention is the incorporation of WC in SiC ceramics. As SiC has higher hardness and oxidation resistance, and WC has better strength and fracture toughness, superior wear resistance is expected for SiC-WC composites.

In order to thoroughly assess the potential for different tribological applications such as bearings for the liquid rocket engine turbopumps, bearings for rotary shafts, nozzles, heat exchangers, transportation medium for hot abrasive materials, turbine blades, cylinder liners, and cutting tools etc., a systematic investigation on the behaviour of hot pressed SiC-WC composites in continuous/reciprocated sliding wear and solid particle erosive wear conditions is made for the first time in the present work. The study particularly emphasizes the effect of WC content in SiC ceramics and wear test parameters on tribological behaviour of SiC-WC composites, and provides understanding on material degradation mechanisms. First chapter contains a brief introduction of SiC ceramics and major objectives of present thesis. The second chapter gives a comprehensive literature review on sliding and erosion behaviour of SiC ceramics and SiC based composites. Particularly, effect of microstructure and mechanical properties on tribological behaviour of SiC based ceramics is highlighted. The third chapter deals with the details of experimental procedure carried out in line with scope of the work. Details of composition and method of preparation of investigated materials is reported and this is followed by characterization of microstructures and evaluation of mechanical properties of SiC-WC composites. Details of experimental techniques involved in estimating tribological behaviour of the composites in sliding wear, reciprocating sliding wear and erosion wear conditions are explained. The analytical methods to understand the surface

of unworn or worn composites are also explained. Further, techniques used for surface and subsurface characteristics of worn surfaces are described. The present work mainly includes four major parts.

The first study dealt with continuous sliding wear behaviour of SiC-WC composites. In this part of the study, hot pressed SiC ceramics was subjected to dry sliding wear at 5 N, 10 N and 20 N load against SiC (Hardness: 28 GPa), WC-Co (Hardness: 14 GPa) or steel (Hardness: 7 GPa) ball. Experimental results indicated highest friction against WC-Co ball and highest wear against SiC ball at a given load. Mechanical fracture and abrasion are observed as major mechanisms for material loss against any ball. Extensive fracture of worn surfaces observed for SiC ceramics against SiC ball as compared WC-Co or steel ball at 20 N load. Considering maximum wear at 20 N load against any ball, SiC-WC composites were subjected to sliding wear against different counterbody at 20 N load. Friction decreased with WC content against SiC or WC-Co ball while it increased against steel ball. Generation of hard iron tungsten oxide ($FeWO_4$) debris in ceramics during sliding against steel is believed to cause high friction. The increased fracture toughness of SiC ceramics with WC content caused reduction in extent of fracture during sliding against any ball and led to reduced wear. Significant change in major wear mechanism of SiC-WC composites is observed with change in counterbody. Against SiC ball, SiC-WC composites showed mechanical fracture as dominant wear mechanism, while worn surfaces of composites revealed tribochemistry with increased WC content against WC-Co or steel ball. Frictional behaviour of composites was independent of ball hardness, while wear influenced by the hardness of counterbody and fracture toughness of SiC-WC composites.

The second part of study was aimed to understand the tribological behaviour of SiC-WC composites in reciprocated sliding wear conditions. Based on the highest wear obtained against SiC ball in first part of the study, the investigated composites were subjected to unlubricated reciprocating sliding wear against SiC balls at 6 N, 9 N or 19 N load at room temperature and 500^{o}C. The friction decreased with load and WC content at room temperature. SiC-WC composites exhibited maximum wear resistance with 50 wt% WC in room temperature and 30 wt% WC at high temperature and 19 N load. Effect of high humidity (55±5% RH) (compare to (40 ±10% RH) in continuous sliding study) is observed to dominate responsible mechanisms of material removal in SiC-WC composites. Worn surface analysis indicated tribochemistry and microfracture as dominant wear mechanisms for sliding in ambient conditions, whereas microfracture dominated at 500^{o}C. Wear results obtained at high temperature are in consistent with the lateral fracture model for wear volume estimation. Friction and wear results in reciprocated

sliding conditions advocated the effect of fine grain size and improved mechanical properties of SiC-WC composites.

In the third part of study, the SiC-WC composites were subjected to SiC particle erosion wear at high temperature (800^{o}C). In particular, influences of WC particles and angle of impingement (30^{o}, 60^{o} or 90^{o}) of erodent on erosion performance were evaluated. The erosion rate of the composites increased with increased impingement angle from 30^{o} to 90^{o}, and decreased up to 30 wt% WC content. SiC ceramics prepared with 30 wt% WC exhibited highest wear resistance at a given angle of impingement of erodent. Maximum erosion wear rates were obtained for SiC-50 wt% WC composites at normal impact. Worn surfaces revealed grain fracture and pull-out as major mechanisms of material removal for the composites in selected high temperature erosion conditions. Reduction in grain fracture and pull-out observed with decrease in angle of impingement. Owing to the highest hardness the SiC-30 wt% WC composites showed lowest erosion loss. Weak bonding with agglomerated WC particles and severe fracture of SiC grains at normal impact led to a large amount of material loss for SiC-50 wt% WC composites.

It is observed from the experimental results that the performance of the composites in wear conditions is largely influenced by the dominant wear mechanisms of material removal. Therefore subsurface of worn composites were systematically studied in the last part of the thesis to elucidate source of material loss. Subsurface analysis under the worn region after dry sliding wear of SiC-WC composite against SiC ball was studied to assess the source of material removal mechanism. Focused ion beam (FIB) cross sectioning on worn surface of SiC and SiC-50wt%WC composite is done to investigate the damage beneath the worn surface. SiC ceramics showed significant damage of ~ 1 μm thickness beneath the worn region, while damage beneath the worn region of SiC-50 wt% WC composites limited to ~ 300 nm. Beneath the damage region, cracks were initiated as microcracks and extended up to ~2 μm downwards the worn surface for SiC ceramics; eventually leading to material removal. TEM analysis of damaged zone of SiC-50 wt% WC composite demonstrated a network of stress induced dislocations and twins in SiC grains. Considerable restriction in the crack propagation by deflection/bridging is observed by WC particles in the SiC-50 wt% WC composites.

Results obtained from the series of experiments in the present research truly illustrate the significant role of composition (microstructure), mechanical properties and experimental conditions on the tribological performance of SiC-WC composites. A variation in WC content leads to a considerable difference in

microstructure and mechanical properties, and hence affected the tribological behaviour of composites. Wear test parameters like load, counterbody, temperature and angle of impingement additionally influence friction and wear characteristics of SiC-WC composites by changing the dominant wear mechanisms.

In the backdrop of the present experimental research, it can be concluded that addition of WC is recommended for applications in wear conditions. SiC-50 wt% WC composites are not recommended for use in sliding wear conditions at elevated temperatures. Overall 30 wt% WC addition would be beneficial in any wear conditions when compared to monolithic SiC ceramic.

Keywords: *Silicon carbide; Tungsten carbide; Sliding wear; Erosion wear; Subsurface; Counterbody; Erodent; High Temperature.*

ACKNOWLEDGEMENTS

First of all, I would like to express my deepest gratitude, sincere thanks and acknowledgement to my respected supervisor Dr. B. V. Manoj Kumar, Associate Professor, Department of Metallurgical and Materials Engineering, Indian Institute of Technology Roorkee, for showing his faith in me and giving me the wonderful opportunity of doing research under his supervision. His constant motivation and support throughout my entire research tuner helped me to achieve this milestone in my life. He gave me valuable time for discussions and suggestions for making the good explanation and easy understanding of research work. His immense enthusiasm and unlimited zeal have been major driving force during my Ph.D work which helped me a lot to develop myself professionally. I have learnt a lot from him, without his help I could not have finished my PhD thesis successfully. It is very difficult for me to express my gratitude toward him in few words. I could not have imagined having a better advisor and mentor for my Ph.D. work than him. To him, I shall remain, professionally and emotionally obliged.

I would like to thank Dr. Ujjwal Prakash Departmental Research Committee (DRC) chairman; Dr. S. K. Nath, chairman, Student Research Committee (SRC), and Dr. G. P. Chaudhari, Internal Member, Dr. S. C. Sharma, External Member of my SRC committee for taking efforts in reading and providing the constructive suggestions with valuable comments throughout the thesis work. I would also like to thank Dr. Young-Wook Kim, Professor, University of Seoul, Korea, for his valuable comments and suggestions throughout my research work. I would like to acknowledge Dr. Mitjan Kalin, Professor, University of Ljubljana, Slovenia for allowing me to work in his laboratory for some of the experimental works.

I am deeply obliged to present my regards to Head of the Department Dr. Anjan Sil, Professor, Metallurgical and Materials Engineering Department, for his help and providing the facilities in the department for my research work. I would also like to show my appreciation to our technical staff who have helped me through the experimental work, especially, Mr. R. K. Sharma for supporting me in the usage of departmental facilities.

Thanks are also due to my seniors, colleagues and friends Dr. Ashish W. Selokar, Dr. Vipin Sharma, Mr. Shiv Kumar, Prabhat, Sameer, Blaz Jugelz, Gajendra, Manoj, Abhishek, Neeraj, Nishi, Surya, Sanjeev, Vijay Sharma, Bilal, Vaibhav, Luv Gurnani, Vivek, Mukesh, Yashpal, Supriya,

Samanvay, Dinesh, Kapil, Sonali, Abhishek Gupta, Ajay, Surendra, Anirudha and Vikas for all the support and making my journey pleasant.

My heartfelt gratitude and sincere thanks goes to my parents, Shri. Gorakh Nath Sharma and Smt. Sandhya Sharma, and my brother Shri. Saurabh Kumar Sharma, and my sister Smt. Prity Sharma, and my Bhabhi Smt. Anamika Sharma, and my Jija Shri Yogesh Kumar and to my nieces for their support both morally and spiritually, and for their patience, love, guidance, encouragement and prayers during this research period.

I also like to thank everyone who supported me for completing this work successfully and I express my apology that I could not mention everyone individually.

Above all, to the Great Almighty, the author of knowledge and wisdom, for His everlasting love and strength that He bestowed upon me throughout my life.

SANDAN KUMAR SHARMA

CONTENTS

LIST OF FIGURES

LIST OF TABLES

List of Publications

1. **Sandan Kumar Sharma**, B. Venkata Manoj Kumar, Young-Wook Kim, Tribological Behavior of Silicon Carbide Ceramics - A Review, ***Journal of the Korean ceramic society***, 2016; 53 [6]:581-596.
2. **Sandan Kumar Sharma**, B. Venkata Manoj Kumar, Young-Wook Kim, Effect of WC addition on sliding wear behavior of SiC ceramics**, *Ceramics International*** 2015;41:3427-3437.
3. **Sandan Kumar Sharma**, B. Venkata Manoj Kumar, Young-Wook Kim, "Effect of impingement angle and WC content on high temperature erosion behavior of SiC-WC composites", ***International journal of refractory metal and hard materials*** *(Minor revision submitted).*
4. **Sandan Kumar Sharma**, B. Venkata Manoj Kumar, Young-Wook Kim, "Tribology of WC reinforced SiC ceramics: Influence of counterbody", ***Friction*** (*Under review*).
5. **Sandan Kumar Sharma**, B. Venkata Manoj Kumar, Blaz Brodnik Zugelj, Mitjan Kalin, Young-Wook Kim, Room and high temperature reciprocated sliding wear behavior of SiC-WC composites, **Ceramics International** (*Under review*).
6. **Sandan Kumar Sharma**, Luv Gurnani, B. Venkata Manoj Kumar, Amartya Mukhopadhyay, Young-Wook Kim, "Post-wear subsurface analysis of worn SiC-WC composites using FIB and HR-TEM", *(*manuscript *to be submitted JECS).*

CHAPTER 1

Introduction

Silicon carbide (SiC) also known as carborundum, a well-recognized structural ceramic material has been used in industries for a long period owing to its unique combination of properties such as high hardness, high modulus, high temperature strength, good oxidation resistance, excellent wear resistance, good thermal shock resistance and high thermal conductivity [Buchheit 2009; Youn 2014; Roewer 2002; Silvestroni 2010].

The fundamental structure of covalently bonded silicon carbide is a coordinated tetrahedron, either SiC_4 or CSi_4. Although a great variety of SiC polytypes is known, important are cubic polytype referred as β-SiC, and non-cubic structures (hexagonal or rombohedral) as α-SiC [Shaffer 1969; Iwata 2003; Izhevskyi 2000; Jeong 2014]. The strong covalent bond and extremely low self-diffusion coefficient (10^{-13}-10^{-14} cm^2/sec) pose difficulties in densification of SiC powders at lower temperatures. The densification is possible only at extremely high pressures (30-100 MPa) and temperatures exceeding 2100ºC. In order to achieve high density at lower temperatures and pressures, use of sintering aids is necessary [Hase 1980; Negita 1986; Sciti 2000; Basu 2011a, b; Zoli 2017].

Metal oxides, Al-B-C, AlN–metal oxides as sintering additives during liquid-phase sintering tailor the microstructure and improve fracture toughness of SiC ceramics [Rixecker 2001; Lee 2001; Kumar 2011; Ortiz 2012]. The platelet-reinforced microstructures exhibit enhanced toughness due to the combination of intergranular crack mode, introduced by the glassy grain boundary phase, and energy dissipating processes in the crack wake [Silvestroni 2015; Becher 1991]. Sintering additive composition also affect the crystallinity of grain boundary phase of SiC ceramics. Further details on sintering and microstructure can be found elsewhere [Sciti 2000; Choi 2002, 2004; Kim 2005, 2007a,b; Kumar 2009].

In an industrialized society, an important part of the gross national product is spent on damages as a consequence of wear [Blau 1992; Kosel 1992]. Therefore, very high growth in the demand of advanced materials has been reported [Gurunath 2007; Basu 2011; Gebretsadik 2011; Bijwe 1997; Lundmark 2009; Kim 2012; Krishna 2003, 2006, 2015; Fahrenholtz 2017; Monteverde 2016]. Owing to attractive properties, advanced materials like SiC based ceramics are preferred for several tribological and structural applications such as turbine parts, heat exchanger tubes, mechanical seals, bearings,

cylinder liners, burner parts in fluidized bed combustion system, bullet proof vests, cutting tools etc. [Sonber 2017; Kim 2007; Herrmann 2014; Kim 2014; Lim 2014; Grasso 2015; Placette 2015]. Some typical structural applications of the SiC ceramics are shown in **Figure 1.1**. A thorough understanding on tribological behavior of SiC ceramics is required for their efficient use as triboelements. Accordingly, extensive research has been carried out towards estimating tribological potential of SiC and SiC-based composites [Hsu 2004; Zum-Gahr 2001; Lopez 2005a,b, 2007a,b,c; Ciudad 2012; Ortiz 2012; Dulias 2005; Kim 1998; Li 2014]. Available literature on tribology of SiC ceramics can be broadly divided into two categories: sliding and erosion.

Figure 1.1. Typical structural applications of SiC based ceramics

Based on the conditions of sliding and characteristics of SiC and SiC based composites, the coefficients of friction (COF) in unlubricated sliding studies are reported to vary in a wide range of 0.2–0.8, which decreased up to 0.02 in lubricating media like water, paraffin oil etc [Lopez 2005a,b, 2007a,b,c; Ciudad 2012; Ortiz 2012; Gates 2004; Hsu 1996; Kato 2002]. Wear rates in sliding conditions varied in the order of 10^{-7} - 10^{-4} mm^3/N.m [Cranmer 1985; Dong 1995; Zum-Gahr 2001; Murthy 2004; Jordi 2004; Udayakumar 2011]. When SiC ceramics are subjected to sliding, complex friction and wear behavior can be described by several mechanisms of material removal. According to Hsu et al. [1996], a

transition in material removal mechanisms occurs from abrasion in air or water at a low speed of 1.9 mm/s and a low load of 2 N to intergranular fracture at a high speed of 0.6 m/s and a high load of 360 N. Kumar et al. [2011] reported a change in sliding wear mechanism from microcracking at 1 N load to tribochemical wear at 13 N for SiC ceramics containing a small amount of additives. In case of SiC-based composites, worn surfaces reveal adhesion, plastic deformation and/or tribooxidation [Woydt 1993]. Umeda et al. [1993] observed only polishing and grooves without any cracks when SiC/ (ZrB_2 + B_4C) composites were subjected to wear in ambient conditions. For liquid-phase-sintered SiC-TiB_2 composites, wear is reportedly initiated by grooving and a subsequent grain pull-out process [Cho 1996]. Micele et al. [2010] observed an almost 400-fold increase in wear when the sliding speed reduced from 2.0 m/s to 0.5 m/s in SiC–$MoSi_2$ composites. In other study [Sang 2000], fine SiC particles used in preparing Si/SiC-Ni composites exhibited increased wear resistance when sliding tests were conducted at 0.45 m/s sliding speed and 20 N applied load.

Erosion of SiC ceramics is mainly studied in solid particle erosion conditions, while that in cavitation conditions is limited [Dulias 2005]. Solid particle erosion of SiC and SiC-based composites is reported to occur generally by brittle fracture as a result of lateral and radial cracking. The erosion rate ranges from 10^{-1} to 10^3 mm^3/kg based on erosion test parameters, and microstructural and mechanical characteristics of SiC ceramics [Routbort 1980, 1983; Wang 1990; Wang 1995; Kim 1998; Sharma 2014; Li 2014]. The complex tribological behavior of SiC ceramics and their composites in solid particle erosion conditions was mostly explained by several material removal mechanisms such as mechanical fracture, chipping, plastic deformation, ploughing, and/or formation and removal of tribooxide layer [Basu 2011; Routbort 1980, 1983; Wang 1990; Wang 1995; Kim 1998; Sharma 2014; Li 2014].

Jianxin et al. [2007] studied erosion wear behavior of SiC/(W, Ti)C laminated ceramic nozzles produced by hot pressing in dry sand blasting processes. They reported that the laminated ceramic nozzles were superior to the homologous stress-free ceramic nozzle due to the formation of compressive residual stresses in the nozzle entry region. Kim and Park [1998] observed that the erosion rates of hot-pressed monolithic SiC ceramics and SiC–TiB_2 composites did not increase monotonically with increasing particle size. Rather, the erosion rate was higher for the SiC-TiB_2 composite with higher fracture toughness but had a lower hardness compared to monolithic SiC. Large erodent particle size and elevated temperatures are reported to lead to lower erosion rates for SiC-TiB_2 composites when compared against SiC ceramics [Colclough 1997].

A new combination that has received much less attention is the incorporation of tungsten carbide (WC) in SiC ceramics. Improved wear resistance is expected by adding tough and strong WC in the hard SiC matrix. Powder metallurgy route is suitable for manufacturing such composites. Pang and Li [2009] prepared porous SiC-WC composites by solid reaction of Si and WC for applications that involve low thermal expansion. Zhang et al. [1998] prepared dense and strong SiC-Si composites reinforced by WC particles by hot pressing. The understanding on tribological behaviour of dense SiC-WC composites is limited.

In the present work, hot pressed SiC ceramic composites with varying WC content (0 to 50 wt %) were studied for understanding their tribological behaviour. Considering the importance of the influence of microstructure and mechanical properties in different wear conditions, SiC-WC composites were investigated in continuous sliding, reciprocated sliding and solid particle erosion wear conditions. The effects of material parameters (WC content) and wear test parameters (load, counterbody, temperature, angle of impingements etc.) are systemically studied. The important part of the thesis work is to elucidate the mechanisms of material removal of investigated SiC-WC composites in the given wear conditions. The major parts of the present thesis work are schematically presented in **Figure 1.2**. An attempt is made to understand the effect of composition (microstructure), mechanical properties on tribological behaviour of the SiC-WC composites.

1.1. Objective of the thesis:

The present study is conducted to understand the tribological behaviour of hot pressed SiC-WC composites in different wear conditions. The following are major objectives (also represented in **Figure 1.2**):

- To study the effect of WC content on friction and wear behaviour of SiC-WC composites in continuous sliding wear conditions.
- To study friction and wear characteristics of SiC-WC composites in continuous sliding conditions with respect to test parameters i.e. effect of load and counterbody materials (SiC ball, WC ball and steel ball).
- To understand the effect of WC content, load and temperature on tribological behaviour of composites during reciprocated sliding wear.

- To understand the solid particle erosion behaviour of SiC-WC composites at high temperature (800ºC) as function of angle of impingement of SiC erodent particle and WC content.
- To elucidate dominant mechanisms of material removal of SiC-WC composites as function of WC content and wear test conditions.
- To propose a relation of composition (microstructure)-mechanical property-wear test parameters-tribological behaviour of the investigated composites.

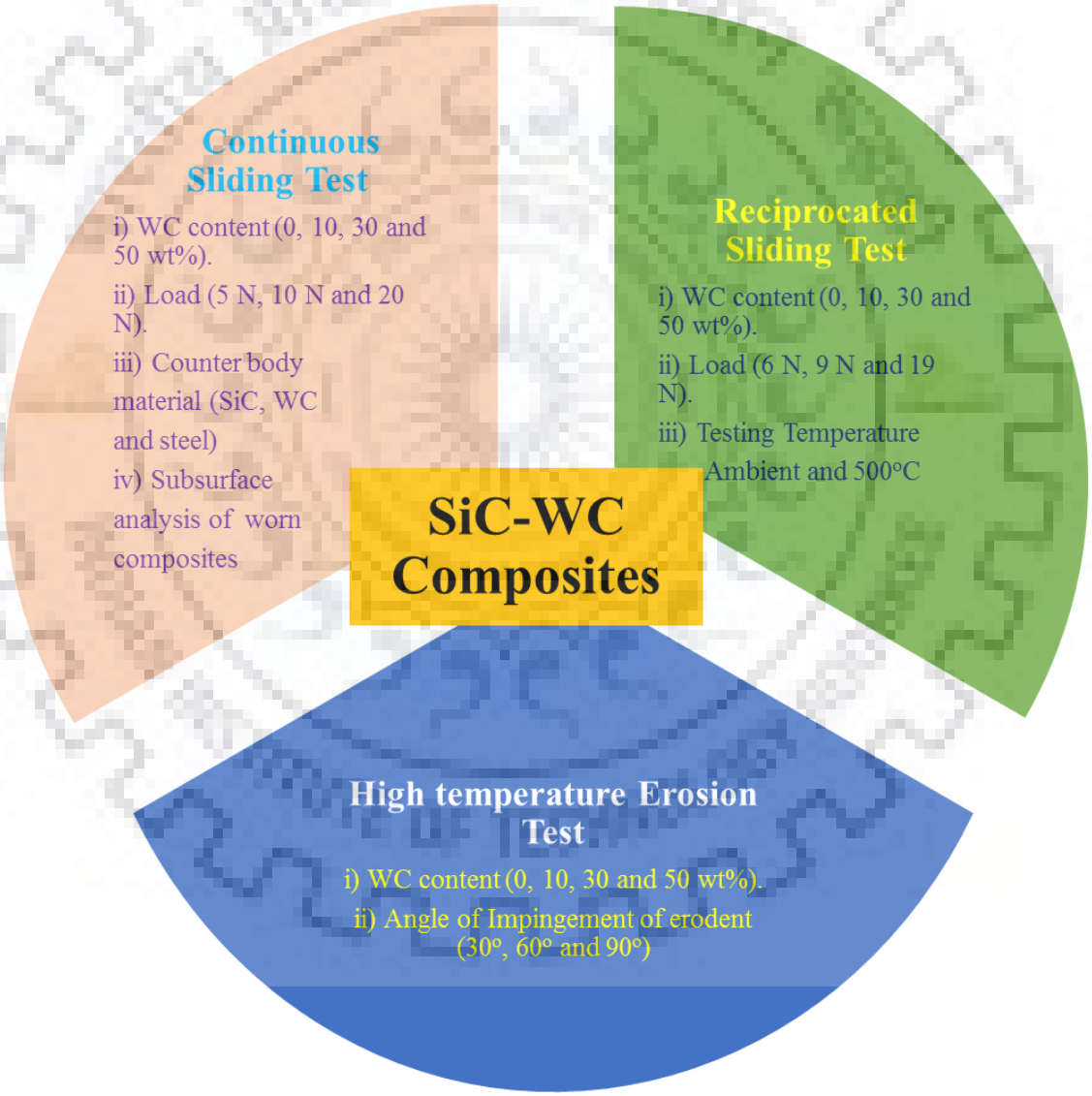

Figure 1.2. Schematic representation of the major parts of the present thesis.

1.2. Structure of the thesis:

In order to envisage the above listed objectives, the thesis is structured as per the following:

Chapter-2: Literature review

A comprehensive review on sliding and erosion behaviour of SiC ceramics and SiC based composites as function of microstructure and mechanical properties is provided in this chapter.

Chapter-3: Experimental techniques

Basic characterization of the investigated composites is explained. This is followed by details of experimental techniques involved in estimating properties of the composites in sliding wear, reciprocating sliding wear and erosion wear conditions. The analytical methods to understand the surface of unworn or worn composites are also explained.

Chapter-4: Effect of counterbody material on sliding wear behavior of SiC-WC composites

In this chapter, the effect of load (5 N, 10 N and 20 N) on friction and wear behavior of SiC ceramics is studied in continuous sliding wear conditions. Effects of WC content in the composites and counterbody (SiC, WC and steel) materials on tribological behavior during sliding wear are particularly discussed. This is followed by the study of major material mechanisms in different tribological conditions.

Chapter-5: Reciprocated sliding wear behavior of SiC-WC composites

Major results obtained in understanding the tribological behaviour of the composites in reciprocated sliding wear conditions are provided in this chapter. First, the effect of load on friction and wear behaviour of SiC ceramics is explained. Further, tribological behaviour of the SiC-WC composites is discussed as function of (10-50 wt%) WC content and temperature (ambient and 500^{o}C). Finally, major material removal mechanisms are elucidated.

Chapter-6: High temperature erosion wear studies of the SiC-WC composites

This chapter deals with high temperature (800^{o}C) solid particle erosion response of SiC-WC composites against SiC erodent. Effect of WC content and angle of impingements of SiC erodent on

erosion behaviour of SiC-WC composites is highlighted. Changes in material removal mechanisms with varying erosion test parameters and WC content in the composites are explained.

Chapter-7: Subsurface studies of worn SiC-WC composites using FIB/HR-TEM.

In this chapter, subsurface analysis using focused ion beam (FIB)/FEG-SEM cross sectioning of worn SiC and SiC-50 wt% SiC composite after sliding wear against SiC ball at 20 N load is performed. Damaged region is investigated for the origin of macrocracks during wear such as generation of stress induced dislocations or twins under HR-TEM.

Chapter-8 Conclusions and future scope

In the first part of this chapter, major conclusions obtained in the present study on the tribological behavior of SiC-WC composites as function of composition (WC content) in SiC-WC composites and test parameters in wear conditions like load, counterbody in continuous sliding, temperature in reciprocated sliding, angle of impingement and temperature in erosion etc. are highlighted. A clear understanding on the material removal mechanisms in respective wear conditions is particularly provided. Further, relations among microstructure, mechanical properties, experimental parameters and tribological properties of the composites are given. In the other part of the chapter, outcomes of the present research are used to list out potential directions for further research in assessing the potential of the SiC-WC composites. An outline of the present doctoral investigation is presented as **Figure 1.3.**

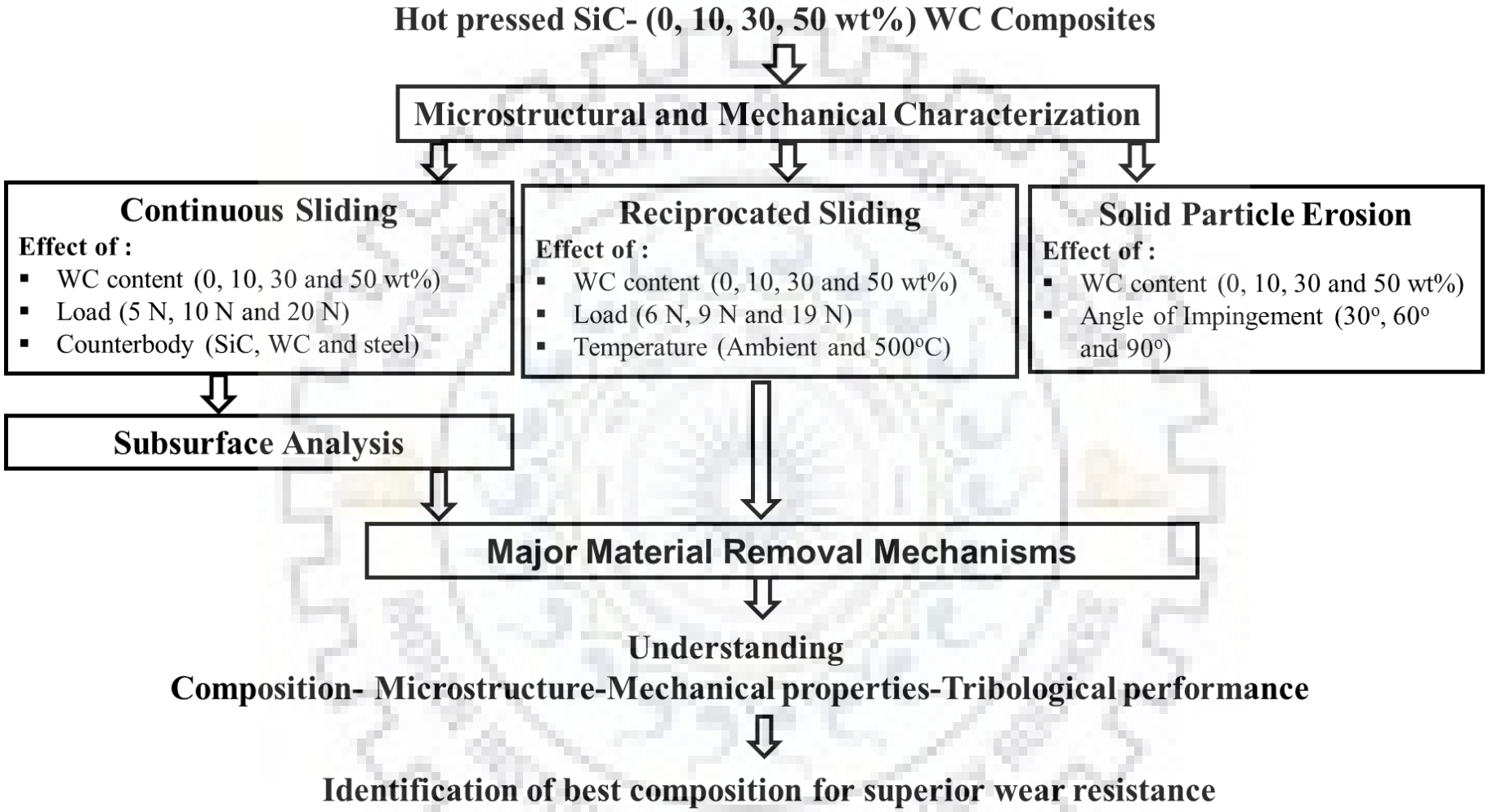

Figure 1.3. The schematic outline of the doctoral investigation

CHAPTER 2

Literature review

In this chapter, a comprehensive review on the available literature on sliding and solid particle erosion wear characteristics of silicon carbide (SiC) ceramics and SiC-WC composites is provided. Sliding or erosion wear behavior of ceramics is dependent on various material characteristics as well as test parameters. Results obtained between varieties of pairs of SiC ceramics that indicate complexity in understanding dominant mechanisms of material removal are discussed. Effects of microstructural and mechanical properties of SiC ceramics are particularly focused to understand tribological performance of SiC ceramics. Also, the effect of test parameters like load, temperature on tribological behaviour of SiC based ceramics are discussed.

2.1. Sliding wear of SiC ceramics

Sliding wear of SiC ceramics are reported mainly using ball-on-disk or pin-on-disk tribometer. SiC ceramics showed complex behavior of wear influenced by sliding test parameters, material or environmental parameters in lubricated/unlubricated sliding conditions[Adewoye 1981; Andersson 1994; Wang 1996; Basu 2011; Ciudad 2012, 2013; Lopez 2005a,b, 2007a,b,c; Cho 1996; Murthy 2004]. In this section effect of microstructure and mechanical characteristics on sliding wear of SiC ceramics is discussed. This is followed by detailed understanding on dominant wear mechanism of SiC ceramics in sliding conditions.

2.1.1. Effect of microstructure

Lopez et al. [2007] studied the sliding wear behavior of liquid phase sintering (LPS)-SiC ceramics with different microstructures like elongated SiC grains *(in situ* toughened LPS SiC), coarse equiaxed SiC grains, and fine equiaxed SiC grains. Sliding wear resistance of elongated grain SiC ceramics was better than that of equiaxed SiC ceramics owing to a hard interlocking network of *in situ* toughened LPS SiC grains ***(see Figure 2.1)***. The isolated nature of the yttrium aluminum garnet (YAG) second phase also played a role in enhancing wear resistance of *in situ* toughened LPS-SiC. This was in contrast to the equiaxed SiC ceramics, where the grains were embedded within a continuous YAG phase matrix.

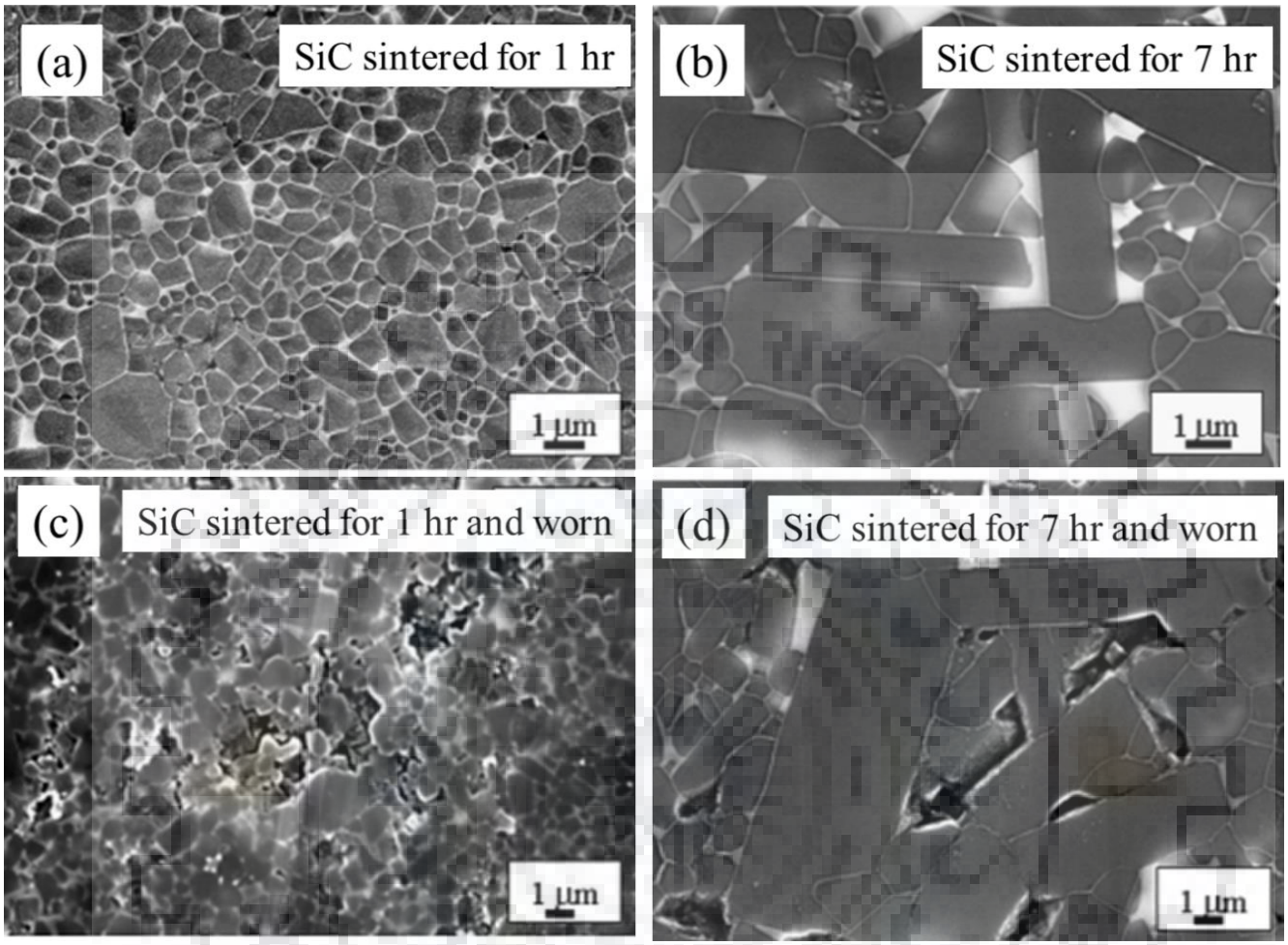

Figure 2.1. Typical SEM images of SiC ceramics (a, b) unworn and (c, d) after sliding against Si_3N_4 ball. Note the presence of elongated grains in (b) and equiaxed grains in (a), and comparatively less wear in (d) than in (c). Other conditions of sintering and sliding wear can be found in [Lopez 2007].

In sliding of SiC ceramics prepared with YAG (Y_2O_3:Al_2O_3 = 3:5), Lopez et al [2005a] suggested reduced content of the intergranular phase or grain size for improvement in wear resistance of LPS α-SiC ceramics. Reduced content of intergranular phase and the grain refinement resulted in reduction of rate of transition from deformation-controlled wear to fracture-controlled wear and hence in wear loss. A simple model by Lawn et al. [1994] provided a framework for estimating the sliding wear properties in polycrystalline ceramics. The proposed model states that the plastic-deformation damage accumulates within the grains during deformation-controlled wear. This damage is in the form of

dislocation pile-ups, confirmed using transmission electron microscopy [Cho 1989; Cho 1995; Sanchez 1998].

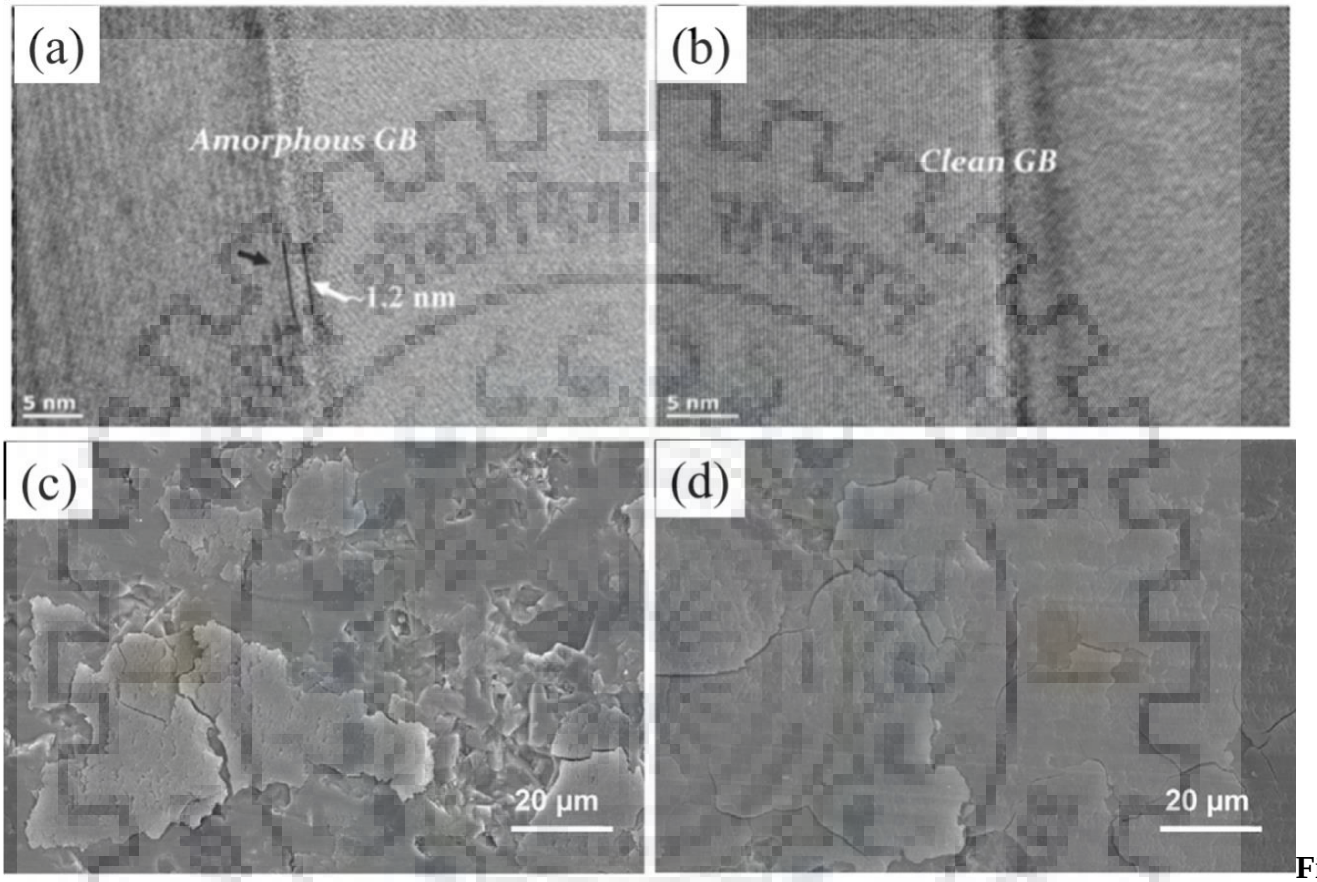

Figure 2.2. TEM images of SiC ceramics revealing (a) amorphous grain boundary in SiC ceramics prepared with 3 wt% (AlN-Y_2O_3) additive (b) clean grain boundary in SiC ceramics prepared with 3 wt% (AlN-Sc_2O_3). Worn surfaces of (a) and (b) are respectively shown in (c) and (d) [Kumar 2011].

It was earlier concluded that SiC ceramics sintered using 3 wt% AlN–Y_2O_3 additives revealed mostly large equiaxed grains with amorphous grain boundary phase, while SiC ceramics prepared using 3 wt% AlN–Sc_2O_3 (SCSc3) additives exhibited duplex microstructure of elongated and fine equiaxed grains with clean grain boundary phase ***(see Figures 2.2 a and b)***. SiC ceramics prepared using 3 wt% AlN–Sc_2O_3 additives resulted ~ 18% less wear at 13 N load. Worn surfaces SiC ceramics sintered with 3 wt% (AlN-Y_2O_3) and 3 wt% (AlN-Sc_2O_3) are shown in **Figures 2.2(c), and (d)**, respectively [Kumar 2011].

Murthy et al. [2004] observed that SiC ceramics doped with different p-type (Al, Mg) or n-type (P) doping elements had influence on the wear behavior in two ways: (i) by directly affecting thermodynamics of tribochemical reactions or (ii) by modified frequency of grain boundaries having same orientation angle and change in the kinetics of tribochemical reactions. It was found that doping elements partly made a sloid solution with SiC and rest were segregated along grain boundaries. Segregated Al reduced solubility of silica largely in water, whereas P and Mg reduced solubility to a lesser extent [Iier 1979]. Kinetics of formation of hydrated silica varied with solubility and hence led to change in frictional characteristics of SiC ceramics.

For improvements in the sliding-wear resistance of pressureless liquid phase sintering (PLPS)-SiC under diesel lubrication, Ciudad et al. [2013] suggested (i) reduction in intergranular phase (second phase) content, and (ii) decrease in grain size or increase in grain aspect ratio. They reported that SiC ceramics with similar grain size (of 1.1 μm) but having large amount of second phase exhibited high wear. Second phase led to decrease in hardness and increase in wear. Ortiz et al. [2012] proposed a colloidal processing route to produce dense SiC ceramics via pressureless liquid-phase sintering. In addition to uniform mixing, the colloidal processing route resulted in a nano film of ~5 nm thickness on the surface of SiC particles. Compared to conventional mixing and sintering, complete densification achieved in shorter sintering time and minimum defects found in ceramics sintered using colloidal processed powders. The time required for the transition from mild to severe wear was more than double for SiC ceramics prepared by colloidal processing as compared to that for the SiC ceramics prepared by conventional processing. It was advocated that, though the microstructures were similar in terms of the size and morphology of grains for ceramics prepared through both processing routes, the clear interface with fully dense structure led to a superior wear resistance *(see **Figure 2.3**)*.

Zhou et al. [2003] reported that silicon carbide-graphite (SiC-C) composites exhibited lower coefficients of friction during sliding than the monolithic SiC. The flake like graphite particles present in SiC-C composites *(see **Figure 2.4**)* were expected to provide solid lubrication with easy shear during sliding. However, in the high contact stress condition (pin-on-disk tests), wear rates enhanced sharply from 0.38 to 3.90 X 10^{-6} mm^3/N.m for SiC-C composites which was attributed to the fracture of graphite flakes despite lowered coefficients of friction when compared to low contact stress condition (block-on-ring test) *(See **Table 2.1**)*.

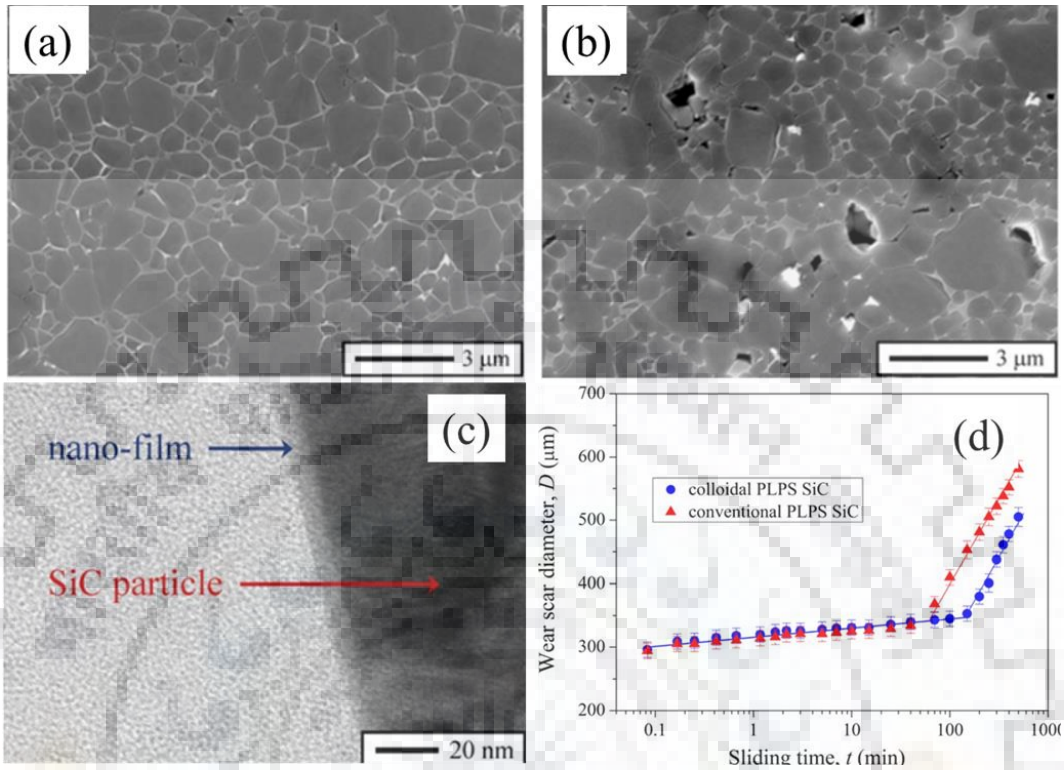

Figure 2.3. SEM images of the plasma-etched cross-sections of the (a) colloidal pressureless liquid-phase sintering SiC ceramic and (b) conventional pressureless liquid-phase sintering SiC ceramic. TEM image of the SiC powder particles, showing the presence of a nano-film on the surface of the SiC particles after the colloidal processing (c), and wear scar diameter representing wear of SiC ceramics (d) [Ortiz 2012].

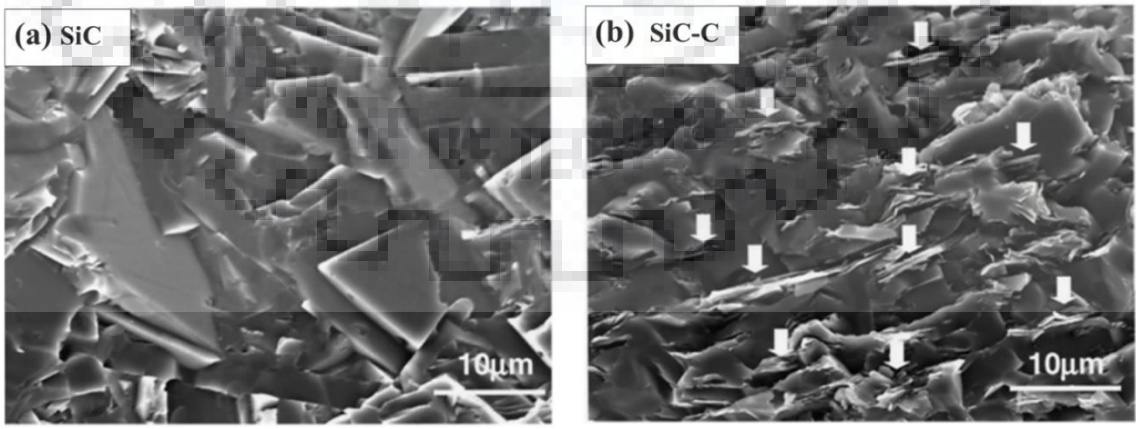

Figure 2.4. Fracture surfaces of (a) SiC and (b) SiC- 20 vol% graphite (SiC-C) composite. The graphite particles in SiC–C composite remain flake like, as indicated by the arrows [Zhou 2003].

Table 2.1. Friction and wear data for SiC-C ceramics for different tribo-configurations [Zhou 2003].

Specimen	Average coefficient of friction		Wear rate (X 10^{-6} mm^3/N.m)	
	Block-on-ring	Pin-on-disk	Block specimen in block-on-ring test	Pin specimen in pin-on-disk test
SiC	0.64	0.28	4.60	0.38
SiC- 10 vol. %C	0.55	0.15	3.20	2.90
SiC- 20 vol. %C	0.49	0.14	6.20	2.30

2.1.2. Effect of mechanical properties

Mechanical properties such as fracture toughness, hardness, and elastic modulus have influence on sliding wear characteristics of SiC ceramics. Hardness and fracture toughness of SiC ceramics are reported to generally range from 16 GPa to 27 GPa, and 2.3 MPa.$m^{½}$ to 8.3 MPa.$m^{½}$, respectively based on types of sintering/additives, microstructure etc [Lopez 2005, 2007; Guo 2010; Yeom 2015; Llorente 2016; Yang 2016]. Particularly, the influence of hardness and fracture toughness on friction and wear behavior was debated in most of the reports.

A sharp indenter model and a blunt indenter model were proposed to estimate the sliding wear in the tribocontact of brittle materials in absence of any layer formation. According to Marshall et al. [1982] for the tribocontact of sharp indenters, wear in brittle materials occurs due to the formation and propagation of lateral cracks *(see **Figure 2.5**)*. For a given applied load (P), total sliding distance (S), hardness (H), fracture toughness (K_{Ic}) and elastic modulus (E), wear volume of the brittle solid (V_S) can be assessed using the following equation [Marshall 1982]:

$$V_S = \alpha \frac{P^{9/8}}{K_{Ic}^{1/2} H^{5/8}} \left(\frac{E}{H}\right)^{4/5} S \qquad \text{..... (2.1)}$$

where α is a material constant. In case of blunt indenter pressed against a brittle solid, surface ring cracks are generated, which propagate towards downwards with repeated sliding contact and develop conical cracks to cause pull-out of material [Lawn 1994].[78)] Following Hertzian analysis, when there was no tribochemical layer formation, Tewari et al. proposed following relation for estimating wear volume (V_B) for brittle materials in ball-on-disk fretting wear contacts [Tewari 2009].

$$V_B = \frac{2\pi\beta^2 s}{3}\left(\frac{3PR}{4E}\right)^{2/3}\sqrt{\left(\left(\frac{4\chi^2 EP}{3\beta^3 K_{Ic}^2 R}\right)-1\right)} \quad \text{..... (2.2)}$$

where R is radius of the ball, χ and β are constants, and s is the stroke length in fretting contact.

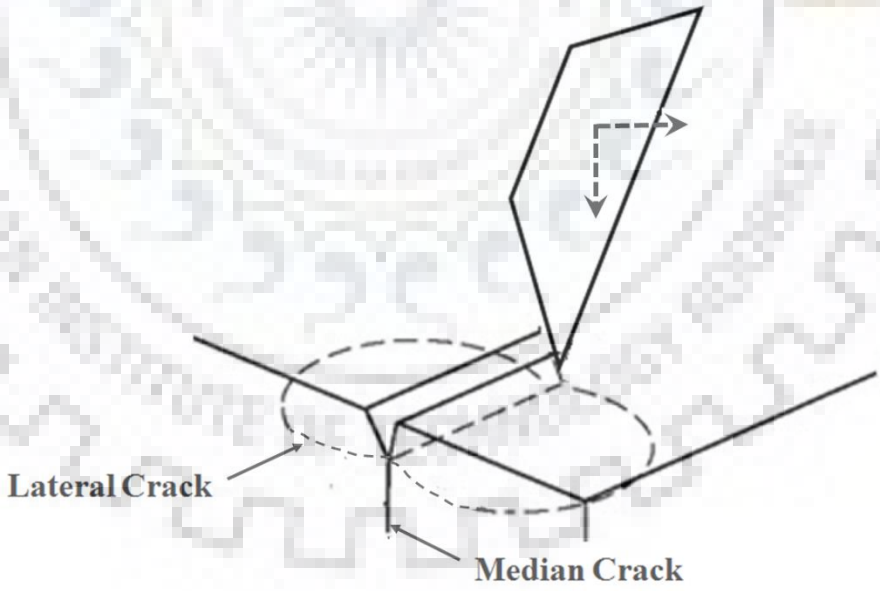

Figure 2.5. Wear mechanism of brittle material dominated by lateral and median crack [Marshall 1982].

SiC ceramics sintered with small amount (0.2 wt%) of Y_2O_3 additives attributed to high strength (561 MPa) and high hardness (27.7 GPa) than the SiC ceramics sintered with large amount (3wt%) of Y_2O_3 additives (542 MPa and 26.1 GPa), and exhibited superior wear resistance [Gupta 2015]. Li et al. [1998] found that toughened SiC prepared by hot pressing showed high hardness and fracture toughness compared to the SiC ceramics prepared through pressureless sintering or reaction sintering. The same trend reflected for resistance against friction and wear in water-lubrication conditions against SiC counterbody. Lopez et al. [2005] reported that elongated-grain LPS SiC, despite having lower hardness, showed almost a half of the wear rate than that obtained for equiaxed-grain LPS SiC, and reflected less extent of dislocation plasticity. They also differentiated the extent of wear as mild wear dominated by hardness and severe wear dominated by fracture toughness of LPS SiC ceramics. Kovalcikova et al. [2014] used brittleness index (H/K_{1c}) for qualitative estimation of specific wear rate of SiC against Si_3N_4. Their results showed that resistance to wear increases with increased index number.

Llorente et al. [2016] studied tribological nature of SiC composites prepared with different types and amounts of graphene-based sources. They demonstrated the importance of graphene fillers in resisting wear during sliding. According to them, the choice of the most suitable amount and type of graphene in SiC composites for tribological and mechanical applications is dependent on their specific working requirements. SiC composites with 20 vol% graphene nanoplatelets (GNPs) clearly exhibited 72% higher wear resistance compare to the monolithic SiC (*see* ***Figure 2.6***). It was demonstrated that an optimum combination of mechanical properties is required to provide the best wear resistance for SiC ceramics.

Amirthan et al [2011] studied the reciprocated sliding friction and wear characteristics of cotton fabric/teak wood/jute fiber based Si/SiC. Among the investigated composites, fine teak wood and cotton based samples exhibited less COF of 0.25 and 0.23 and less wear rate of 3.0×10^{-6} and 1.24×10^{-6} $mm^3/N.m$, respectively in dry sliding condition. This was attributed to the carbon film formation that acted as lubricating media on the wear track. Alumina particles, generated as debris from alumina counterbody balls acted as third body for harder surfaces. Third body abrasion of the surfaces led to high wear of harder chemical vapor infiltration treated cotton based sample. On the other hand, porous nature of the coarse wood particle and jute fiber based sample surfaces exhibited high wear.

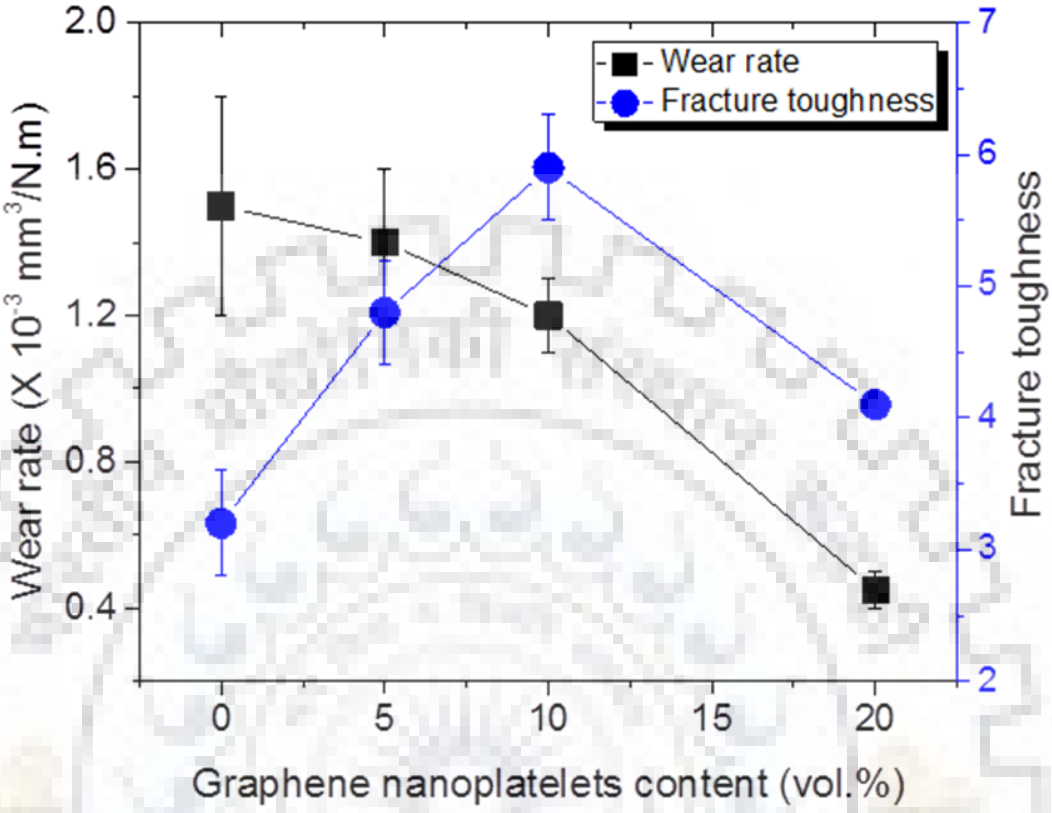

Figure 2.6. The wear rate and fracture toughness of SiC- graphene nanoplatelets composites as function of content of graphene nanoplatelets [Llorente 2016].

Candelario et al. [2014] introduced graphite nanodispersoids into the microstructure of a fine-grained LPS SiC ceramics fabricated by spark plasma sintering and studied sliding wear characteristics in regular diesel fuel (viscosity of ~3.8 cSt) lubricating conditions. Addition of graphite nanodispersoids was detrimental to mild wear and transition from mild to severe wear occurred in shorter time due to softer graphite particles. On other side, the addition of graphite nanodispersoids led to increased fracture toughness and provided external lubrication after grain pull-out. This was resulted in effectively decreasing wear damage for a prolonged sliding. Important findings from sliding wear studies of SiC based ceramics are listed in **Table 2.2**.

Table 2.2. Summary of major findings from sliding wear studies of SiC based ceramics.

Materials (SiC based ceramics/ Counter body)	**Sliding test parameters**			**Major findings**	**References**
	Speed	Load	Environment or Lubrication		
SiC pin/SiC disk	2 mm/s	5, 30, 50, 100 N,	50±2% RH and 19±2^{0}C	A hydrated silicium oxide film forms and functions as a lubricating film to reduce friction and wear.	[Takadoum 1994]
SiC ball/SiC disk	10mm/s 1 m/s	250 mN 1N	vacuum Air	In vacuum, the transition from severe to mild wear was connected with smoothening of surface roughness.	[Zum-Gahr 2001]
Si_3N_4 ball/LPS-SiC disks	~0.04 m/s to ~0.01 m/s	240 N to 100 N	Diesel (viscosity ~3.8 cst)	Resistance to sliding decreases with increasing contact load and sliding speed.	[Ciudad 2013]
Si_3N_4 ball/LPS-α-SiC disk	~0.04 m/s	70 N	Paraffin oil (viscosity ~34 cst)	The superior sliding wear resistance of low-cost *in situ* toughened SiC ceramic was most likely due to the formation of interlocking networks of elongated SiC grains.	[Lopez 2005]
SiC ball/SiC-3 wt% (AlN–Sc_2O_3 or AlN– Y_2O_3	0.21 m/s	1 N, 6 N or 13 N	20 -580 ^{o}C and 50 -10% RH	SiC ceramics sintered with 3 wt% AlN–Sc_2O_3 additives exhibited less wear. Surface grooving and microcracking occurred at low load	[Kumar 2011]

) disk				(1 N). Tribochemical wear was dominant at 6 and 13 N loads for all the ceramics.	
α-SiC ball/ Al, Mg or P-doped SiC	36 mm/s	1 N,	30% - 60% RH	At higher humidity (60% RH), the friction coefficient value (0.25) is almost independent of doping elements. At lower humidity (30% RH), the effect of doping elements (Al, Mg and P) is more pronounced. As the humidity increases from 30% to 60%, the nature of damage changes from mechanical to tribochemical.	[Murthy 2004
SiC–$MoSi_2$ /Alumina cylinder	0.5, 1.0 and 2.0 m/s	15, 30 and 50 N	20–25 ^oC and 35–55% RH	Mild to severe wear transition with speed (high wear at high speed of 2 m/s)	[Micele 2010]
SiC_f-SiC pin/hardened steel disc	~100 to ~850 rpm	11 N	Dry Atmosphere	SiC_f/SiC composite with carbon interface shows high hardness and least wear rate. SiC_f/SiC composite with BN interface, subjected to an intermediate heat treatment showed lower hardness and higher wear rate	[Udayakum -ar 2011]

SiC or Al_2O_3 balls/ Pressure less sintered SiC disk	Stroke 100-1600µm, frequency 2.5 - 20 Hz	1-10 N	1 to 100% RH	Tribo-oxidation was determined as the main wear mechanism.	[Wasche 2004]
SiC cylinder/SiC plate	Stroke 8mm, frequency 10 Hz	60 N	Isooctane and distilled water	The self-mated ceramics showed greater values of friction coefficient in isooctane than in distilled water	Dulias 2005]

2.1.3. Mechanisms of material removal in sliding wear

In this section, studies related to material removal mechanisms during sliding wear are discussed in terms of material characteristics. Different results for frictional behavior between varieties of pairs of SiC ceramics during wear indicate complexity in frictional mechanism. Kato [1990] divided wear mechanisms of SiC ceramics in sliding wear conditions into two modes: (a) mechanical wear, where various types of cracks like lateral, median and radial cracks are generated by friction around the Hertzian contact zone *(see **Figure 2.7**)*, and (b) tribochemical wear, where silicon oxide was found on the surface in unlubricated sliding wear [Hotta 1988; Chen 2007]. Wang et al. [1996] found that tribological contact stresses predominantly affect mechanisms of material removal. They found that SiC ceramics removed via plastic deformation induced microfracture for less stress on contact surface. As the contact stress increased to a critical level, varieties of cracks like partial cone cracks, lateral/shallow cracks, and radial cracks etc. are generated. Further increase in contact stress propagates cracks to intersect each other and detach chunks of material. The detached material crushed into fine particles by further tribological contact and evolved as wear debris. The dominant damage patterns with contact stress severity for indentation, scratch, and sliding wear tests are synchronized in **Table 2.3**.

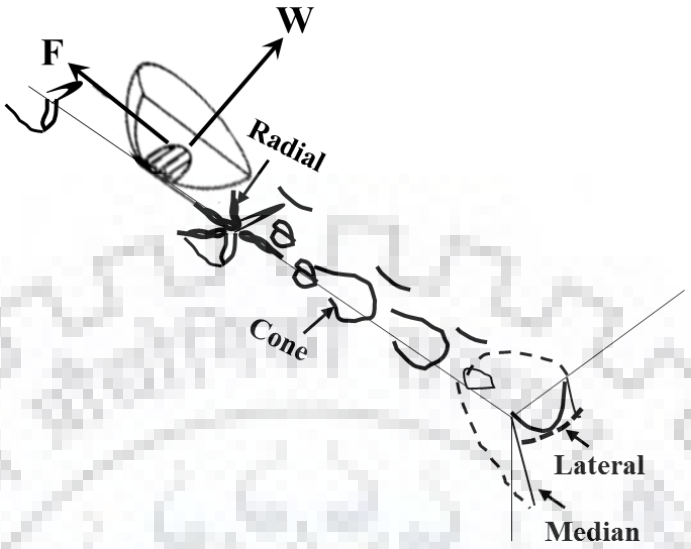

Figure 2.7. Various types of cracks induced by friction in unlubricated sliding wear conditions [Hotta 1988] (where W is load and F is frictional force).

Table 2.3. Stress severity against damage patterns for SiC ceramics in different contact [Wang 1996].

Contact Stress	**Dominant damage patterns in sliding of SiC ceramics**		
	Indentation	**Scratch**	**Sliding wear**
Small (below the elasticity limit)	No damage (Elastic Deformation)	No damage (Elastic Deformation)	No damage (Elastic Deformation)
Moderate (below the plastic limit)	Plastic deformation	Plastic deformation	Plastic deformation controlled wear
Large (near the critical failure stress)	Cone/Ring cracks	Partial Cone/Ring cracks	Microcrack controlled wear or grain pull-out
Very large (exceeds the critical stress)	Radial crack Lateral crack	Microfracture caused by the intersection of radial, lateral and partial cone cracks	Microfractured-controlled wear

Lopez et al. [2005] reported that for equiaxed-grained SiC ceramics, sliding wear initiated with plastic deformation as mild wear and led to sever wear, with fracture and pull-out of material [Hsu 2004; Cho 1989; Li 1998; Liu 1993; Cho 1992]. For coarser microstructures, transition in wear mechanism occurred sooner and exhibited poor wear resistance [Wang 1996; Cho 1996; Lopez 2005; Cho 1989; Cho 1995; Cho 1992; Dong 1993; Rainforth 2004; Wang 2005]. However, these mechanisms were not observed for highly heterogeneous ceramics such as elongated-grain LPS-SiC [Lopez 2005]. For elongated grain LPS SiC ceramics, despite the grain-boundary fracture, interlocking network was responsible for the surface integrity of worn surface which delayed transition in wear mechanism (*see* ***Figure 2.8***).

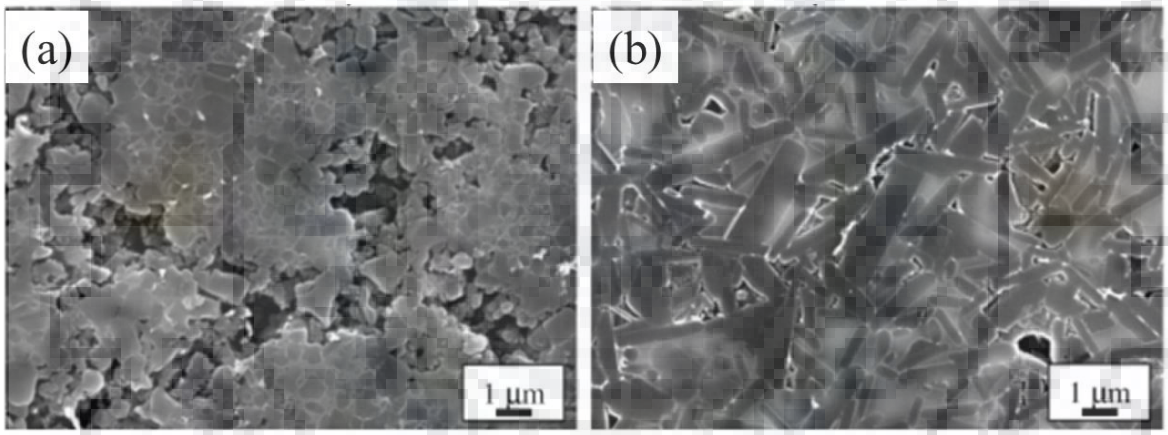

Figure 2.8. Worn surface of (a) equiaxed-grain LPS SiC and (b) elongated-grain LPS SiC [Lopez 2005].

Kovalcikova et al. [2014] studied wear mechanisms for SiC ceramics slid against different counterparts Si_3N_4, Al_2O_3, WC-Co and ZrO_2 materials. They found microfracture and removal of oxides against any counterpart. But the extent of material removal was different. The steady state coefficient of friction and specific wear rate were affected with different tribological partners. The SiC/Si_3N_4 couple exhibited the highest friction probably due to chemical similarity of counterparts *(see* ***Figure 2.9****)*.

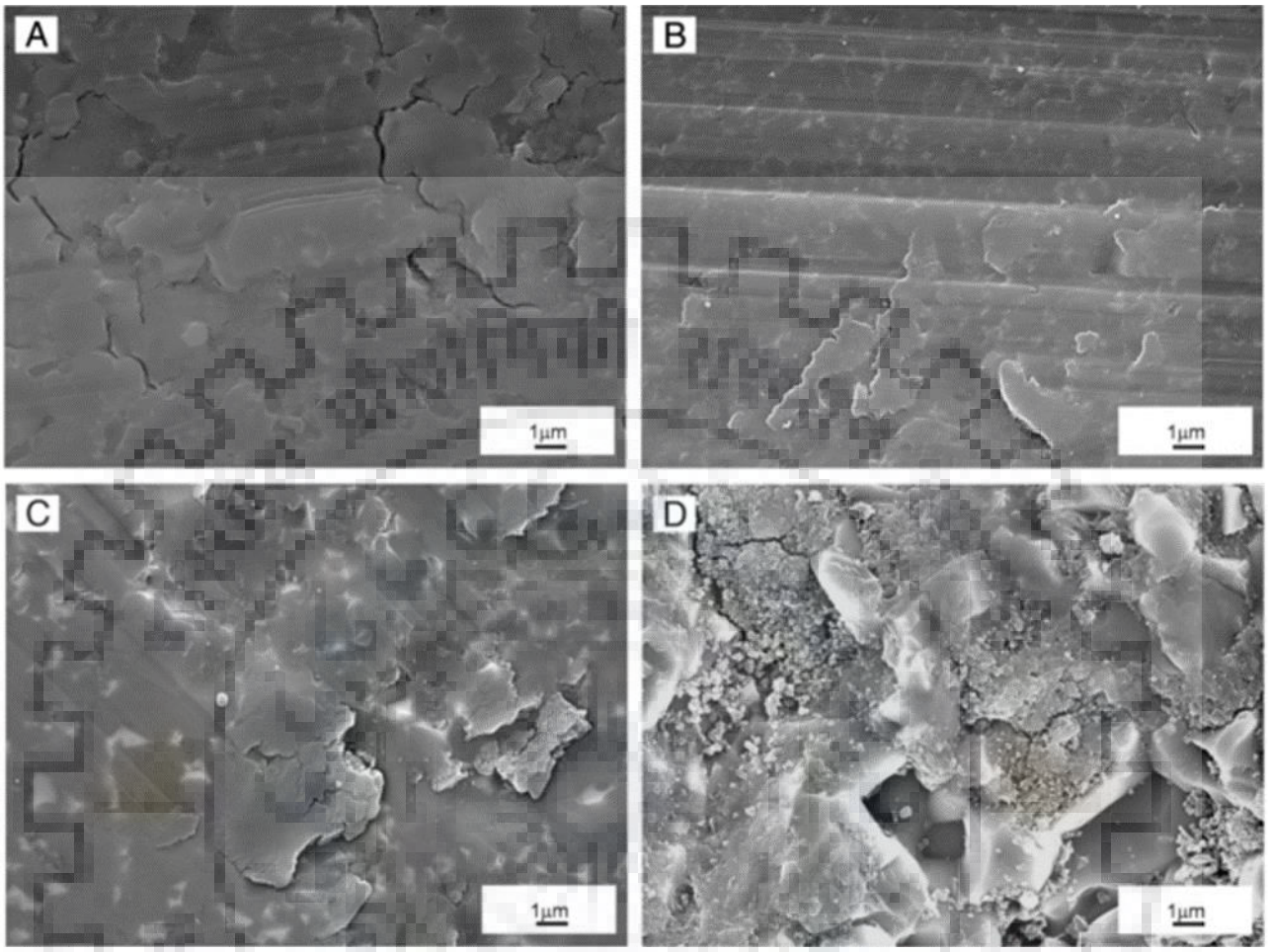

Figure 2.9. The surface of SiC worn against (A) ZrO_2 ball; (B) WC-Co ball; (C) Al_2O_3 ball; and (D) Si_3N_4 ball [Kovalcikova 2014].

Andersson et al. [1994] reported two types of oxidation in sliding at elevated contact temperatures: passive oxidation and active oxidation. At elevated temperature (usually above 575 ^oC), SiC oxidizes to SiO_2 according to the following reactions [Frisch 1988; Singhal 1976]:

$$2SiC + 3O_2 \rightarrow 2SiO_2 + 2CO \text{ (passive oxidation)} \quad \text{..... (2.3)}$$

$$SiC + 2O_2 \rightarrow SiO_2 + CO_2 \text{ (passive oxidation)} \quad \text{..... (2.4)}$$

Above reactions occur at an appropriate pressure in oxygen environment. If temperature is above 1000 ^{o}C, and partial pressures of oxygen, the following reactions might occur on SiC ceramic surface [Singhal 1976]:

$$SiC + 2SiO_2 \rightarrow 3SiO + CO \text{ (active oxidation)} \quad \ldots\ldots\ldots\ldots (2.5)$$

$$SiC + O_2 \rightarrow SiO + CO \text{ (active oxidation)} \quad \ldots\ldots\ldots\ldots... (2.6)$$

The SiO powder formed was brownish to yellowish in color and often formed with β-SiC powders in an argon thermal plasma jet [Kong 1987]. Under passive oxidation layer, loose wear debris consisting of SiO_2 formed a protective and less shear strength tribofilms which further favored to reduce wear rates. Against passive oxidation layer, wear rates varied from 10^{-6} to 10^{-5} mm^3/N.m and the coefficients of friction was approximately 0.5. As SiO did not form tribofilms and favored to active oxidation to some extent, wear rates increased to 10^{-5} -10^{-4} mm^3/N.m and the coefficients of friction to 0.8. It was found that the additive composition had minimal effect on frictional behavior of SiC ceramics in dry sliding conditions when compared to sliding load.[2)] Wear mechanisms changed from surface grooving and micro-cracking at lower load (1 N) to dominant tribochemical wear at higher (6 or 13 N) load for all the ceramics. In other study [Gupta 2015], sliding wear behavior of SiC ceramics sintered with (0.2 wt.% or 3 wt.%) Y_2O_3 additive, microcracks induced fracture and pull-out were found responsible for the material removal.

In self-mated sliding of SiC ceramics, Zum-Gahr et al. [2001] reported that running-in period was much longer in vacuum than in humid air and would favor tribochemical smoothening of surface roughness. At a tribocontact of relatively smooth surface, formation of thin water film led to increased friction owing to menisci formed at asperities. On the other hand, thick water films separated the mated bodies and resulted for reduced friction due to low viscosity of H_2O and assumed a proper wettability of tribosurfaces with water film, i.e. hydrophilic surfaces.

Available data on the effect of humidity on coefficient of friction and wear rate of self-mated SiC ceramics is compiled and presented as **Figure 2.10** [Murthy 2004; Li 1998; Wasche 2004; Hotta 1988]. Murthy et al. [2004] found that in sliding at less humid conditions (30%), major wear mechanism was fracture of tribosurface followed by attrition, while tribochemical reaction (oxidation or hydrolysis) was a leading wear mechanism in high humid condition (60%). Owing to the availability of more water molecules, oxidation ($SiC + 2H_2O \rightarrow SiO_2 + CH_4$) and hydrolysis ($SiO_2 + H_2O \rightarrow Si(OH)_4$) reactions were accelerated at higher humidity. The faster kinetics of tribochemical reactions resulted in decreased wear with a narrow difference in friction.

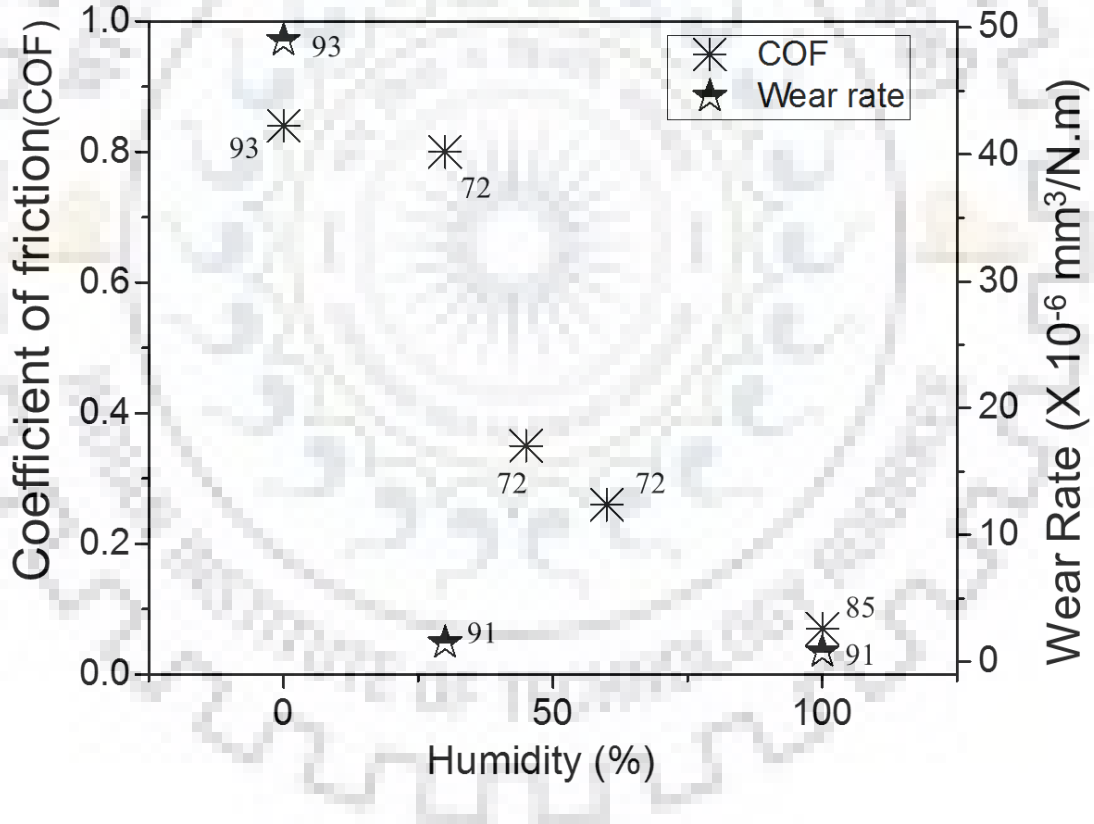

Figure 2.10. Average steady state coefficient of friction and wear rate of SiC ceramic with respect to humidity against SiC counterbody [Murthy 2004; Li 1998; Wasche 2004; Hotta 1988].

Li et al. [1998] observed difference in wear mechanism during sliding in water lubrication conditions for SiC ceramics prepared through different processing routes. The wear occurred by pull-out of grains, which was mainly controlled by free Si along grain boundary for the reaction sintered SiC. Tribochemical oxidation in water and local grain fracture occurred due to its low toughness for the pressureless sintered SiC. Excellent wer resistance and less friction were attributed for the hydrodynamic lubrication for the toughened SiC. It was believed that tribochemical oxidation took place and an ultraflat surface consisting of SiO_2 and ($SiO_2.nH_2O$) formed on the worn track.

Candelaria et al. [2014] found less wear of SiC with graphite nanodispersoids compared to SiC ceramics, due to the combination of (i) higher toughness, which hinders the crack propagation and coalescence responsible for the grain pull-out, (ii) lower hardness of the wear debris due to its lower SiC concentration, and (iii) external lubrication imposed by pull-out of graphite nanoparticles, which reduced abrasion by third bodies. Zhu et al. [1999] studied polishing of SiC ceramics in oxidant solution of 3 wt% CrO_3. The removal of material by a chemical dissolution, stimulated by friction was referred as tribochemical.

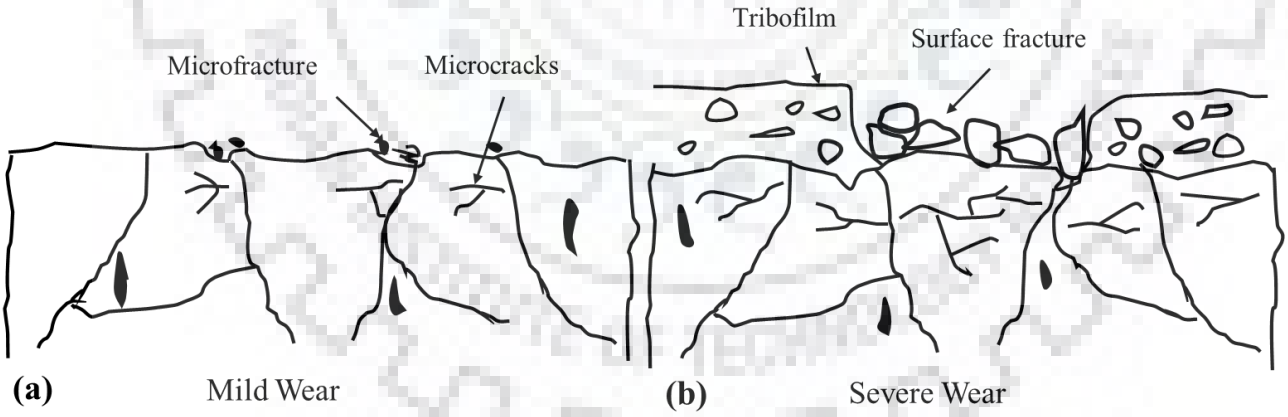

Figure 2.11. Schematic illustrations of worn surface characteristics of SiC ceramics after sliding in diesel in (a) mild wear and (b) severe wear regimes [Sanchez 1998].

Ciudad et al. [2013] studied wear mechanisms in diesel for pressureless liquid phase sintered-SiC ceramics. They found a two-step wear process, initially controlled by plastic deformation

(corresponding to mild wear regime) followed by fracture of materials (corresponding to severe wear regime). Major characteristics of surfaces in mild wear and severe wear regimes are schematically illustrated in **Figure 2.11**. Erickson et al. [1993] observed chemical wear on mated surface as major deterioration mechanism in oil/water lubricated sliding conditions along with several mechanisms like plastic deformation, subsurface microcrack formation, microfracture and microabrasion of the surface of worn SiC. The absence of tribofilm on the contact surface indicates that wear debris transported out of the system or directly dissolved by the oil/water lubricant as water is able to dissolve SiO_2 easily [Tomizawa 1987; Lancaster 1990; Sasaki 1988].

Zhou et al. [2003] reported that the tribochemical reaction led to material removal for monolithic SiC and SiC-C (graphite) composite. For SiC, they found rough worn surfaces resulted in fracture and three body abrasion, whereas graphite particles exerted a lubricating effect and resulted lower coefficients of friction for the SiC-C composites. Micele et al. [2010] studied the tribological characteristics of SiC-$MoSi_2$ composites against alumina in dry sliding conditions. The material loss was caused by ploughing effects, while no significant effect of brittle fracture observed on the worn surface of the ceramic composite. Wasche and Klaffke [1999] studied wear mechanisms for SiC–TiC–TiB_2 in water when slid against SiC or Al_2O_3. In case of SiC/SiC and Al_2O_3/SiC, no films were formed. An oxide film was formed during wear of SiC–TiC and SiC–TiC–TiB_2 materials. Reduction in wear of materials was affected by formation of titanium oxide at the tribocontact. In case of Al_2O_3 ball and composite disk system, the tribooxidatively formed layer was partly adhered on to the ball. The wear of SiC–TiC or SiC–TiC– TiB_2 disk against SiC or Al_2O_3 ball was reduced by a factor of 10 compared to monolithic SiC disk system.

2.2. Erosion wear of SiC ceramics

Erosion can be defined as removal of material from a surface due to interaction between the surface and a fluid, or impinging liquid or solid particles [Kumar 2006; Rattan 2007; Wang 1995; Medvedovski 2010; Evans 1977]. Considerable research has been carried out in understanding solid particle erosion wear behavior of SiC ceramics and their composites [Wang 1995; Routbort 1980a,b, 1983b; Kim 1998; Medvedovski 2010; Evans 1977; Nava 2002; Wiederhorn 1983; Jianxin 2007].

2.2.1. Effect of microstructure and mechanical properties

Solid particle erosion of SiC ceramics and their composites is reported to occur generally by brittle fracture as a result of lateral and radial cracking [Routbort 1980a,b; Kim 1998; Evans 1977; Nava 2002; Wiederhorn 1983; Jianxin 2007]. Bell and Rogers [1987] noted fracture toughness as predominant factor in estimating erosion wear characteristics of brittle materials at normal impact of erodent [Wang 1995; Gautier 1993], whereas hardness was found important at low impingement angles. Shetty et al. [1982] also reported hardness as predominant property of reaction-bonded SiC ceramics to estimate erosion behavior of ceramics. Routbort and Matzke [1983b] studied the erosion for SiC ceramics prepared through hot-pressing and reaction-bonded sintering techniques. The Vickers hardness (H) and fracture toughness (K_{Ic}) of these ceramics were used to estimate the erosion rate (ΔW) of ceramics using following realtion:

$$\Delta W = C\, H^{a}\, K_{1c}^{b} \quad \text{---------- (2.7)}$$

where, *C* is proportionality constant and the exponents *a* and *b* valued according to details of the used erosion model [Routbort 1983b] (*see* ***Table 2.4***).

Table 2.4. Values of (H^{a} K_{Ic}^{b}) calculated for the various steady-state erosion models and experimentally measured erosion rates for SiC ceramics [Routbort 1983b]. Hot pressed-SiC and reaction bonded-SiC respectively indicate hot pressed SiC and reaction bonded SiC, while H and K_{Ic} indicate hardness and fracture toughness, respectively.

Materials	$H^{0.11}\, K_{Ic}^{-1.3}$	$H^{-0.25}\, K_{Ic}^{-1.3}$	$H^{0.48}\, K_{Ic}^{-1.9}$	**Measured erosion rate ($X\ 10^{-3}$ g/g)**
HP-SiC	0.54	0.01	11.10	2.00
RB-SiC	1.34	0.03	40.00	12.00
RB-SiC + 0.2 vol% Si	0.73	0.02	16.20	10.00
RB-SiC + 0.13 vol% Si	0.80	0.02	18.00	4.50

However, the wear rates estimated using existing wear models were not in agreement with the experimentally measured wear rates. This can be primarily attributed to the fact that these models neglected important contributions from microstructure of the target material in estimating erosion loss [Wang 1995; Routbort 1980a,b, 1983a,b; Wiederhorn 1983]. Wang et al. [1995] studied the effect of microstructure on erosive wear of SiC ceramics, prepared by pressureless sintering, hot pressing and hot isostatic pressing techniques. Microcracking with some extent of plastic deformation was observed as main material removal mechanism at higher impact angles [Wang 1990; Finnie 1967]. Grain refinement and reduction in the amount and size of pores of hot isostatically pressed SiC resulted in superior wear resistance. Wang and Levy [1990] studied the erosion behavior of SiC fiber reinforced SiC composite at 25^{o}C and 850^{o}C and found an inverse relation of density and hardness to the erosion rate of the composite. The erosion rate reduced by one order of magnitude at 850^{o}C (0.10 mg/g) compared to that at 25^{o}C (2.20 mg/g). At 850^{o}C, the difference between erosion rates at 90^{o} and 30^{o} (0.02 mg/g) was much less than that found at 25^{o}C (1 mg/g), which attributed to increased ductility of composite at 850^{o}C *(see **Table 2.5**)*.

Table 2.5. Erosion rate of SiC_f-SiC composite as function of impingement angle and temperature [Wang 1990].

Erosion Temperature (^{o}C)	**Erosion rate at 30^{o} impact angle (mg/g)**	**Erosion rate at 90^{o} impact angle (mg/g)**
25	1.20	2.20
850	0.08	0.10

Similarly in a recent study [Li 2014], solid particle erosion rate of SiC-Si_3N_4 composite at elevated temperature increased first up to 800^{o}C, and then decreased with increase in temperature to 1400^{o}C *(See **Figure 2.12**)*. At lower temperature (up to 800^{o}C), wear occurred by brittle fracture where stripping of aggregates of composite resulted in loss of protection from the matrix. On the other hand [Wang 1990], plastic deformation and oxidation protection dominated at higher temperature (beyond 800^{o}C). The

highest erosion rate at 800°C for SiC-Si_3N_4 is contradictory to the lowest erosion at 850°C for SiC ceramics.

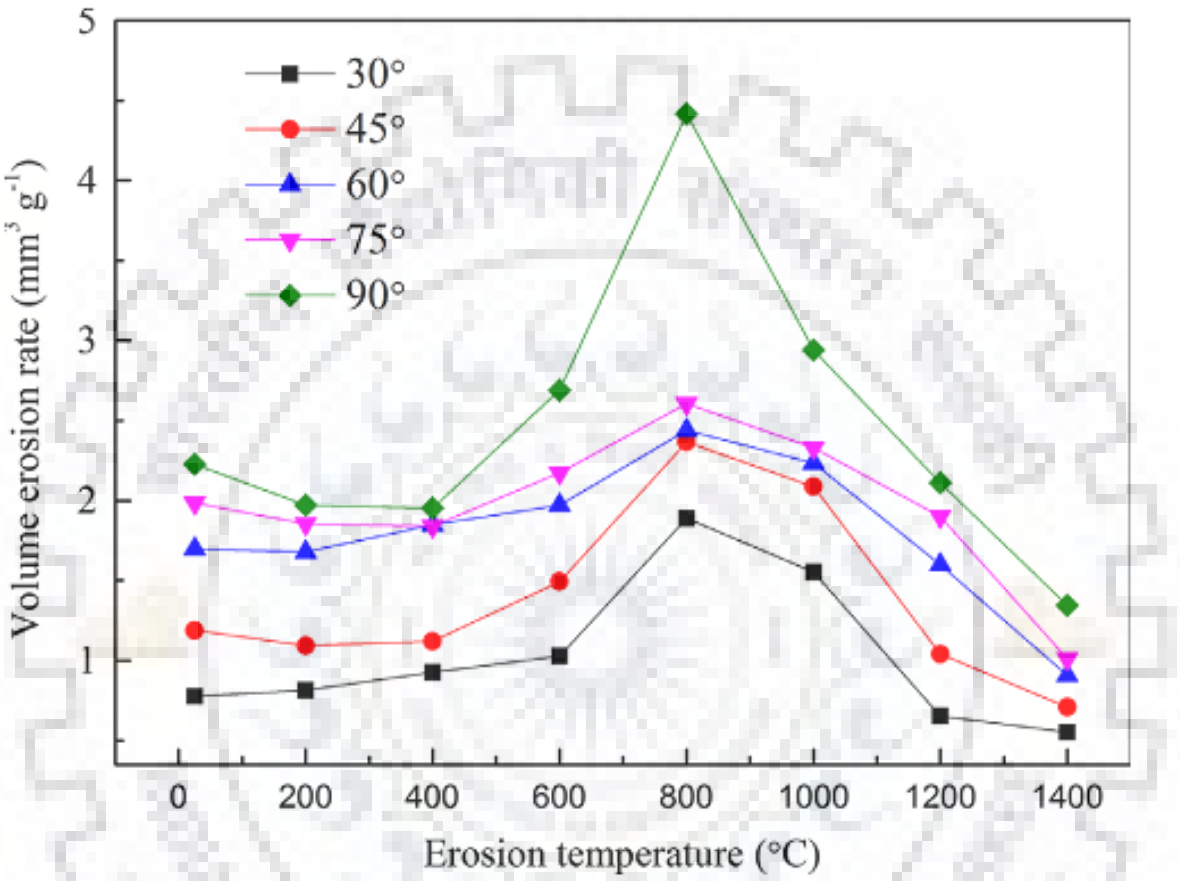

Figure 2.12. Change in the volume erosion rates with respect to the erosion temperature at different impingement angles for SiC–Si_3N_4 composite [Li 2014].

Amirthan et al. [2010] found cleavage like brittle fracture on biomorphic Si/SiC composite surface exposed to erosion. Fine teak wood particle based Si/SiC composite showed least erosion compared to other Si/SiC composite. Further, coarse teak wood particle based Si/SiC composite with large pores caused the highest erosion rate. A. Lopez et al. [2004] studied the erosion behavior of biomorphic (eucalyptus and pine reinforced) SiC, reaction-bonded SiC, and hot-pressed SiC and found that erosion resistance was highest for biomorphic based SiC ceramics. Owing to the highest hardness, hot-pressed SiC exhibited least erosion rate.

2.2.2. Mechanisms of material removal in erosion wear

The dominant mechanisms of material removal in solid particle erosion wear conditions of brittle ceramics are elastic-plastic deformation based micro-fracture, and crack formation below the plastic zone of subsurface [Kim 1998; Routbort 1980a,b; Evans 1977; Nava 2002]. Major findings from studies on erosion wear mechanisms for SiC ceramics are listed in **Table 2.6**.

Table 2.6. Summary of major findings from studies on erosion wear mechanisms for SiC based ceramics.

Materials (SiC based ceramics/ erodent)	**Erosion test parameters**			**Major findings**	**References**
	Particle velocity& feed rate	Impact angle	Environment		
Reaction Bonded SiC/ Angular Al_2O_3	Velocity varied from 53.8 m/s to 150.7 m/s	Impact Angle Varied from 10^o to 90^o	Normal atmosphere	The steady state erosion rate was lower for smallest erodent particle. With leading brittle fracture, some plasticity also observed in the SEM micrographs.	[Routbort 1980b]
Biomorphic SiC, Reaction-bonded SiC, and hot-pressed SiC/ Angular SiC	Particle velocity = 100 m/s, feed rate of 8 gm/min	Normal Impact	Vacuum (approx. 500 mTorr),	Both lateral and radial cracks formed for biomorphic SiC ceramics, whereas reaction-bonded SiC eroded by formation and propagation of only lateral cracks. Hardest hot-pressed SiC ceramic found as the most erosion	[Finnie 1967]

				resistant.	
α-SiC target specimens/SiC	Velocity 35, 65 and 90 m/s, feed rate of 10 g/min,	Impingement angles of 15, 45, 60 and 90°,	Ambient Temperature	Reduced amount and size of pores, and reduced grain size led to improved wear resistance. Microcracking and some extent of plastic deformation was found as dominant material removal mechanism is mainly with some extent of plastic behaviour of materials.	[Wang 1995]
Hot-pressed monolithic SiC and SiC–TiB_2/ Angular SiC	Velocity 40–100 m/s, feed rate: 0±0.5 gm/min,	Impact angles: 30–90°	Room temperature	The erosion rate was lower for monolithic SiC with higher hardness value than SiC-TiB_2 composite of higher fracture toughness. Erosion of these materials was controlled significantly by the plastic deformation.	[Kim 1998]
SiC_f -SiC / Silica sand	Particle velocity: 32 m/s and 44 m/s,feed rate: 1 kg/min,	Impinge angle: 15°, 30°, 45°, 60°, 90°	Ambient Temperature	Higher hardness of SiC_f -SiC composite with carbon interface led to least erosion. Composite with boron nitride interface showed lower hardness and higher erosion loss.	[Udayakumar 2011]

A detailed investigation of impact sites of worn surface in brittle materials exhibits an intense plastic deformation beneath the immediate area of the contact [Hockey 1975, 1978; Wiederhorn 1983; Lawn 1980]. The elastic-plastic zone at the impact site is the major driving force for the surface fracture that led to material loss on erosion [Evans 1978, 1979; Marshall 1982]. The residual stresses generated under plastic zone on impact of erodent to the brittle materials originate small lateral cracks to grow beneath the impact sites. Initially, these cracks propagate parallel to the impacted zone of target surface and further interact to the surface resulting in material loss. Wang and Mao [1993] observed that size and type of cracks generated on the eroded surface are dependent on several factors like erodent shape and size, mass flow rate, velocity and angle of impingement of erodent, temperature and hardness, toughness and microstructure of target material [Wiederhorn 1983; Routbort 1983b; Wang 1995; Sharma 2014]. Two types of crack systems are generally found in erosion at low velocities; (a) cone cracks generated due to impact of blunt (rounded) erodent [Wiederhorn 1983; Chaudhri 1978; Knight 1977] and (b) lateral and median cracks generated due to impact of sharp (angular) erodent angular [[Wiederhorn 1983; Hockey 1978; Lawn 1978; Chaudhri 1980]. In case of high velocity erosion, material is removed by plowing, severe cracking and chipping [Evans 1977, 1978, 1979; Wiederhorn 1983; Chaudhri 1978]. In other study [Routbort 1980], precise mechanisms for the erosion of reaction bonded-SiC were not found clear, but reduced erosion wear rate of mixed phase SiC-Si region was related to either by arresting cracks around the small SiC grains or by increased apparent volume fraction of uncovered erosion resistant fine SiC grains.

Suh et al. [2011] studied the effect of SiC fiber reinforcement on erosion wear of SiC ceramics. During erosion of the composite, SiC fibers were detached from the interface and matrix of SiC and subsequently eroded out. Pores present in matrix with aperture around the fibers led to easy removal of material from the impact sites. The erosion wear was also attributed to issues regarding durability and reliability that depend on geometric discordance, irregular performance, and related energy dissipation. Gochnour et al. [1990] studied erosion behavior of SiC-Al_2OC composites against alumina erodent. They found surface appeared smooth and polished, with grain pull-out regions in erosion of SiC-5wt % $A1_2OC$ composites. Softer Al_2OC phases resulted in grain pull-out regions and smooth zones were corresponded to wear of harder SiC phase. However, severe grain pull-out occurred in erosion of SiC-50 wt % $A1_2OC$ composite and resulted in isolated smooth regions only *(see **Figure 2.13**)*. The steady-

state erosion rate (ΔE) for brittle materials was proportional to erodent radius (R) and found to be related as [Wada 1987; Wiederhorn 1983].

$$\Delta E \propto R^{2/3} \quad \text{.....(2.8)}$$

This was predicted by both the dynamic [Wiederhorn 1983] and the quasi-static [Wada 1987] theories of erosion for brittle materials. However, Kim and Park [1997] found that erosion rates of SiC and SiC-TiB_2 were not increased monotonically with the increased erodent size, in contrast to the prediction by theories. The eroded surface of SiC exhibited deformed lips and cracks, whereas intergranular fracture and deformed lips were observed for SiC-TiB_2 composites.

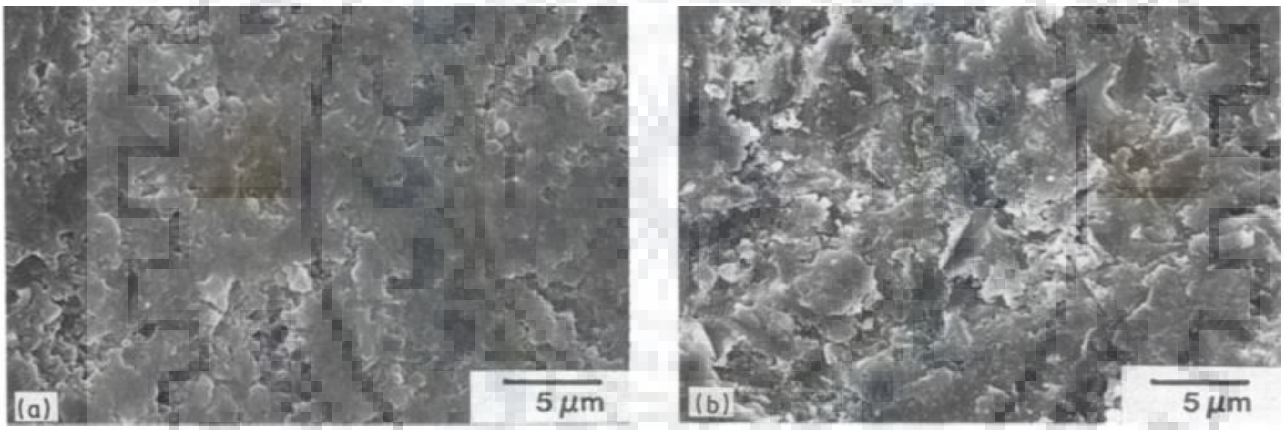

Figure 2.13. Eroded surfaces of (a) SiC-5 wt % $A1_2OC$, and (b) SiC-50 wt % $A1_2OC$ composite [Gochnour 1990].

Limited reports are available on erosion behavior of SiC ceramics and composites as function of temperature. Wang and Levy [1990] reported that erosion for SiC fiber reinforced SiC composite at 25°C occurred by cracking and chipping of the matrix as well as the fibers, while erosion rates considerably decreased at 850°C owing to the increased ductility. Li et al. [2014] studied the erosion mechanism for SiC-Si_3N_4 composites at different temperatures (25°C-1400°C). At low temperature, material removed occurred mainly by brittle fracture and stripping of aggregates as the protection from the matrix was lost. At higher temperature, erosion mechanisms were primarily ascribed to plastic

deformation as well as oxidation protection. Oxidation of Si_3N_4 and SiC on the material surface at 1400^oC generated a thin dense layer of SiO_2 glassy film, which further reduced direct contact of erodent with the material surface at a certain extent and resulted in less loss of the material ***(see Figure 2.14)***. The dominant mechanisms of material removal are further illustrated schematically in **Figure 2.15**.

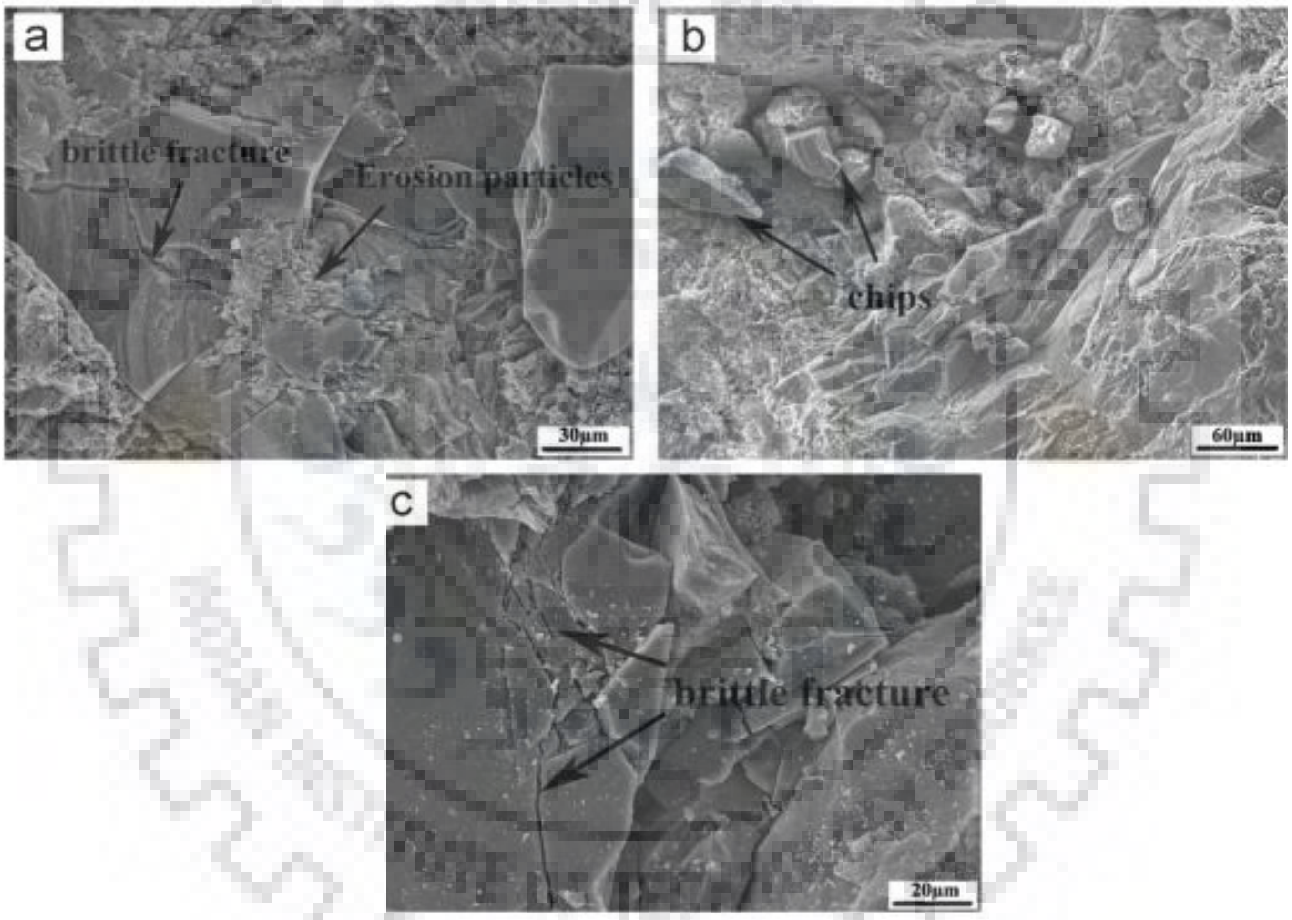

Fig. 2.14. The brittle fracture erosion morphologies of SiC–Si_3N_4 composite eroded at (a) 25 ^oC, (b) 800 ^oC and (c) 1000 ^oC [Li 2014].

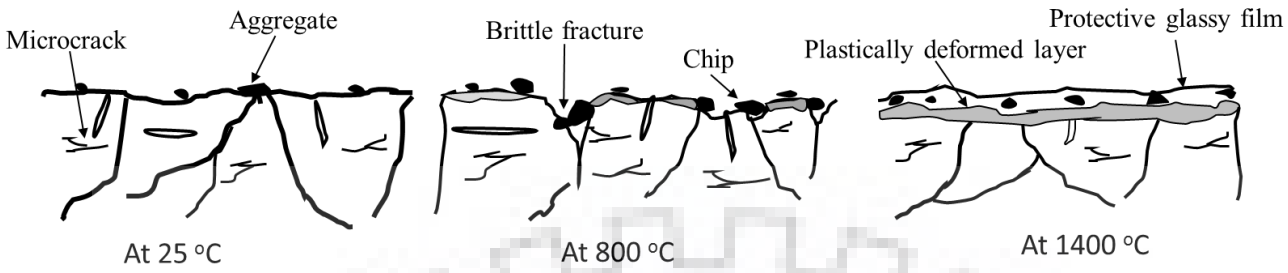

Fig. 2.15. Schematic representation of erosion mechanisms for SiC-Si_3N_4 composites at different temperatures.

2.3. Summary of literature reviewed

Considering the wide range of tribological applications, wear behavior of SiC and SiC based composites is extensively studied. In the present review, tribological characteristics of SiC ceramics and composites in sliding and solid particle erosion conditions are comprehensively discussed.

It is found during sliding that wear and friction characteristics of SiC ceramics vary with microstructural alteration. Hard interlocking network of elongated grains or high aspect ratio grains led to enhanced wear resistance. Second phases and intergranular phases also play a dominant role on wear and friction behavior. SiC ceramics with reduced weak second phase content and grain refinement exhibited improved wear resistance. Further, SiC ceramics with clear grain boundaries showed improved wear resistance compared to amorphous grain boundaries. The transition from mild to severe wear occurs for SiC ceramics with coarse grain structure than with fine grain structure. Doping elements affect kinetics of tribochemical reaction and lead to different characteristics of friction and wear. In understanding the influence of mechanical properties on wear of SiC ceramics, research is mainly debated on the dominant effect of fracture toughness and hardness. It is widely accepted that crack deflection or crack bridging by reinforced phase led to less extent of material removal during sliding wear of SiC composites. Furthermore, the ratio of hardness and fracture toughness (H/K_{1c}), known as brittleness index is found to give qualitative estimation of wear for SiC ceramics. Superior resistance to wear was found for ceramics with high brittleness index. Reinforced phases like graphene nanodispersoids led to an increase in fracture toughness and reduced hardness, the combination of which reduced the mild to severe wear transition.

Sliding wear mechanisms of SiC ceramics and composites can be categorized into two groups: mechanical and tribochemical. In mechanical wear, cracks and abrasion dominate the worn surfaces of SiC ceramics, whereas oxides were found on the tribosurface in tribochemical wear. With regards to contact stress conditions, wear occurred trough plastic deformation induced microfracture in low contact stress, whereas cracks induced fracture led to material removal in high contact stress. High friction is found against the counterbody having chemical similarity with SiC ceramics, whereas composition of sintering additives had minimal effect on frictional behavior of SiC ceramics. At elevated sliding temperature, two types of oxidation: passive oxidation with reduced wear and active oxidation with increased wear are reported for SiC ceramics. Running-in period is reported to be higher in vacuum than in humid air for SiC ceramics. Tribochemical smooth layer formed in humid air led to less friction. In oil/diesel fuel lubricated conditions, wear occurred in two steps: initially controlled by plastic deformation and then followed by subsurface microcrack formation, microfracture and micro-abrasion.

Solid particle erosion rate is found to be higher and steady states attained earlier against harder erodent particles. Erosion resistance is improved for harder SiC ceramics. Grain refinement and reduced amount and size of pores resulted for superior resistance against erosion. Erosion rates of SiC ceramics were estimated by semi-empirical models with mechanical properties like hardness, fracture toughness and elastic modulus. Since none of the proposed models for erosion prediction/estimation was completely satisfactory, it is highlighted necessity for incorporation of microstructural aspects into erosion theories. Incorporation of SiC fibers in SiC matrix resulted in improved erosion resistance at elevated temperature. The difference in erosion rate with change in impingement angle of erodent also found to be less at high temperature. In general, erosion rate of SiC composites increased with increase in temperature up to 800^{o}C and attributed to brittle fracture and stripping of aggregates. Further increase in temperature up to 1400^{o}C resulted in the formation of silica based glassy film and decreased erosion.

Solid particle erosion for SiC ceramics is reported to occur by elastic-plastic deformation based microfracture followed by subsurface crack formation beneath the plastic zone. Size and type of cracks are found to dependent on erodent shape and size, mass flow rate, velocity and angle of impingement of erodent, temperature, hardness toughness and microstructure of target materials. In case of low

velocities of erodent, dependent on shape of the erodent, two types of cracks were generally reported. On impact of blunt erodent, generation of cone cracks are observed whereas lateral and/or median cracks are generated beneath the plastically deformed surface against sharp erodent. For high velocities impact of erodent, material removal from target surface is removed by plowing, severe cracking and chipping. Erosion wear of SiC based composites was also dependent on the characteristics of second phase such as geometry, durability, energy dissipation etc. During erosion, SiC fiber reinforced SiC composites initially detached out of matrix which further left pores and then resulted in easy removal of SiC ceramics. Shape, size and size distribution of erodent particles influence erosion of SiC ceramic composites.

An incorporation of tungsten carbide (WC) in SiC ceramics has received much less attention. Improved wear resistance is expected by adding tough and strong WC in the hard SiC matrix. The successful densification of SiC-WC composites at a temperature as low as 1800^{o}C through liquid-phase sintering [Sharma 2014] increased interest in structural and tribological properties liquid-phase sintered SiC-WC composites. Until now only ambient temperature erosion wear behavior of hot pressed SiC-WC composites is reported by our group [Sharma 2014]. It was found that the SiC ceramics containing 30 wt% WC exhibited better erosion resistance when eroded by SiC or alumina particles. The erosion wear was found maximum at normal incidence of erodent particles. No other literature has been reported on the study of tribological behaviour of this novel SiC-WC composites.

Owing to the expected use of SiC-WC composites in applications like ball bearings, nozzles, heat exchanger tubes, etc. their performance potential under sliding and erosion wear conditions is systematically investigated in the present doctoral thesis work. The dominant material removal mechanisms in the selected wear conditions are particularly elucidated as function of WC composition and applied sliding load.

CHAPTER 3

Experimental Technique

In this chapter, experimental techniques used for tribological characterization of novel SiC-WC composites are mentioned. First, details about material compositions and their processing is provided. This is followed by details of microstructural and mechanical behaviour of the composites. Major techniques to understand the tribological behavior of the composites are explained in detail. Finally, details about techniques to characterization and analyses of worn surface are also provided.

3.1. Materials

Dense silicon carbide ceramic composites used in the present study were prepared by hot pressing mixtures of SiC and WC powders (0, 10, 30 or 50 wt%) at 1800°C for 1 h under 40 MPa of pressure in an argon atmosphere. Al_2O_3, Y_2O_3 and CaO were used as sintering additives. The batch composition and sintered density of the composites are shown in **Table 3.1.**

Table 3.1. Sample designation, batch composition, and sintered density of the investigated powder mixtures.

Sample designation	Batch composition (wt %)						Sintered density (g/cc)
	β-SiC	α-SiC	WC	Al_2O_3	Y_2O_3	CaO	
SW0	94.05	0.95	0	3.5	1.0	0.879	3.23
SW10	84.15	0.85	10	3.5	1.0	0.879	3.51
SW30	64.35	0.65	30	3.5	1.0	0.879	4.31
SW50	44.55	0.45	50	3.5	1.0	0.879	5.45

The sintered sample surfaces were polished to obtain an arithmetic average surface roughness (R_a) of 30 – 70 nm. Surface roughness characteristics of polished surfaces were studied using AFM analysis (NT-MDT NTEGRA, Moscow, Russia). **Figure 3.1.** shows a typical AFM image of a polished surface of SiC (0 wt% WC) ceramics.

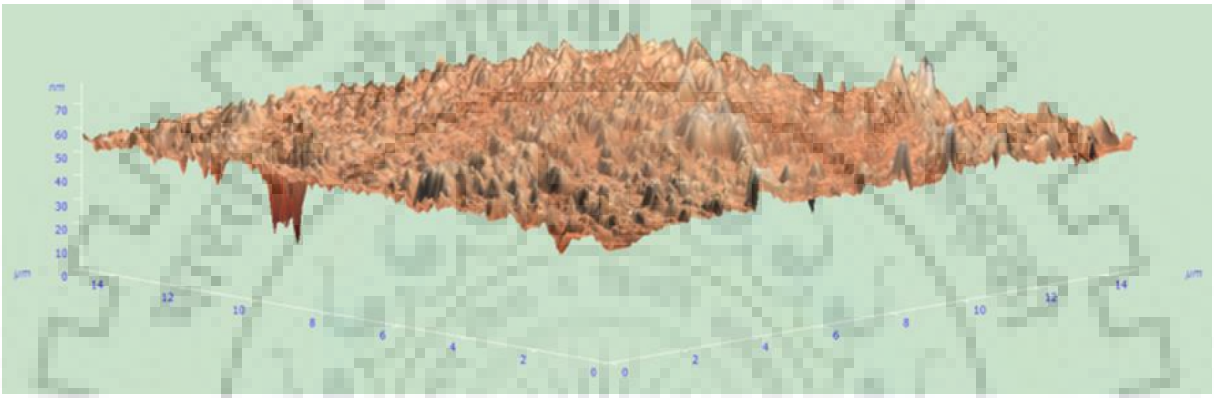

Fig.3.1. Three-dimensional profiles of polished SiC ceramics.

Scanning electron microscopy (SEM) was used to observe the etched or fractured surfaces. Typical microstructures of etched and fractured SiC specimens prepared with 0, 10, 30 and 50 wt% WC particles are shown in **Figure 3.2** and **3.3**. Etched microstructures exhibited a reduction in the average size of the near equi-axed SiC grains from 835 to 578 µm with 50 wt% WC addition. Fractured surfaces demonstrated the domination of transgranular fracture with WC addition to SiC ceramics. Hardness and fracture toughness values of sintered composites are provided in **Table 3.2**. The hardness of sintered composites varied from 24.0 GPa to 26.3 GPa, whereas the fracture toughness varied from 5.85 MPa.$m^{1/2}$ to 6.66 MPa.$m^{1/2}$ with WC addition. The fracture toughness increased to a maximum when 50 wt% WC was added, whereas the maximum hardness of 26.3 GPa obtained for SiC-30 wt% WC composites. Since the present thesis is focused on characterization of SiC-WC composites when subjected to complex tribological conditions, only brief details of sintering, microstructures and mechanical properties are provided. Complete details are provided in [Sharma 2014].

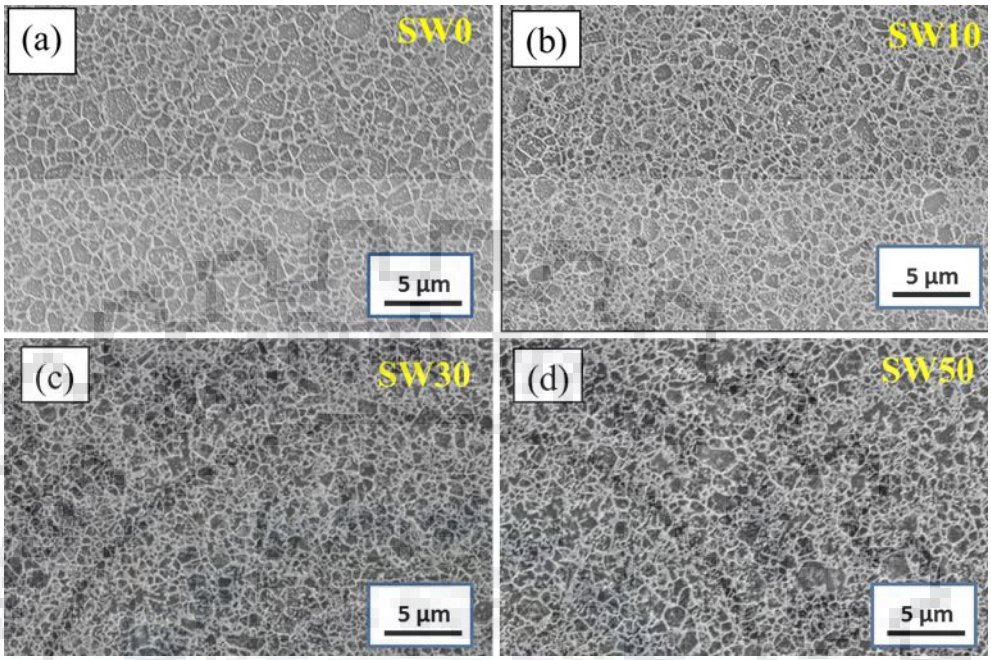

Figure 3.2. Typical SEM images of etched surfaces of SiC ceramics prepared with (a) 0% WC, (b) 10% WC, (c) 30% WC, and (d) 50% WC.

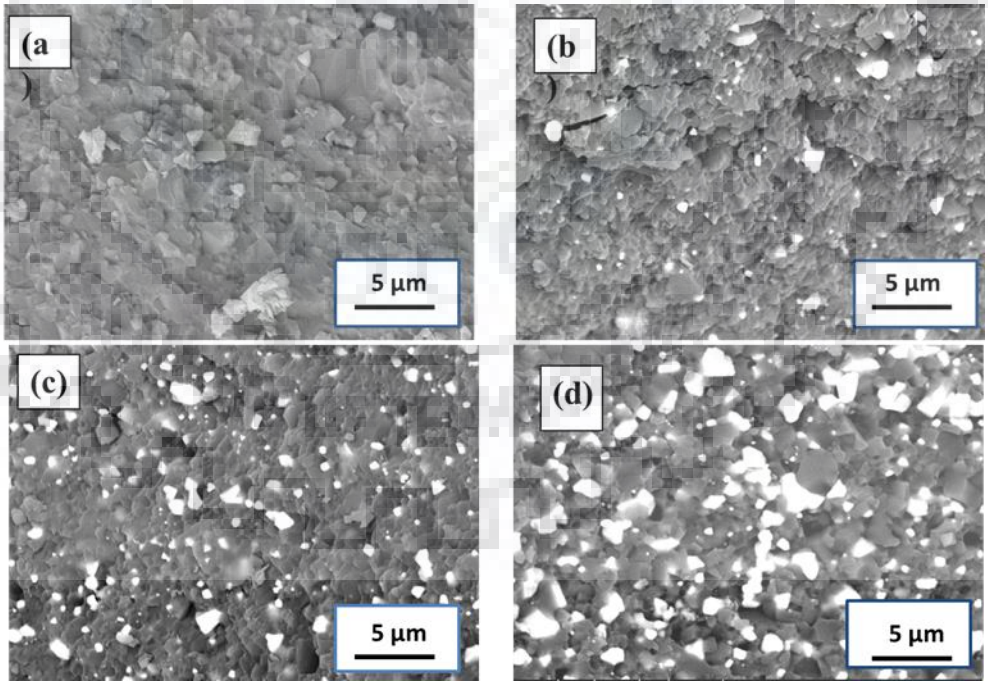

Figure 3.3. SEM images of fractured surfaces of SiC ceramics sintered with (a) 0% WC, (b) 10% WC, (c) 30%WC, and (d) 50% WC.

Table3.2. Sintered density, hardness and fracture toughness of the investigated SiC-WC composites.

WC (wt%)	**Sintered density (g/cc)**	**Hardness (GPa)**	**Fracture toughness ($MPa.m^{1/2}$)**
0	3.23	23.95±0.97	5.85±0.30
10	3.51	24.02±1.12	6.36±0.22
30	4.31	26.33±0.71	6.47±0.13
50	5.45	24.26±1.12	6.66±0.12

3.2. Pre-Wear Characterization:

Sintered SiC-WC composites were analyzed for initial surface treatment and characteristics before subjected to tribological performance tests. The surfaces of the sintered SiC-WC composites will be prepared using standard techniques involving polishing with successively finer grades of emery papers and diamond suspensions (Buehler PlanarMet 300, India) on auto polisher. The sample surfaces were polished to obtain an arithmetic average surface roughness (R_a) of 20-70 nm. Surface roughness characteristics of polished surfaces were studied using Stylus profilometer or AFM analysis (NT-MDT NTEGRA, Moscow, Russia).

3.3. Wear Testing:

A systematic wear tests were executed to understand the complete tribological potential of novel SiC-WC composites. Influences of applied normal load, counterbody, temperature and angle of impingement on friction and wear behavior of the composites were explored. Basically tribological behavior were executed in three distinct wear conditions: (1) Continuous sliding, (2) Reciprocated sliding (3) Solid particle erosion.

3.3.1. Continuous Sliding Wear Tests:

The friction and wear behavior of monolithic SiC and SiC-WC composite disks in continuous sliding wear conditions was studied against commercially available SiC (SBB Tech. Co., Suwon,

Korea), WC and steel (bearing grade AISI 52100) balls of 6.35, 10 and 6.35 mm diameter respectively. The frictional force was continuously recorded using an electronic sensor to generate a real time coefficient of friction (COF). Tests were performed using a ball-on-disk tribometer (TR-201E-M2, DUCOM, Bangalore, India). A photograph of tribometer is shown in **Figure 3.4**.

Figure 3.4. Ball-on-disk tribometer used to perform continuous sliding wear test.

As per the information from manufacturer hardness of the balls were 28, 14 and 7 GPa for SiC, WC and steel ball respectively. Before tribological testing, both disk samples and balls were cleaned using acetone in an ultrasonic bath for 15 minutes, followed by drying in a hot air stream. The balls was kept stationary under the applied load to make a track radius of 6 mm, while the disk was rotated at 500 rpm (a linear speed of 0.16 m/s) for 30 min (total sliding distance of 283 m). Sliding wear tests were done in ambient conditions (27 ±5^{o}C and 40 ±10% RH) at three loads: 5, 10 and 20 N. The maximum (initial) Hertzian contact stresses varied between 1.07 GPa and 1.85 GPa with applied load and reinforced WC

content in SiC. The frictional force was continuously recorded using an electronic sensor to generate a real time coefficient of friction (COF). The surface profiles of worn disk samples were studied to determine the depth and width of wear scars using a profilometer (SJ 400, Mitutoyo, Japan).

At least 10 orthogonal measurements per track and three tracks for each composition were made to obtain average values of width and depth of wear scars. Results of width and depth were used for quantification of the extent of volumetric wear damage in the disk. Further, the estimated wear volume of the disk was divided by the applied load and total sliding distance, and is reported as a specific wear rate. The average of the wear rate and the coefficient of friction data are reported after conducting at least three sliding experiments.

3.3.2. Reciprocated Sliding Wear Test:

The friction and wear characteristics of SiC-WC composites were studied against SiC counterbody using a ball-on-disk tribometer (shown in **Figure 3.5**). The tribometer had stationary base with sample holder system on it. The upper part of the holder was connected with oscillating motion mechanism to hold ball and equipped with a load cell.

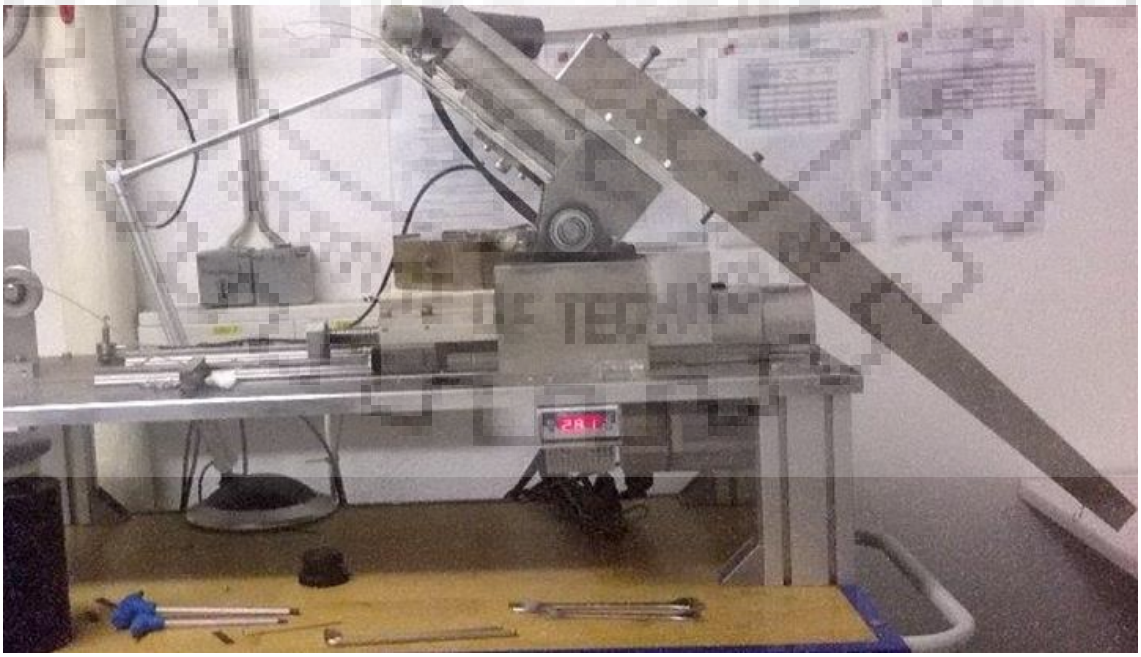

Figure 3.5. Ball-on-disk tribometer to perform reciprocated sliding wear test.

All the tests were performed against SiC ball (Ra ~8 nm, and hardness of 28 GPa, as claimed by the manufacturer SBB Tech. Co., Suwon, Korea) of diameter 6.35 mm Frequency for the test was maintained at 8.3 Hz with a stroke of 4.71 mm (speed ≈ 78 mm/s) for 1000 cycles. Control experiments were conducted for SiC ceramics at 6, 9.3 or 19.3 N to understand the effect of load on friction and wear behavior in ambient conditions (28±2^{o}C and 55±5% RH), while the effect of (10, 30 or 50 wt%) WC content on sliding wear behavior of SiC-WC composites at 19.3 N load was systematically studied in both ambient and elevated temperature (500^{o}C) conditions. At least three experiments were performed for determining the average coefficient of friction (COF) for each combination of composition, load and temperature. An optical profilometer (Contour GT-k0. Bruker, USA) was used for three dimensional analysis of wear scar to determine depth and width of wear scar. Wear volume was further calculated using wear scar depth and width.

3.3.3. Solid particle erosion wear test:

Erosion tests were performed using an air jet erosion machine equipped with furnace to heat up the sample surface. Silicon carbide erodent particles of 40-70 µm in size were dried in an oven at 100^{o}C for 1 h and were mixed with air. The mixed air jet passed through a WC nozzle of 3 mm diameter and were subjected to erode the polished surface of the composite at a stand-off distance of 10 mm. Air pressure was controlled to maintain the particle velocity at 47 m/sec with a flow rate of 3 g/min. Erosion tests were done at 800^{o}C temperature with different angles of impingement: 30, 60, and 90^{o}. High temperature erosion tester (TR-201E-M2, DUCOM, Bangalore, India) is shown in **Figure 3.6**.

The weight loss of the sintered ceramics was measured to an accuracy of ±0.1 mg after 15 min of erosion. The test was continued considering a steady state weight loss for the composites on the basis of our previous investigation [Sharma 2014]**.** The average weight loss in steady state was converted to average volume loss and steady state erosion rate E in mm^3/kg was determined as per the following:

$$E = \frac{V}{M} \quad \text{.....(3.1)}$$

where V is volume of the material removed in steady state in mm^3 and the M is the mass of the erodent particles used in steady state in kg.

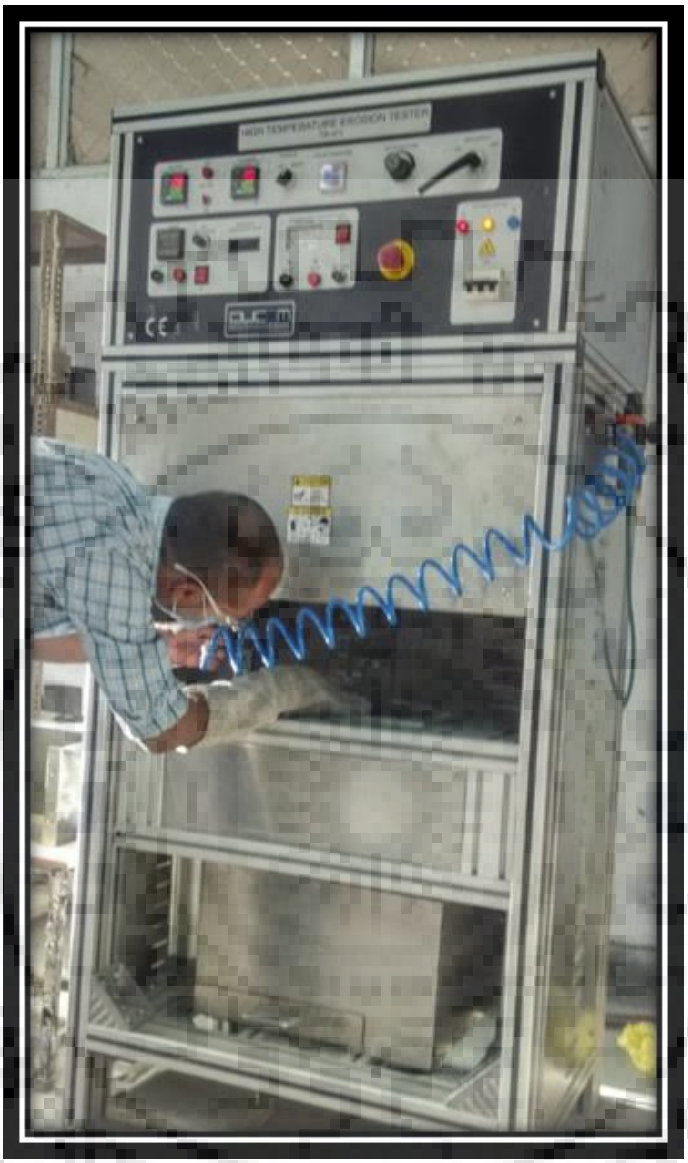

Figure 3.6. High temperature solid particle erosion tester**.**

The erosion results were checked for the reproducibility by conducting whole experiment at least twice for each composition and angle of impingement. Material removal mechanisms were elucidated using SEM-energy dispersive spectroscopy (EDS) (ULTRA plus, Carl Zeiss, Germany) analysis of eroded surfaces.

3.4. Post-wear characterization:

The surface profiles of worn disk samples were were studied to determine the depth and width of wear scars using profilometer. Further the worn surfaces of the SiC-WC composites were examined to identify the dominant mechanisms of material removal using scanning electron microscopy (SEM)/Energy dispersive spectroscopy (EDS), FIB (JEOL JSM-7600F), X-ray diffraction (XRD), TEM (JEOL-2100F; Tokyo, Japan).

3.4.1. Surface profilometery:

The surface roughness were estimated for both unworn and worn surfaces using surface profilometer. The surface profiles were used to measure the depth and width of wear tracks towards estimating the volumetric loss of the materials due to wear. The measuring method involved with firstly scanning the wear depth profile across a wear track at various locations, and then determining the average of depth and width using at least 10 measured values. The average of wear track width and depth were further used in computing the wear volume according to following relation:

$$Wear\ volume = (2\pi \times Track\ radius) \times (Track\ width) \times (Track\ depth) \quad \textbf{(3.2)}$$

3.4.2. Scanning electron microscopy (SEM)/Energy dispersive spectroscopy (EDS):

Worn surfaces were examined to understand the major material removal mechanisms and defects in detail. The elemental distribution on the worn surfaces was also studied using energy dispersive X-ray spectroscopy (EDS). Also, SEM/EDS analysis was used for identifying signatures of surface changes or formation of oxide or carbide on the worn surfaces using elemental analysis.

3.4.3. X-Ray diffraction (XRD):

The phase evolution of the SiC-WC composites after wear were studied with varying WC content using XRD. The information about the possible phases were used to estimate the effect of WC reinforcement on tribological behaviour during wear of the SiC-WC composites.

3.4.4. Raman spectroscopy:

The debris particles obtained after sliding wear of SiC-WC composites against different counterbody were carefully collected. Debris collected were analyzed using Raman spectroscopy

(Renishaw invia Raman spectrometer (serial no. 021R88) equipped with argon ion laser (514 nm)) for the reaction product during sliding against different counterbody. Information of reaction product were used to understand the friction and wear behaviour of SiC-WC composites against different counterbody.

3.4.5. Specimen preparations for observation of sub-surface damages:

SEM observations in cross-section mode for the damaged zoned underneath the wear tracks were performed in dual-beam FIB/FEG-SEM (Auriga™ Compact; Carl Zeiss). Cross-section TEM specimens below the wear tracks were prepared using the same dual-beam FIB/FEG-SEM equipped with Omni probe manipulator OP-200 (Oxford Instruments). Initially, a piece of dimensions 10 x 5 x 1 µm was cut from the worn surface down to the bulk of the sample using the Ga-ion milling inside the FIB/SEM sample chamber, which was thinned down to ~80 nm thickness at 30 kV accelerating voltage and 500 pA ion bean current. The lamella was further (precision) polished at 5 kV and 20 pA current for obtaining electron transparent specimen. The TEM observations were performed in high resolution-transmission electron microscopy (HRTEM) (FEI Tecnai G2, F30-300 kV and FEI Titan G2 60 -300 TEM).

CHAPTER 4

Continuous Sliding Wear Behaviour of SiC-WC Composites

In the present chapter of the thesis, results obtained from sliding wear study of SiC-(0, 10, 30 or 50) wt% WC composites are described. Sliding was done in dry unlubricated condition against SiC (hardness: 28 GPa), WC-Co (hardness: 14 GPa) and steel ball (hardness: 7 GPa). In particular, an attempt has been made to answer the following important questions: (i) How does the load (from 5 to 20 N) effect sliding wear behaviour of SiC-ceramics against SiC, WC-Co and steel counterbodies? (ii) Is there effect of WC content on friction and wear characteristics of SiC ceramics? (iii) Does the dominant material removal mechanism of SiC ceramics changes with the addition of WC or counterbody? (iv) What is the influence of mechanical properties on the sliding wear?

4.1. Background:

It is reported that liquid phase sintered (LPS) SiC with fine or elongated grains microstructure resulted improved wear resistance [Lopez 2005; Ciudad 2013; Kovalcikova 2015]. The research results indicate a strong influence of composition (microstructure) and mechanical properties of the composites in different wear conditions. Zum-Gahr et al. [2001] estimated the tribological behaviour of SiC ceramics by oxidation reactions in the presence of oxygen and/or humidity in the surrounding atmosphere. It was also pointed out that as the humidity increased from 30 to 60%, the nature of damage in SiC ceramics changed from mechanical to tribochemical [Murthy 2004]. Formation of oxidative layer may be protective or destructive depending on nature of sliding couple materials, applied load, sliding speed etc. [Skopp 1992; Takadoum 1994]. Hsu et al. [1996] reported a change in wear mechanism from abrasion at a low speed of 1.9 mm/s and a low load of 2 N to intergranular fracture at high speed of 0.57 m/s and a high load of 360 N in air or water. Sliding couples of ceramic materials like silicon carbide, silicon nitride, alumina or zirconia exhibit high friction coefficients in unlubricated conditions [Skopp 1992]. Kovalcikova et al. [2014] studied the influence of counterpart material like Si_3N_4, Al_2O_3, ZrO_2 and WC-Co on the friction and wear behaviour of SiC ceramics. They found mechanical wear and tribochemical wear as major material removal mechanisms against any ceramic counterpart.

However, the difference in wear behaviour of SiC ceramics with the change in counterbody material type from ceramics to cermets or metals is systemically studied.

In the present work, the tribological behaviour of novel SiC-WC composites is investigated in dry sliding conditions (27 ±5°C and 40 ±10% RH) against ceramics (SiC), cermets (WC-Co) and metal (steel) counterbody. In particular, the influence of WC content (0 to 50 wt%) and counterpart material on wear mechanisms of SiC ceramics is elucidated.

4.2. Results obtained in sliding of SiC-WC composites

4.2.1. Friction results

Monolithic SiC ceramics subjected to sliding wear against different counterbody i.e. SiC, WC-Co and steel ball at 5 N, 10 N or 20N exhibited difference in frictional behavior (**Figure 4.1**).

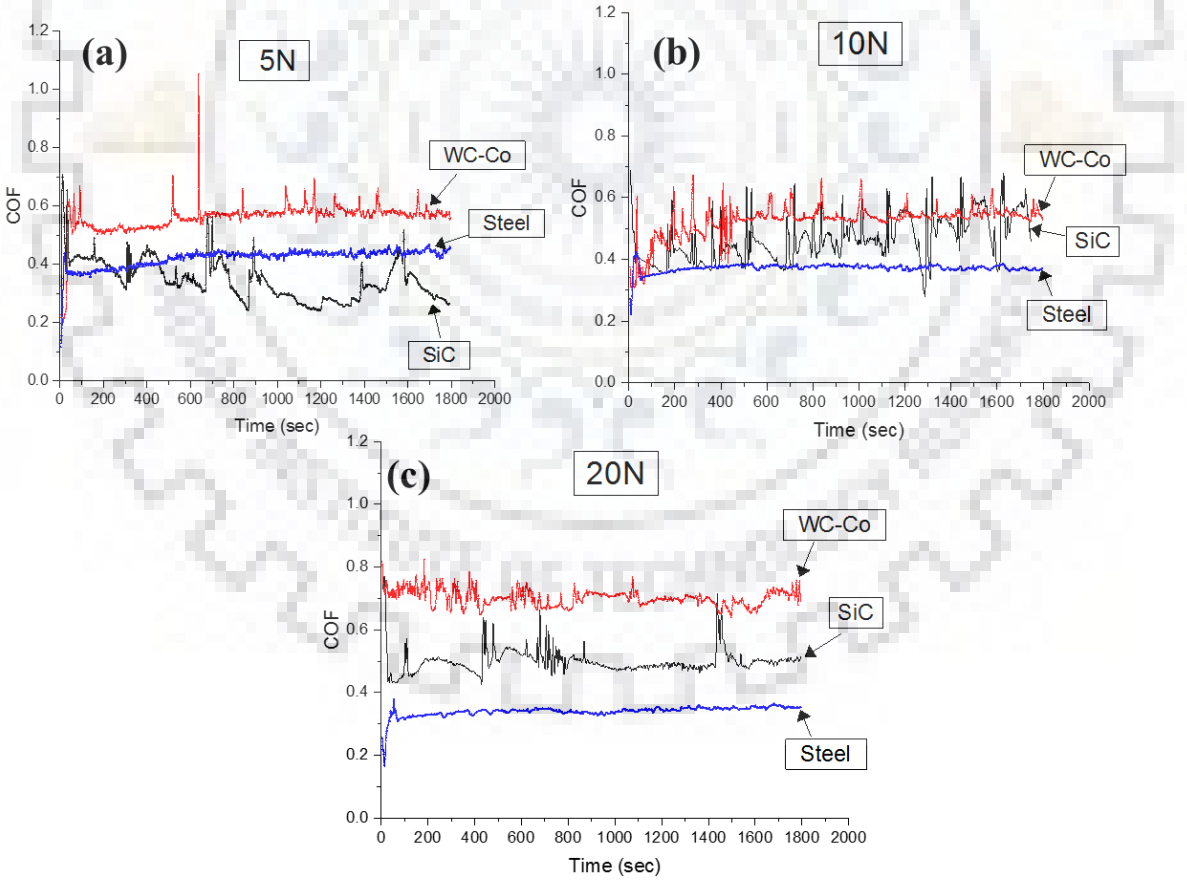

Figure 4.1. Evolution of coefficient of friction for monolithic SiC ceramics at (a) 5 N, (b) 10 N and (c) 20 N, against SiC, WC-Co and steel counterbodies.

It shows significant fluctuations in friction against SiC and WC-Co ball as compared to steel ball. Fluctuations reduced in their intensity with increase in load from 5 N to 20 N for any counterbody. Furthermore, monolithic SiC exhibited highest steady state COF value against WC-Co counterbody at any load. The difference between steady state value of COF against different counterbodies increased from 0.15 to 0.36 as load increased from 5 N to 20 N.

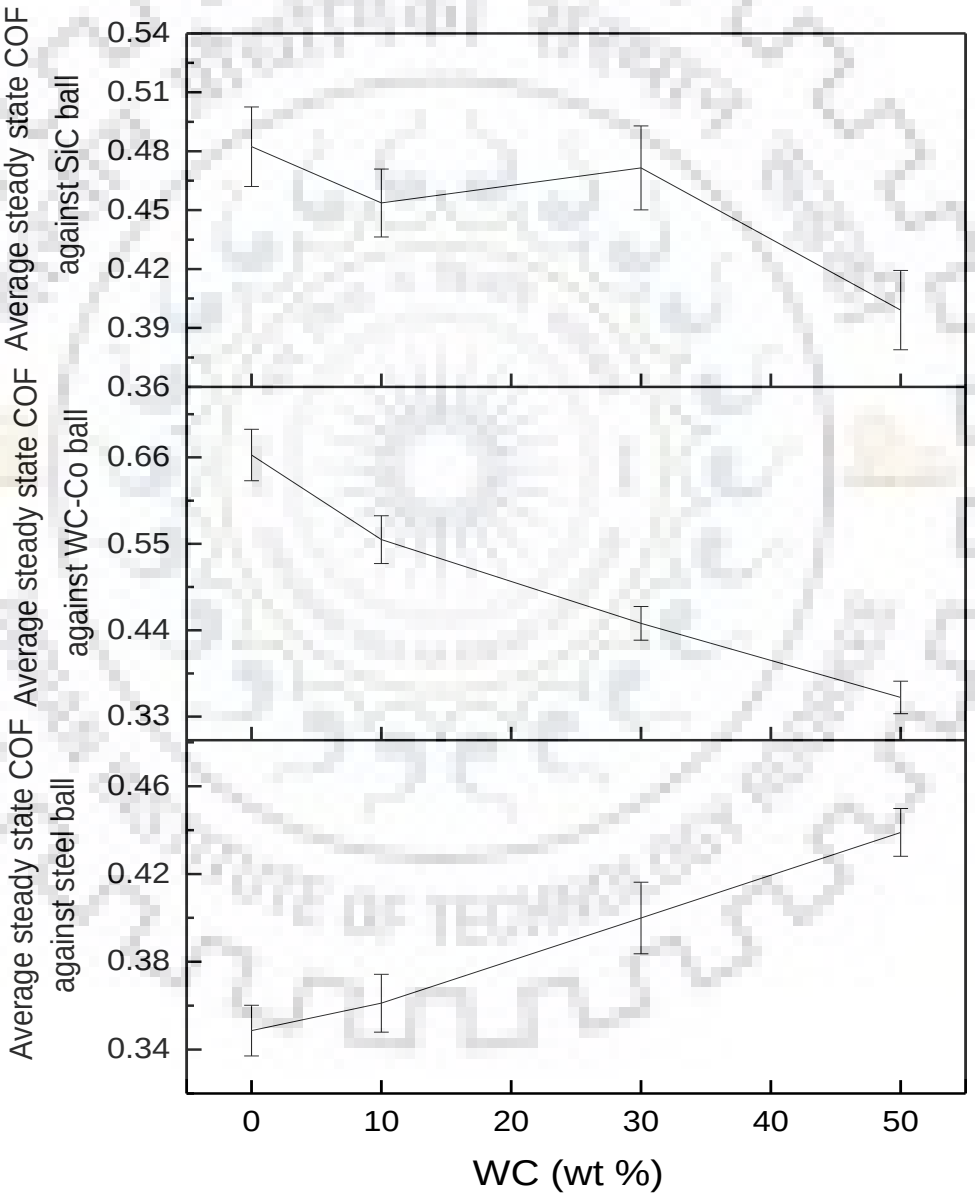

Figure 4.2. Average steady state coefficient of friction of SiC-WC composites against SiC, WC-Co and steel counterbodies at 20 N load.

Figure 4.2 shows the effect of WC content on the average steady state COF of SiC-WC composites when slid against SiC, WC-Co ball and steel ball at 20 N load. With increase in WC content average steady state COF decreased against SiC (from 0.49 to 0.39) and WC-Co (from 0.66 to 0.33) counterbody, whereas it increased against steel ball (from 0.34 to 0.43). Generally, average COF values for SiC ceramics in sliding wear are reported from 0.20 to 0.75 with different parameters and working environments [Lopez 2005a,b, 2007a,b,c; Ciudad 2012; Ortiz 2012; Gates 2004; Hsu 1996; Kato 2002]. For ceramics, high friction mainly results from mechanical wear including third body abrasion, fracture and chipping [Cranmer 1985; Zum-Gahr 2001], while less friction is attributed to the formation of hydrated silica or adhered oxide layer at the contact [Andersson 1994; Murthy 2004; Kumar 2008].

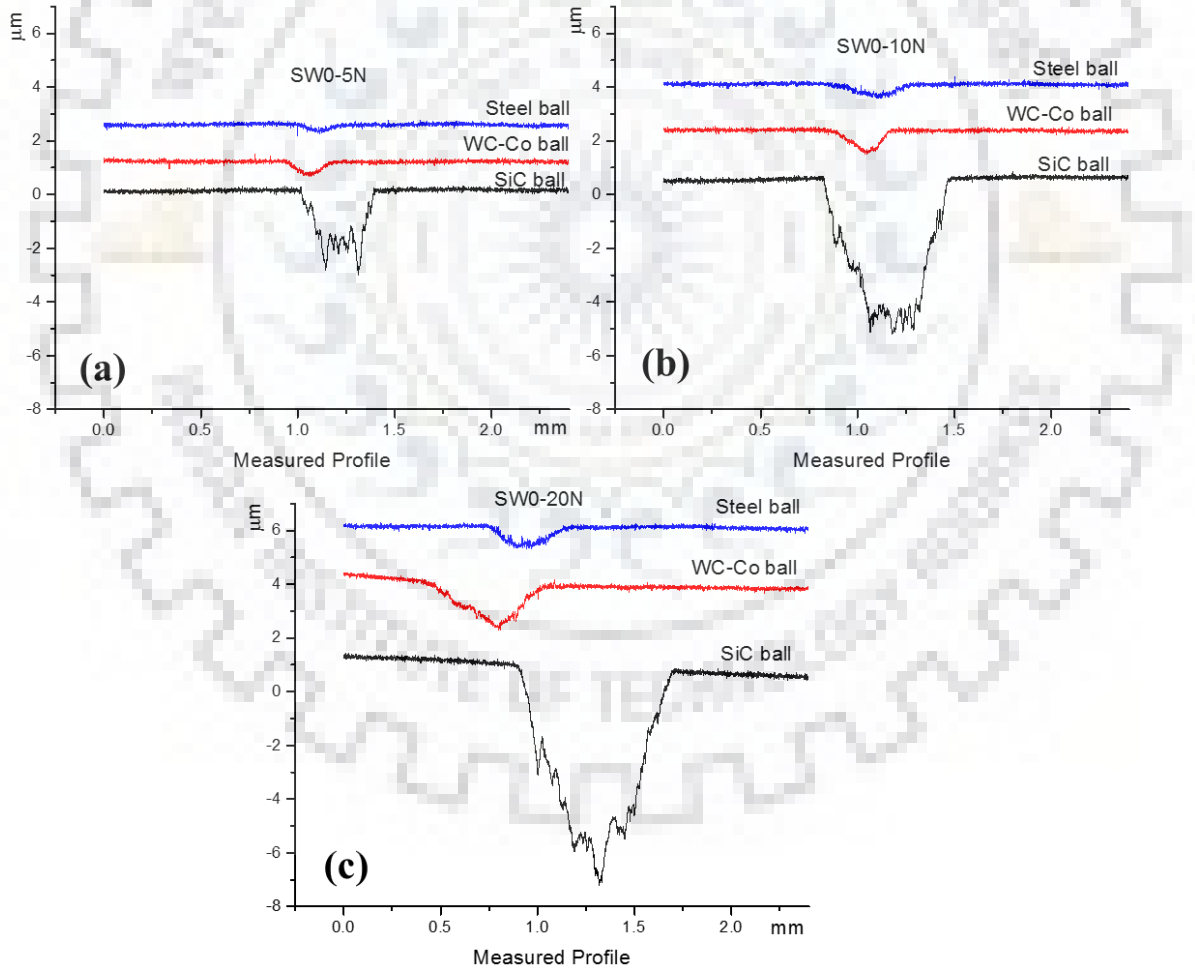

Figure 4.3. Typical surface profile of wear scar on monolithic SiC ceramics at (a) 5 N, (b) 10 N and (c) 20 N, against SiC, WC-Co and steel counterbodies.

Further, surface profiles of wear scar perpendicular to sliding direction are acquired for measuring depth and width of wear scar. Typical surface profiles of wear scars for monolithic SiC at 5, 10 and 20 N load, and SiC-WC composites at 20 N load are respectively shown in **Figures 4.3 & 4.4**. With increase in load from 5 N to 20 N, depth and width varied from 0.23 µm to 2.39 µm and from 0.18 mm to 0.86 mm, respectively. At a given load, the depth and width of the scar are significantly higher against hard SiC counterbody as compared against steel counterbody (see ***Figure 4.3***).

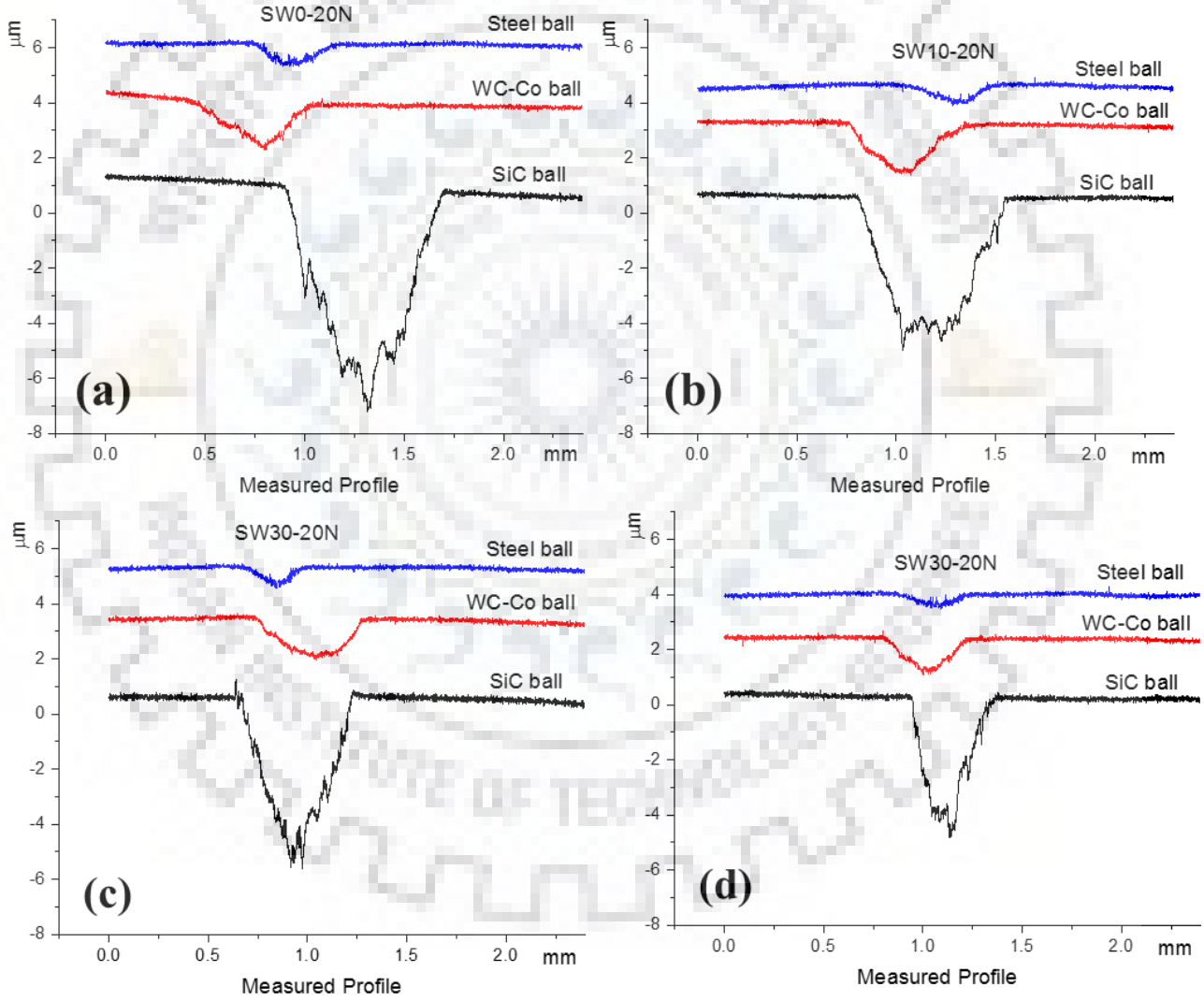

Figure 4.4. Typical surfaces profiles of wear scars against SiC, WC-Co and steel counterbodies at 20 N for SiC ceramics sintered with (a) 0, (b) 10, (c) 30 and (d) 50 wt% WC.

It is observed from **Figure 4.4** that with increased WC content in SiC-WC composites, depth and width reduced against any ball at 20 N load. With increase in WC content from 0 to 50 wt%, depth and width decrease from 0.69 µm to 0.28 µm and from 0.42 mm to 0.29 mm, respectively against steel ball. Depth and width decreased from 1.53 µm to 1.18 µm, and from 0.60 mm to 0.40 mm with increase in WC content against WC-Co ball. Depth and width decreased from 7.08 µm to 3.13 µm and from 0.86 mm to 0.42 against SiC ball with the increase in WC content from 0 to 50 wt% in SiC ceramics. It is clear from the **Figures 4.3 & 4.4** that maximum value of width or depth obtained against SiC ball are independent of load applied and WC content. Therefore, the depth and width of wear scars obtained during sliding wear of the SiC ceramics are significantly influenced by hardness or type of the counterbody.

4.2.2. Wear results:

The wear volume of SiC ceramics against SiC, WC-Co and steel ball at 5 N, 10 N and 20 N load is plotted in **Figure 4.5**. In general, wear volume increased with increase in applied load against any counterbody. It shows continuous increase in wear volume with the change of counterbody hardness from 7 GPa (steel ball) to 28 GPa (SiC ball). SiC ceramics exhibited approximately 5-10 times more wear against SiC counterbody as compared to against WC-Co counterbody. Further, approximately 5-10 times more wear against WC-Co counterbody as compared to against steel counterbody. The wear volume of SiC ceramics varied between 5.9×10^{-4} mm^3 and 8.5×10^{-2} mm^3 with change of load or counterbody. Against WC-Co ball, one order of magnitude increase in wear volume from 5.4×10^{-3} mm^3 to 1.7×10^{-2} mm^3 is observed with increased load. Similarly against steel ball, one order of magnitude increase in wear volume from 5.9×10^{-4} mm^3 to 4.7×10^{-3} mm^3 is obtained with increase in load from 5 N to 20 N. It is also observed that SiC ceramics resulted in maximum wear at 20 N load against any counterbody. Therefore, SiC-WC composites are investigated only at 20 N load to understand the effect of WC content on sliding wear behaviour against different counterbodies.

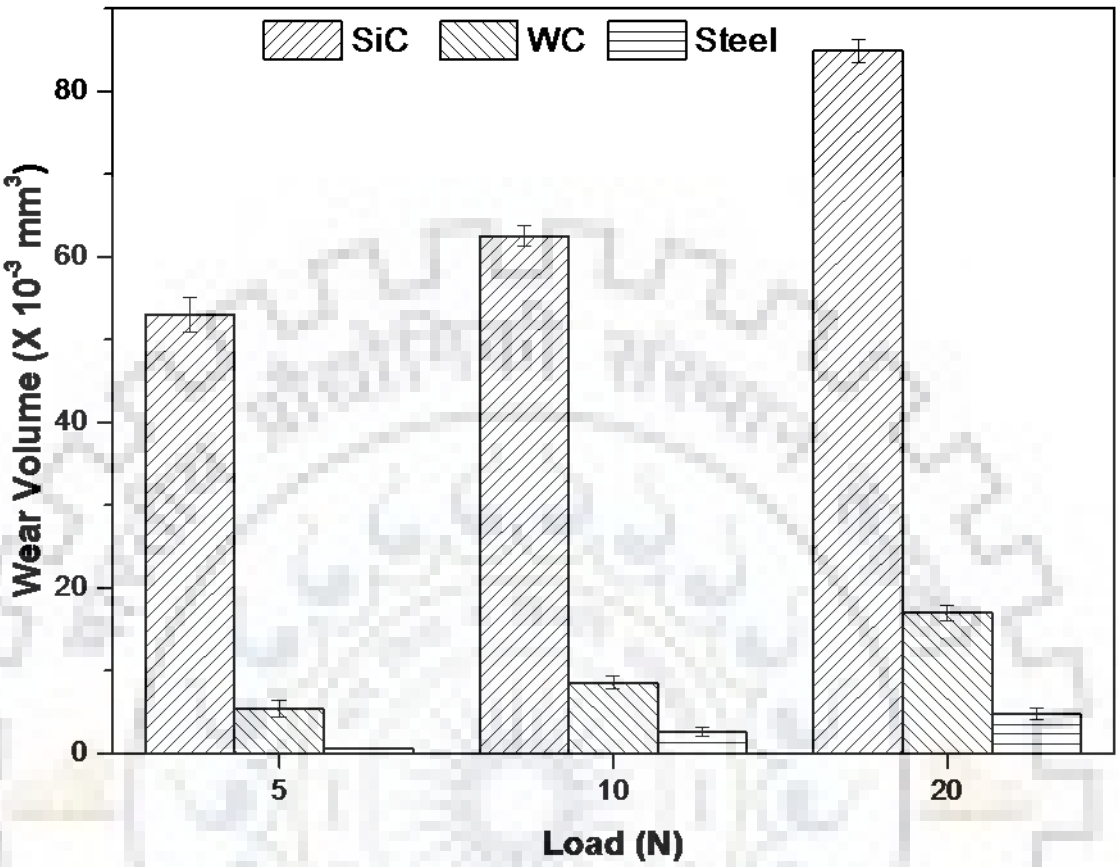

Figure 4.5. Wear volume of SiC ceramics as function of load against SiC, WC-Co and steel counterbodies.

Figure 4.6 shows wear volume of SiC-WC composites as function of WC content against SiC, WC-Co and steel counterbodies at 20 N. Lowest wear volume is obtained for SiC ceramics reinforced with 50 wt% WC against steel ball. SiC ceramics reinforced with large amount of WC exhibit higher fracture toughness led to less mechanical fracture or grain pull-out during sliding wear. With increase in WC content from 10 to 50 wt%, wear volume decreased from 5.2 X 10^{-2} mm^3 to 2.3 X 10^{-2} mm^3 against SiC ball. Wear volume decreased with one order of magnitude from 1.2 X 10^{-2} mm^3 to 5.7 X 10^{-3} mm^3 against WC-Co ball, while a slight change in wear volume from 4.7 X 10^{-3} mm^3 to 2.0 X 10^{-3} mm^3 is observed against steel ball.

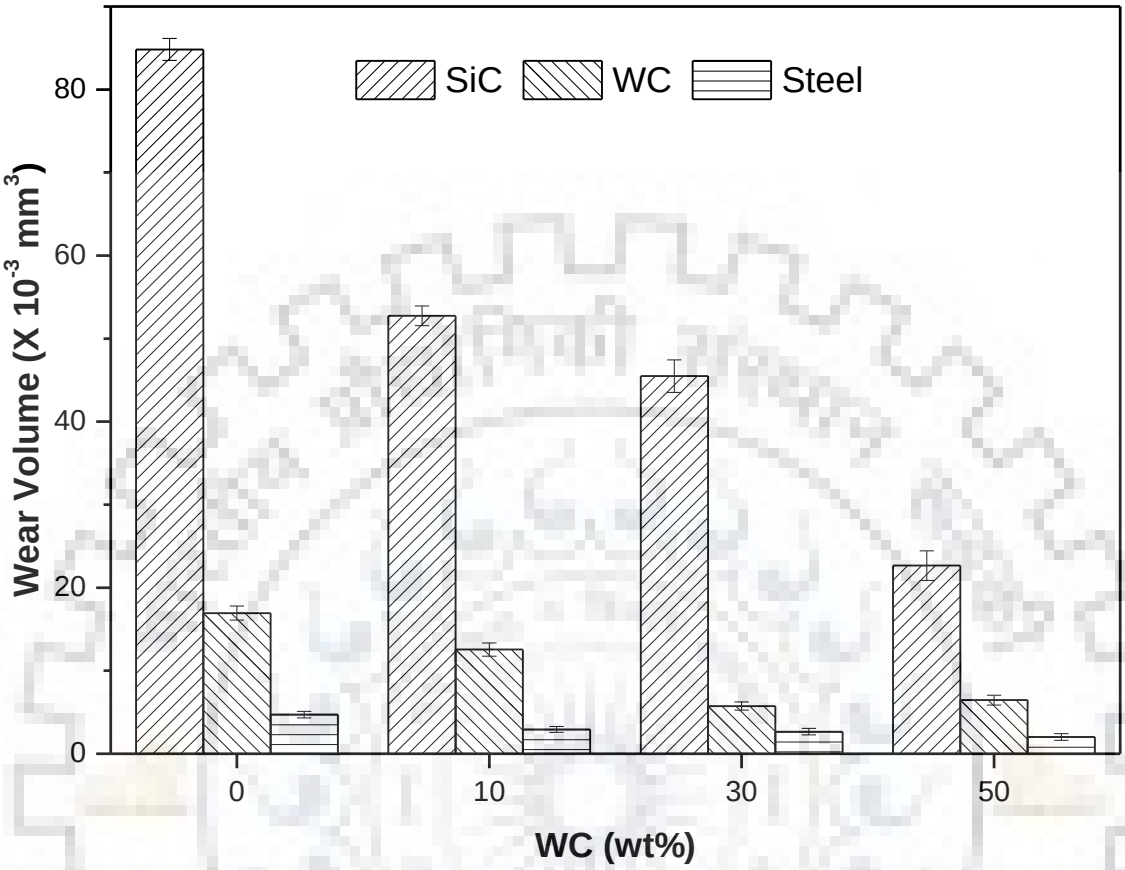

Figure 4.6. Wear volume of SiC-WC composites against SiC, WC-Co and steel counterbodies at 20 N load as function of WC content.

4.2.3. Worn surface analysis:

Typical SEM images of SiC ceramics worn at 5, 10 and 20 N against SiC, WC-Co and steel ball are shown in **Figure 4.7**. It is observed that material removal mechanisms against SiC ball are mainly abrasion, mechanical fracture and grain pull-out. Increased extent of mechanical fracture observed on disk surfaces with increase in load from 5 N to 20 N against SiC ball (***Figures 4.7a to 4.7c***). Against WC-Co ball, extent of abrasion and retained debris on disk surfaces increased with load. In case of steel counterbody, abrasion and retained debris are dominant on worn disk surface of SiC ceramics at low load of 5 N, while surface polishing and suppression of retained debris are observed at high load of 20 N. The EDS analysis of worn surfaces reveales the presence of oxygen along with elements from disk or counterbody (***Figures 4.7j, k & l***).

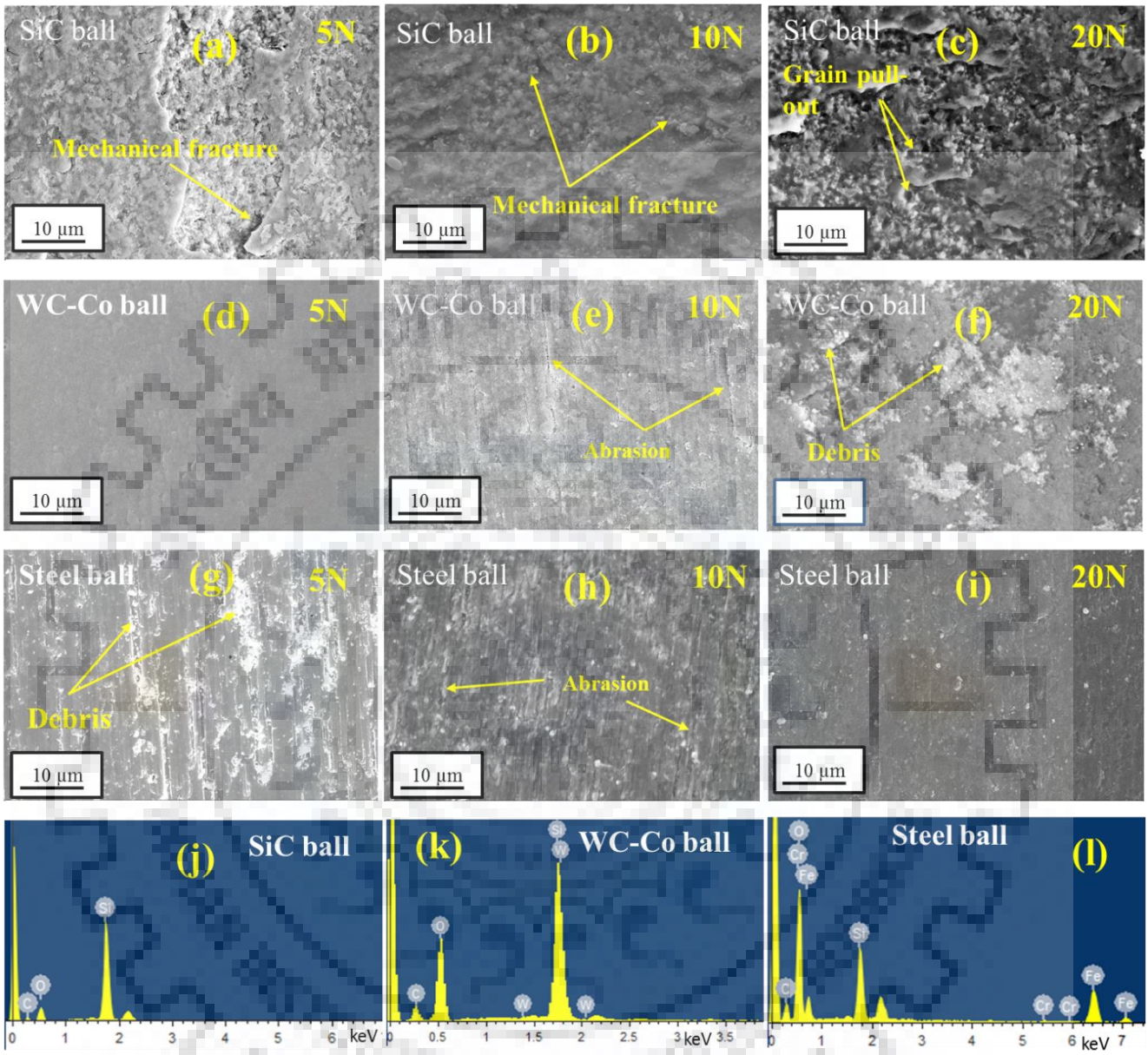

Figure 4.7. SEM images of worn surfaces of SiC ceramics against SiC, WC-Co and steel counterbodies at 5 N, 10 N and 20 N load. EDS analysis of worn surface at 20 N against SiC, WC-Co and steel ball (j, k and l).

Figure 4.8 shows typical SiC-WC composites surfaces worn against SiC, WC-Co and steel counterbodies at 20 N load as function of WC content. Since WC reinforcement led to increase in fracture toughness of the SiC ceramics, the mechanical fracture and grain pull-out from the disk surfaces are decreased when slid against SiC ball. Removal of WC particles from the disk surfaces due

to penetration of SiC ball in disk surfaces cause large amount of material loss in case of SiC ceramics with large amount of WC content. As fracture toughness increases, ball penetration into the disk surfaces decreased with the increase in WC content in SiC ceramics, which led to decrease in fracture (***Figures 4.8a to c***). In case of WC-Co counterbody, significant abrasion and WC particles or retained debris are observed on worn surface of SiC-10 wt % WC composite, while the worn surface is covered with a thick layer in SiC-30 wt% WC and SiC-50 wt% WC composites (***Figures 4.8d to f***). In case of sliding against steel ball, worn surface of SiC-10 wt % WC composite is rough with fracture surface and abrasion, while the reduced fracture and abrasion are observed on SiC-50 wt% WC composite worn surface (***Figures 4.8g to i***). The presence of layer is not observed on the composite surface worn against steel.

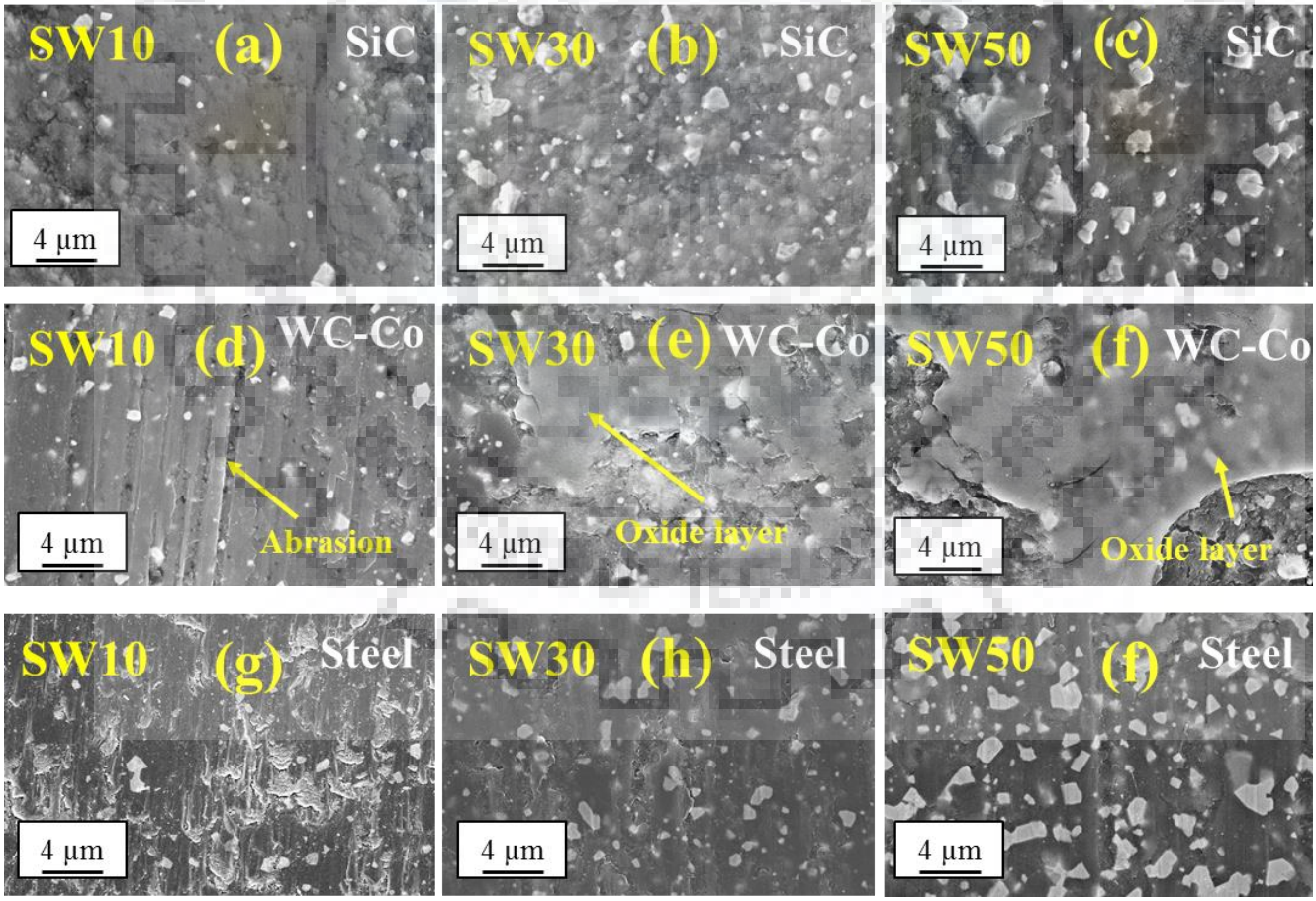

Figure 4.8. SEM images of worn surfaces of SiC-WC composites against SiC, WC-Co and steel counterbodies at 20 N load.

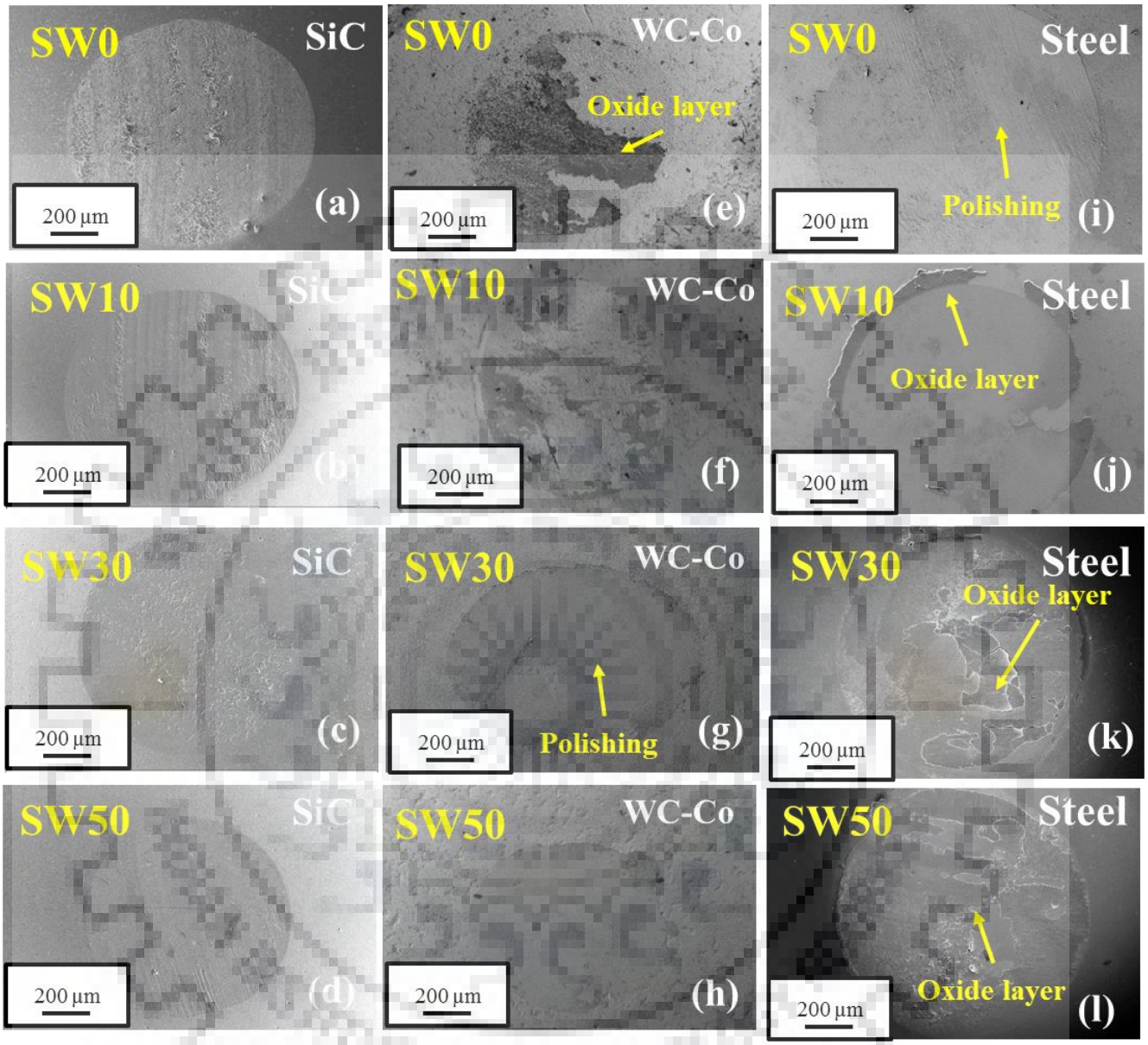

Figure 4.9. Typical worn surfaces of counterbody (SiC, WC and steel ball) slid against SiC-WC composites at 20 N load.

Material removal mechanisms are further understood by observing surfaces of counterbody balls (***Figure 4.9***) worn against SiC-WC composites at 20 N. Worn surfaces show mainly abrasion and pits as material removal mechanisms for SiC ball counterbody, whereas polishing and adhered layer removal for WC-Co or steel ball. Strongly adhered layer is observed on the WC-Co ball surfaces with the increased content of WC in SiC-WC composites. Against monolithic SiC ceramics, the surface of

steel ball is completely polished (***Figure 4.9i***) but, loosely adhered layers are also observed on ball surfaces with increased WC content in SiC-WC composites (***Figures 4.9 k & l***). Owing to less fracture and penetration with increased WC content in SiC ceramics, the scar diameter decreased for any counterbody.

4.2.4. Debris analysis:

SEM images of debris collected after wear of SiC-WC composites against SiC, WC-Co and steel balls are shown in **Figure 4.10**. In general, debris size reduced with increase in WC content. This can be attributed to the reduced grain size of the SiC-WC composites with increased WC content.

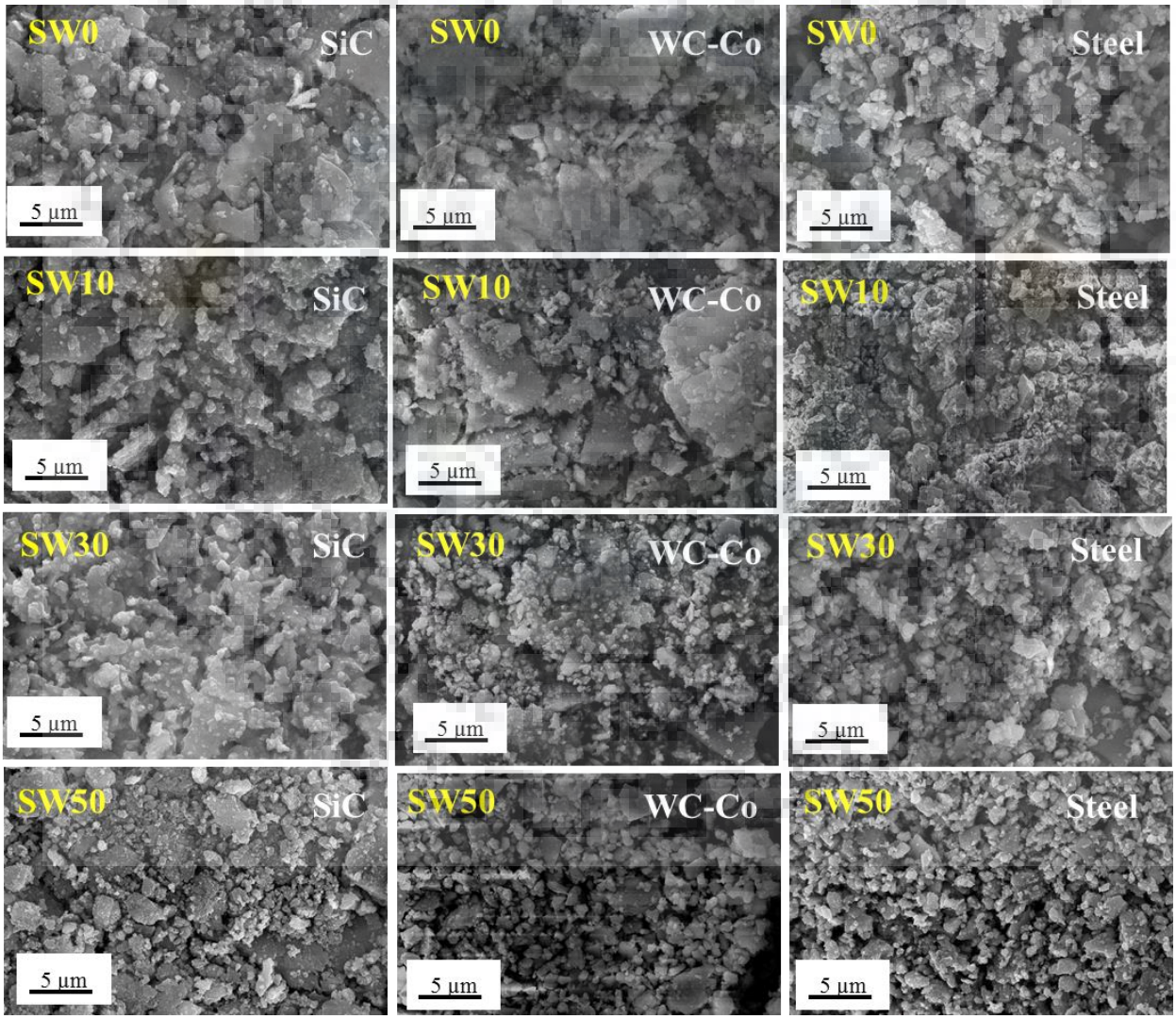

Figure 4.10. SEM images of debris collected after wear of SiC-WC composites against SiC, WC-Co and steel counterbodies at 20 N load.

Figure 4.11 shows Raman spectroscopy analysis of debris particles collected after sliding of SiC-50 wt% WC composite against SiC, WC-Co or steel ball. It validated the formation of silicon oxide [Cortes 2015], tungsten oxide [Luo 2013] and cobalt tungsten oxide [Anspoks 2014] when SiC-WC composites slid against SiC or WC-Co counterbody. In addition, it also supported the formation of iron oxide [Zhang 2013] and iron tungsten oxide [Qian 2014] when SiC-WC composites slid against steel ball.

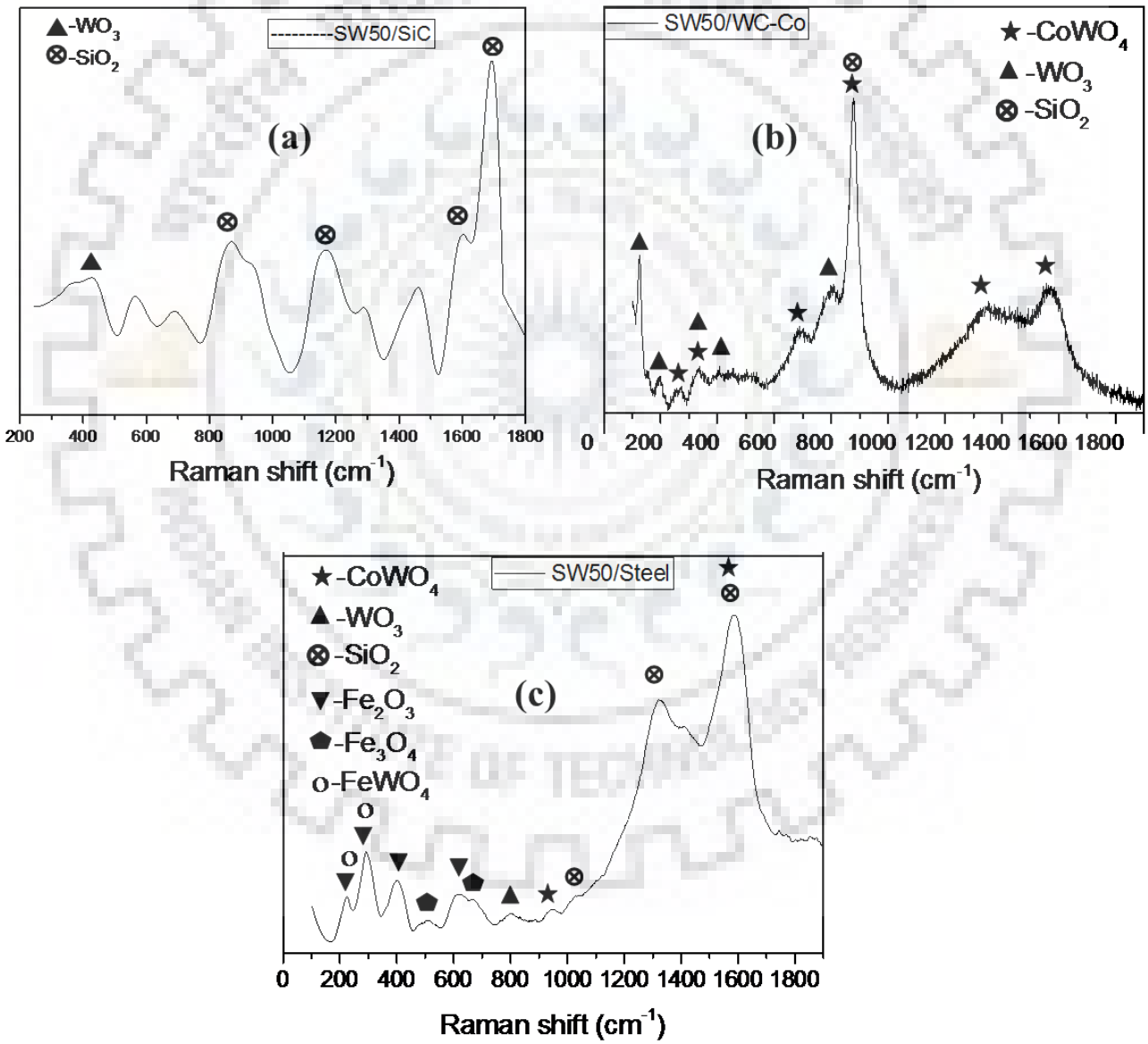

Figure 4.11. Raman spectroscopy analysis of debris collected after sliding wear of SW50 composites against SiC, WC-Co and steel counterbodies.

4.3. Discussion

In this section, phenomenological understanding on the effect of counterbody on frictional and wear behavior of SiC-WC composites as function of WC content is provided. This is followed by the discussion on dominant mechanisms of material removal as function of counterbody and WC content. Also, a short note on the effect of mechanical properties on the wear behavior of SiC-WC composites against different counterbody is provided.

4.3.1. Effect of counterbody on friction and wear behaviour

Fluctuations in friction for monolithic SiC ceramics increased with load when slid against SiC or WC-Co ball (see ***Figures 4.1***) owing to increased mechanical fracture or third body abrasion. Against steel ball, fluctuation reduced with increased load as iron oxide debris particles are suppressed at higher load. SiC ceramics exhibited highest average COF against WC-Co ball and lowest against steel ball at any load. Average steady state COF against SiC counterbody lied in between the value obtained against WC-Co and steel. It was reported earlier that ceramics with dissimilar sliding pairs exhibit different frictional behavior due to difference in the ionic potential of oxides formed between mating surfaces in dry sliding conditions. The tendency for oxide layer formation is large at high sliding load due to friction induced high temperature at the sliding contact [Kumar 2007 & 2008].

In case of composites, reduced fracture with high WC content led to reduced tendency for the formation of hard oxides, leading to less friction [Kovalcikova 2014]. It is also well reported [Rice 1985; Zum-Gahr 1989 &1993] that plastic deformation and transgranular fracture of individual grains are pronounced in microstructures containing fine grains and result in small size debris. The small size debris particles are compressed and plastically deformed into layers in sliding contact and hence led to less friction and wear. Accordingly fine grains resulted fine debris size for SiC-WC composites with large amount of WC content. Also fine debris particles are more prone to get connected to each other in hydrated environment and form layers adherent to the material surface [Zum-Gahr 2001]. Strongly adhered layers resulted in less friction and protected the underneath material from wear. Thus fine grain SiC-WC composites exhibited lowest friction against SiC or WC-Co ball as compared to coarse grained monolithic SiC ceramics.

On the other hand increased friction obtained for SiC-WC/steel system contradicts to reduction in friction with finer grains. This can be understood as per the following: During sliding against steel

counterbody, formation of hard iron tungsten oxide ($FeWO_4$) is expected with increased WC content as per the following reactions:

$$2Fe + O_2 \rightarrow 2FeO \quad \text{---------- (4.1)}$$

$$FeO + WO_3 \rightarrow FeWO_4 \quad \text{---------- (4.2)}$$

The above mentioned reactions are thermodynamically feasible ($\Delta G < 0$) in the 273-973 K range. Formation of hard $FeWO_4$ and loosely bonded iron oxide with WC content participated as third body between the mating surfaces and resulted in high friction during sliding (see ***Figures 4.10 & 4.11***). So, it is worth to note that COF is independent of hardness of counterbody.

In general, wear rates for SiC ceramics in sliding conditions are reported to vary in the order of 10^{-7}-10^{-4} $mm^3/N.m$ [Cranmer 1985; Dong 1995; Zum-Gahr 2001; Murthy 2004; Jordi 2004; Udayakumar 2011]. In the present study, coarse grain SiC ceramics resulted in highest wear against any counterbody at 20 N load. Higher fracture toughness of SiC-WC composites led to reduction in mechanical fracture and grain pull-out, causing reduction in wear volume against SiC counterbody. Wear of disk surface reduced for fine grain SiC-WC composites with less fracture and formation of protective tribolayer on the disk or ball surface during sliding against WC-Co or steel counterbody (see ***Figures 4.10 & 4.11***). The stability of adhered layers also reduced with increased average grain size of the ceramics and led to cracking and/or delamination of the layers and hence increased the wear [Zum-Gahr 1993]. SiC-WC composites exhibited higher wear volume when slid against SiC counterbody compared to wear volume obtained against WC-Co or steel counterbody. Therefore, it is to note that the wear volume of SiC-WC composites is dependent on hardness of the counterbody ball.

4.3.2. Wear mechanisms

With decreased hardness of counterbody, material removal mechanisms changed from mechanical fracture to adhesive wear for the investigated ceramic composites. Large tendency for mechanical fracture of SiC ceramics is found against SiC counterbody as compared against WC-Co or steel ball. Against steel counterbody, polishing of surface observed at higher load. The debris generated between the mating surfaces led to more wear due to third body abrasion for SiC ceramics at higher load. Major wear mechanisms for SiC ceramics against SiC, WC-Co and steel counterbody at 5 N, 10 N and 20 N load are listed in **Table 4.1.**

Table 4.1. Dominant wear mechanisms for the SiC ceramics as function of load and counterbody.

Applied Load (N)	Counterbody		
	Steel	**WC**	**SiC**
5	Embedded debris and abrasion	Abrasion	Mechanical fracture
10	Deep grooves abrasion	Deep grooves abrasion	Mechanical fracture and Grains pull-out
20	Abrasion and polishing	Embedded debris and abrasion	Mechanical fracture and Grains pull-out

Material from the disk composites surface is removed due to abrasion and cracking during sliding of hard SiC counterbody. SiC-50 wt% WC composite with higher fracture toughness restrict crack propagation and exhibits less wear. On the other hand, strongly adhered tribolayer affected the frictional and wear characteristics of SiC-WC composites against WC-Co and steel ball. Adhered tribolayer protected the wear surface by restricting the depth of penetration during sliding. Less penetration of counterbody having low hardness led to removal of less material. It implies that with decreased counterbody hardness from 28 GPa (for SiC ball) to 7 GPa (steel ball), wear of the SiC-WC composite reduced, as extent of abrasion, mechanical fracture and grain pull-out decreased with protective tribolayer (see ***Figure 4.8)***. Dominant wear mechanisms for the SiC-WC composites against SiC, WC-Co and steel ball with respect to WC content in SiC ceramics are summarized in **Table 4.2.** A schematic illustration of major material removal mechanisms for SiC ceramics and SiC-WC composites against SiC, WC-Co and steel counterbody are represented in **Figure 4.12**.

Table 4.2. Major wear mechanisms for the SiC-WC composites against SiC, WC-Co and steel ball as function of WC content.

WC content (wt%)	Counterbody		
	Steel	**WC**	**SiC**
0	Abrasion and Polishing	Embedded debris and abrasion	Mechanical fracture and Grains pull-out
10	Abrasion and adhered debris	Abrasion	Reduced fracture, polishing and pull-out
30	Abrasion	Adhered and compacted oxide layer	Polishing and pull-out
50	Reduced Abrasion	Highly adhered and compacted layer	Polishing and Reduced pull-out

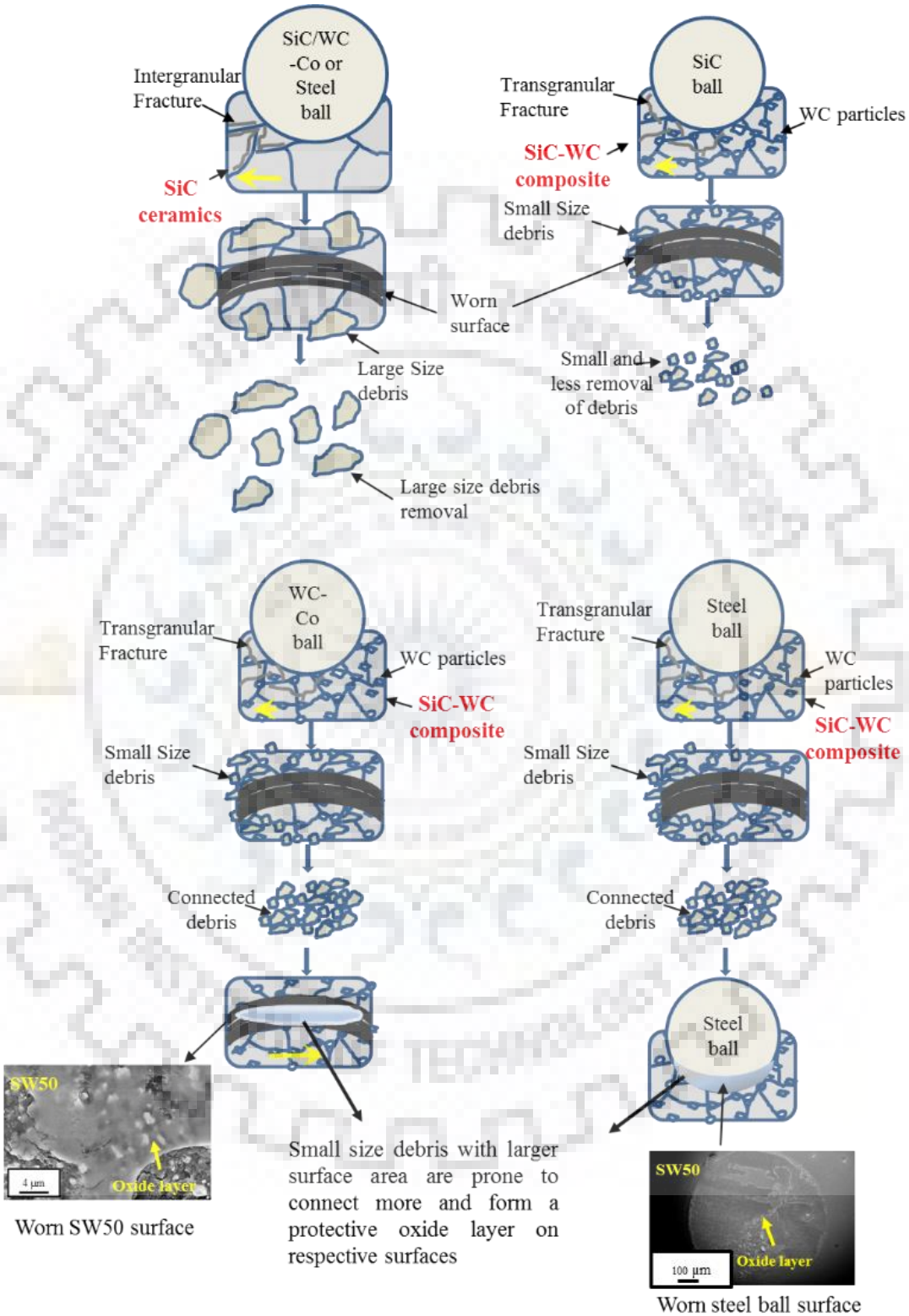

Figure 4.12. Schematic illustration of dominant wear mechanisms for SiC ceramics and SiC-WC ceramics when slid against SiC, WC-Co or steel ball.

4.3.3. Effect of mechanical properties

The complex wear behavior of brittle solids is often reported to be influenced by mechanical properties such as hardness, fracture toughness, and elastic modulus. Tatarko et al. [2010] reported lower specific wear rate for the material with higher hardness. Moreover, Miyazaki et al. [2009] observed that neither hardness nor fracture toughness show any direct relationship to the specific wear rate of Si_3N_4 ceramics. In the present study, the wear rate of studied materials decreased with the increased fracture toughness. The maximum hardness of 26.3 GPa for SiC-30 wt% WC composites is attributed to the homogeneous dispersion of WC particles in the SiC matrix. On the other hand, a maximum fracture toughness of 6.7 $MPa.m^{1/2}$ observed for SiC-50 wt% WC composites is attributed to crack deflection and bridging by a large amount of WC particles [Sharma 2014]. Results from the present study indicate that the minimum amount of material is removed for SiC-50 wt% WC composite against any counterbody, which possessed the maximum fracture toughness. Thus, fracture toughness appeared as more important property than hardness in estimating the extent of sliding wear for the investigated SiC-WC composites.

4.4. Summary

SiC ceramics were investigated for sliding wear behaviour against SiC, WC-Co or steel counterbody at 5 N, 10 N or 20 N load in ambient conditions using a ball-on-disk tribometer. Further, the effect of the addition of WC (10, 30 or 50 wt%) on the friction and wear characteristics of SiC-WC composites is studied against SiC, WC-Co or steel at 20 N load. The following are major conclusions:

(a) At high load, SiC ceramics resulted in higher friction against WC-Co ball due to increased fracture, while less friction observed at high load against steel ball due to the compaction of soft iron oxide debris. The COF is independent of hardness of counterpart materials. The COF value for the SiC ceramics varied from 0.66 against WC-Co ball to 0.34 against steel at 20 N load. SiC ceramics exhibited approximately 100 times more wear against SiC counterbody as compared against steel counterbody. Wear volume varied between 5.9 X 10^{-4} mm^3 and 8.5 X 10^{-2} mm^3 with change in load or counterbody. SEM-EDS analysis of worn surfaces of SiC ceramics indicated abrasive grooves with mechanical fracture responsible for the material removal against SiC or WC-Co counterbody, while abrasive grooves with polishing are observed against steel counterbody.

(b) With increase in WC content from 10 to 50 wt %, average steady state COF decreased from 0.49 to 0.39 against SiC and from 0.55 to 0.33 against WC-Co counterbody for fine grain sized SiC-WC composites. But increased formation of hard $FeWO_4$ with increased amount of WC content in SiC ceramics led to an increase in COF from 0.35 to 0.43 against steel counterbody. The SiC-WC composites with higher WC content exhibited less wear against any counterbody. Lowest wear volume of 2.0 X 10^{-3} mm^3 is obtained for SiC-50 wt% WC composites against steel ball.

(c) Significant change in major wear mechanisms of SiC-WC composites is observed with change in counterbody. Worn surface of SiC-WC composites showed mechanical fracture as material removal mechanism against SiC counterbody, while worn surfaces of composites revealed tribochemistry with increased WC content against WC-Co or steel counterbody. Fine grained SiC-WC composites exhibited small size debris. The compaction of which resulted in the formation of oxide rich layer at the contact against WC-Co or steel. Raman spectroscopy analysis of debris collected from the worn surfaces of SiC-50 wt% WC composites indicated formation of silicon oxide, tungsten oxide, cobalt tungsten oxide particles when slid against SiC or WC-Co counterbody and additional formation of iron oxide and iron tungsten oxide against steel ball.

(d) The wear of SiC-WC composites is in general less against steel ball, whereas SiC-50 wt% WC composite with maximum fracture toughness of 6.7 $MPa.m^{1/2}$ exhibited superior wear resistance against any counterbody.

(e) The present study necessarily demonstrates that the wear behaviour is influenced by the hardness or type of the counterbody and fracture toughness of SiC-WC composites.

CHAPTER 5

Reciprocated Sliding Wear of SiC-WC composites

Considering the highest wear of investigated composites against SiC counterbody in chapter 3, SiC-(0, 10, 30 or 50 wt%)WC composites were further subjected to reciprocated sliding wear in ambient condition (28±2°C and 55±5% RH) and at 500°C against SiC counterbody. Major results obtained are presented in this chapter. In particular, tribological behaviour of SiC ceramics are analyzed as function of load at ambient conditions and WC content at different temperature (RT and 500°C). Dominant material removal mechanisms at different sliding conditions are particularly elucidated.

5.1. Background:

Sliding wear behavior is studied in continuous or reciprocating conditions. The pattern of wear is alike for both wear conditions, but a higher wear is observed in reciprocated sliding. The difference in wear can be understood in terms of characteristics of wear debris remained at the contact for long time in reciprocated sliding conditions [Ward 1970]. Limited research available on wear behavior of SiC ceramics in reciprocated sliding conditions highlighted the role of third body [Wasche 2004; Dulias 2005; Amirthan 2011; Xia 2013]. Wasche et al. [2004] studied the pressureless sintered SiC ceramics against SiC and Al_2O_3 balls in an environment with humidity ranging from 1 to 100% RH. They found increase in wear rate for SiC ceramics worn against SiC balls by two orders of magnitude in dry sliding as compared to sliding in humid environment. Cavities generated by grain pull-out and microcracking in humid conditions acted as reservoir for the debris which further provided lubrication and protected the surface from wear. Amirthan et al. [2011] also found reduced sliding wear of natural materials derived SiC (Si/SiC) ceramics against Al_2O_3 ball in humid environment as compared to sliding in dry conditions. In lubricated conditions, the reciprocating wear of self-mated reaction bonded SiC ceramics decreased with decreasing initial surface roughness. The self-mated ceramics exhibited high COF in isooctane than in distilled water [Dulias 2005]. However, reciprocated sliding wear of SiC based composites has not been reported by any researcher.

Recently, WC reinforced SiC composites have attracted the research community due to the expected improvement in thermal, mechanical or wear properties [Zhang 1994; Pang 2009; Sharma

2014]. The wear resistance of SiC-WC composites against SiC particle erosion was highest for SiC-30 wt% WC composites [Sharma 2014], while in previous part of the study (**Chapter 4**), it was found that the wear resistance in continuous sliding against SiC balls was highest for SiC-50 wt% WC composites. So it is concluded that the optimum composition of SiC-WC composites for superior wear resistance is dependent on the wear conditions.

In order to thoroughly understand the potential of SiC-WC composites for reciprocated wear applications such as bearings for the liquid rocket engine turbopumps, bearings for rotary shaft, transportation medium for hot abrasive materials, turbine blades, etc., a systematic investigation on the behavior of SiC-WC composites in reciprocated sliding conditions against SiC ball is made for the first time in the present part of the thesis. In particular, the influence of WC content (0 to 50 wt%) and temperature (ambient temperature and 500^{o}C) on the friction and wear behavior of SiC ceramics is studied, and the wear mechanisms are elucidated.

5.2. Results and discussion

5.2.1. Frictional behavior

Average steady state COF data for composites obtained in sliding at room temperature is shown in **Figure 5.1.** The COF for SiC ceramics changed from 0.5 to 0.4 with applied load and further it decreased to 0.3 with WC content. The reported COF values for the SiC ceramics slid using different test and materials parameters are in range of 0.2-0.7. High values of COF are reflections of mechanical wear including abrasion, and chipping or fracture of surfaces, whereas lower values are resulted to the formation of hydrated silica at the interface [Zum-Gahr 2001; Cranmer 1985; Murthy 2004]. On this account, the high range of COF observed in the present study can be primarily attributed to mechanical wear. The COF of the composites decreased with increase in load or WC content, indicating the effect of third body at the contact. Further discussion on the nature of contact is provided in later section.

At elevated temperature (500^{o}C), friction between the mated surfaces and SiC ball is found to be 0.7 during initial running in-period and increased continuously beyond 1.0 for all composites in 1000 cycle test. As no steady state for friction was obtained, average steady state COF was not determined. Such frictional behavior of composites is expected to be a reflection of continuous generation and fracture of debris between mated surfaces.

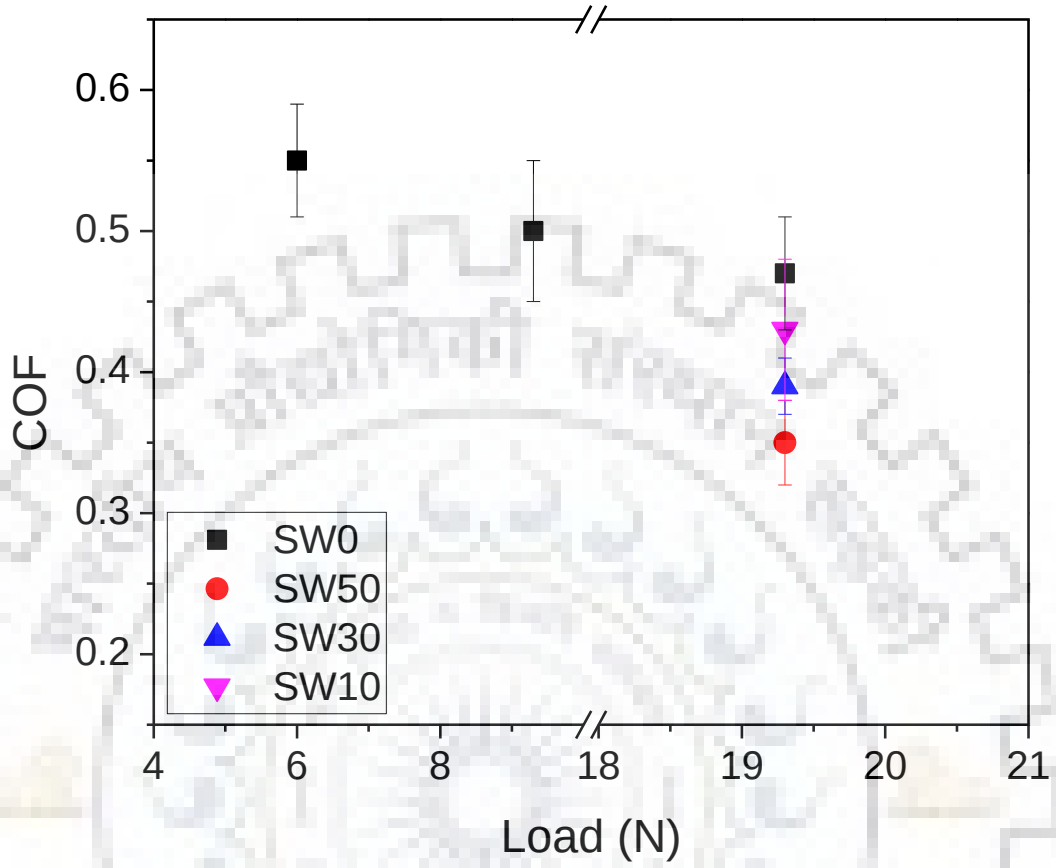

Figure 5.1. Average steady state coefficient of friction (COF) of SiC-WC composites against SiC counterbody at ambient temperature as function of load and WC content.

5.2.2. Wear results

Figure 5.2 shows a typical three dimensional image of surface of SiC ceramics worn at 19 N load in ambient environment. At least 12 measurements in transverse direction of sliding were made using optical images of three worn surfaces for determining the average value of depth and width. **Figure 5.3** shows typical profiles of wear scars in transverse direction of sliding. Average width and depth of scar varied from 0.2 mm to 1.2 mm, and 0.1 µm to 1.3 µm, respectively. The width and depth of scar for SiC ceramics increased with load (***Figure 5.3a***), whereas increased WC content led to their reduction (***Figure 5.3b***) when tested in ambient conditions.

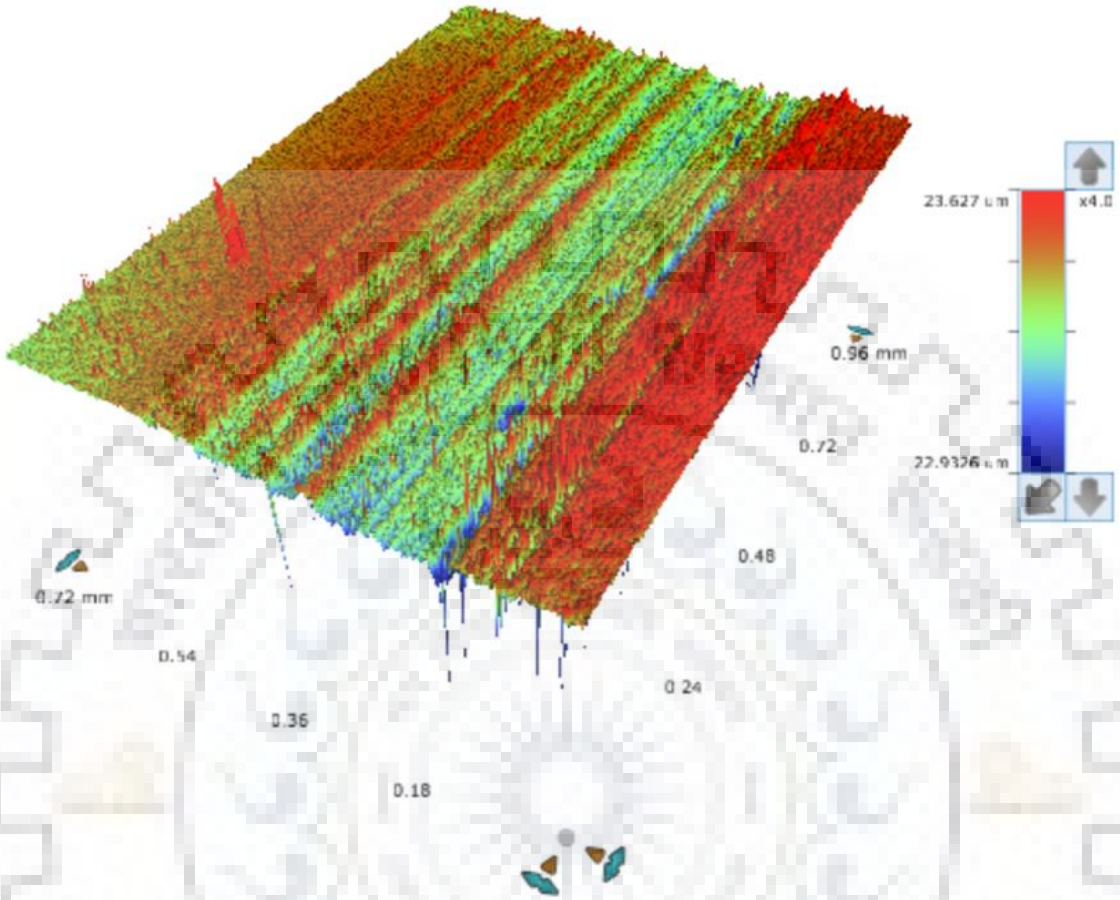

Figure 5.2. Typical three dimensional image of SiC-30 wt% WC composite surface worn at 19 N load.

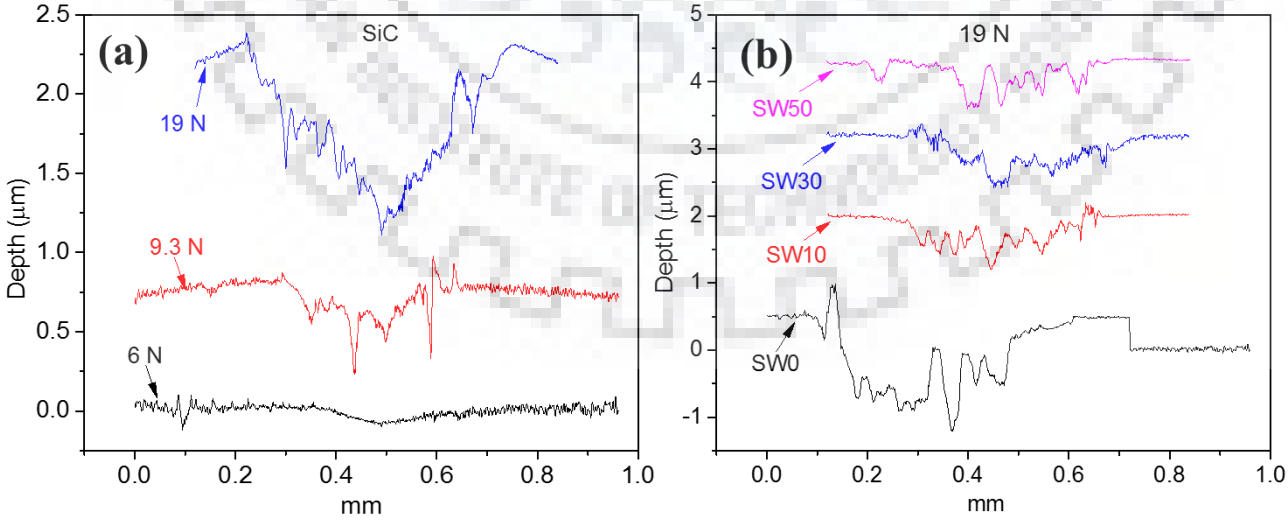

Figure 5.3. Scar profiles of (a) SiC ceramics at different loads and (b) SiC-WC composites worn at 19 N load and ambient temperature.

Compared to ambient temperature, depth and width of scar are much higher for samples worn at 500ºC. Typical scar profiles show change in width and depth with temperature for SiC ceramics (***Figure 5.4a***) and SiC-50 wt% WC composites (***Figure 5.4b***). Depth and width of the scars for composite are almost unchanged up to 30 wt% WC reinforcement. But width and depth notably increased with further increase of WC content up to 50 wt%.

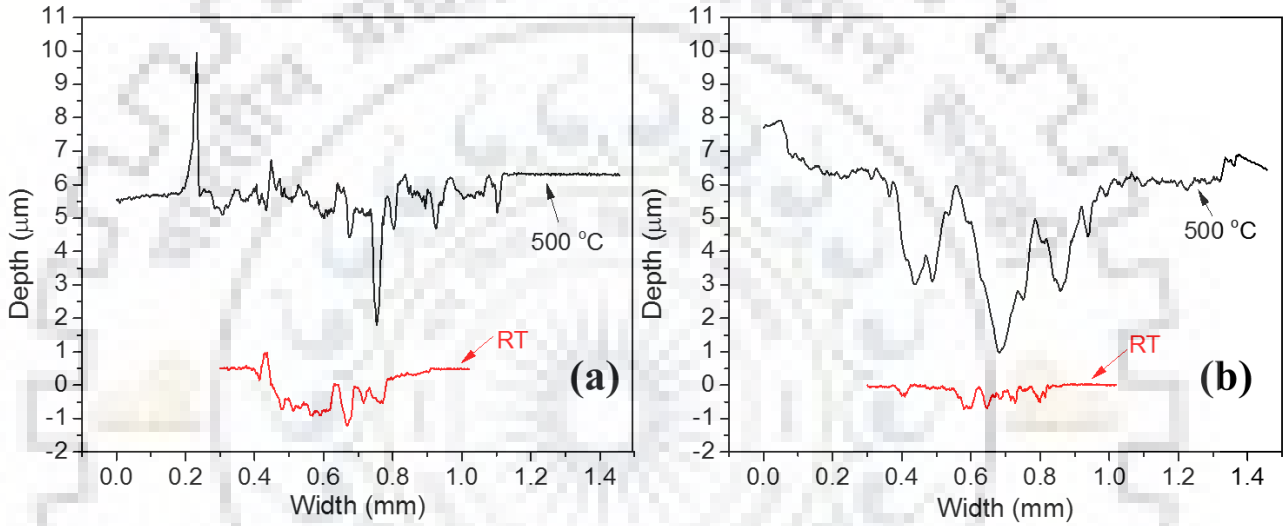

Figure 5.4. Scar profiles of (a) SiC ceramics and (b) SiC-50 wt% WC composites worn at 19 N load and ambient (RT) or 500ºC.

Wear volumes of SiC ceramics and SiC-WC composites are shown in **Figure 5.5**. In ambient condition, at least two orders of magnitude increase in wear volume from 8.2 X 10^{-5} to 2.7 X 10^{-3} mm^3 is observed with change in load from 6 N to 19 N for SiC ceramics (***Figure 5.5a***). With increase in load, increased brittle fracture led to high wear [Cho 1996; Kumar 2011; Gupta 2015]. On the other hand, wear volume reduces from 2.7 X 10^{-3} mm^3 to 2.8 X 10^{-4} mm^3 for SiC-WC composites with large WC content when tested at 19 N load (*see* ***Figure 5.5b***). It is to note from our previous investigation that the fracture toughness increased to a maximum with increase in WC content, owing to crack deflection or bridging [Sharma 2014]. Thus, in reciprocated sliding conditions, the propagation of

fatigue induced crack is effectively prevented by WC particles to result in minimum wear for SiC-50 wt% WC composites.

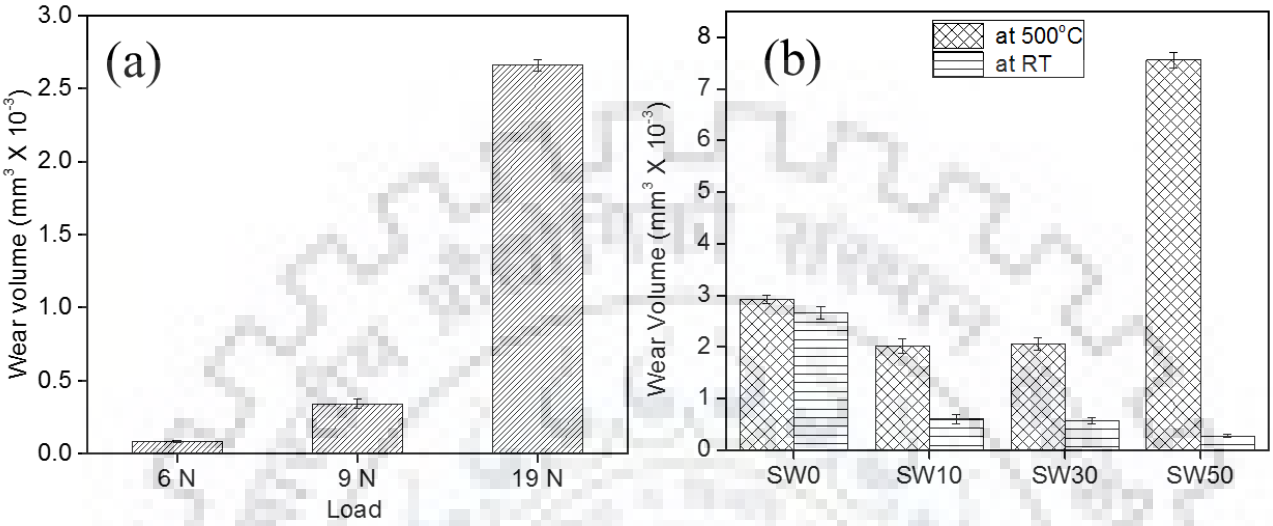

Figure 5.5. Wear volume of (a) SiC ceramics at different sliding loads at ambient temperature (RT) and (b) SiC-WC composites at 19 N load at RT or 500ºC.

In sliding at 500ºC, SiC ceramics does not show significant change in wear volume (**Figure 5.5b**). This can be attributed to the marginal degradation of strength for SiC ceramics at high temperatures [Keppeler 1998]. The wear volume decreased from 2.9 X 10^{-3} mm^3 for SiC ceramics to 2.0 X 10^{-3} mm^3 for SiC-10 wt% WC composites and remains unchanged for SiC-30 wt% WC composite. However, at least 3.5 times increased wear volume from 2.1 X 10^{-3} mm^3 to 7.6 X 10^{-3} mm^3 is observed with increase in WC content from 30 to 50 wt% in SiC ceramics. Such a remarkable change in wear with 50 wt% WC content can be attributed to the change in dominant mechanisms of material removal, which will be clear in later section.

The wear rate for SiC-WC composites ranges from 1.4 X 10^{-6} mm^3/N.m to 4.2 X 10^{-5} mm^3/N.m with change in reciprocated sliding load, temperature or WC content. The liquid-phase sintered SiC ceramics are reported to exhibit wear rate as low as 10^{-7} mm^3/Nm in continuous sliding conditions [Anderson 1994; Murthy 2004]. The higher range of wear rate obtained for SiC ceramics or SiC-WC composites in the present study essentially indicates the corollary of retained debris in the contact in reciprocating sliding conditions.

5.2.3. Worn surface analysis

Worn surfaces of SiC ceramics and SiC-WC composites were subjected to SEM-EDS analysis to elucidate the dominant mechanisms of material removal in the investigated reciprocated sliding wear conditions. **Figures 5.6-5.8** show morphology of worn surfaces of SiC ceramics and composites after sliding at different loads and temperatures. SEM images in **Figure 5.6** demonstrate fatigue induced microcracks (indicated by arrows in **Figure 5.6**) and smooth surface in SiC ceramics, worn in reciprocating sliding. With increase in applied load from 6 N to 19 N, fracture of the SiC surfaces is apparently increased (s***ee Figure 5.6***).

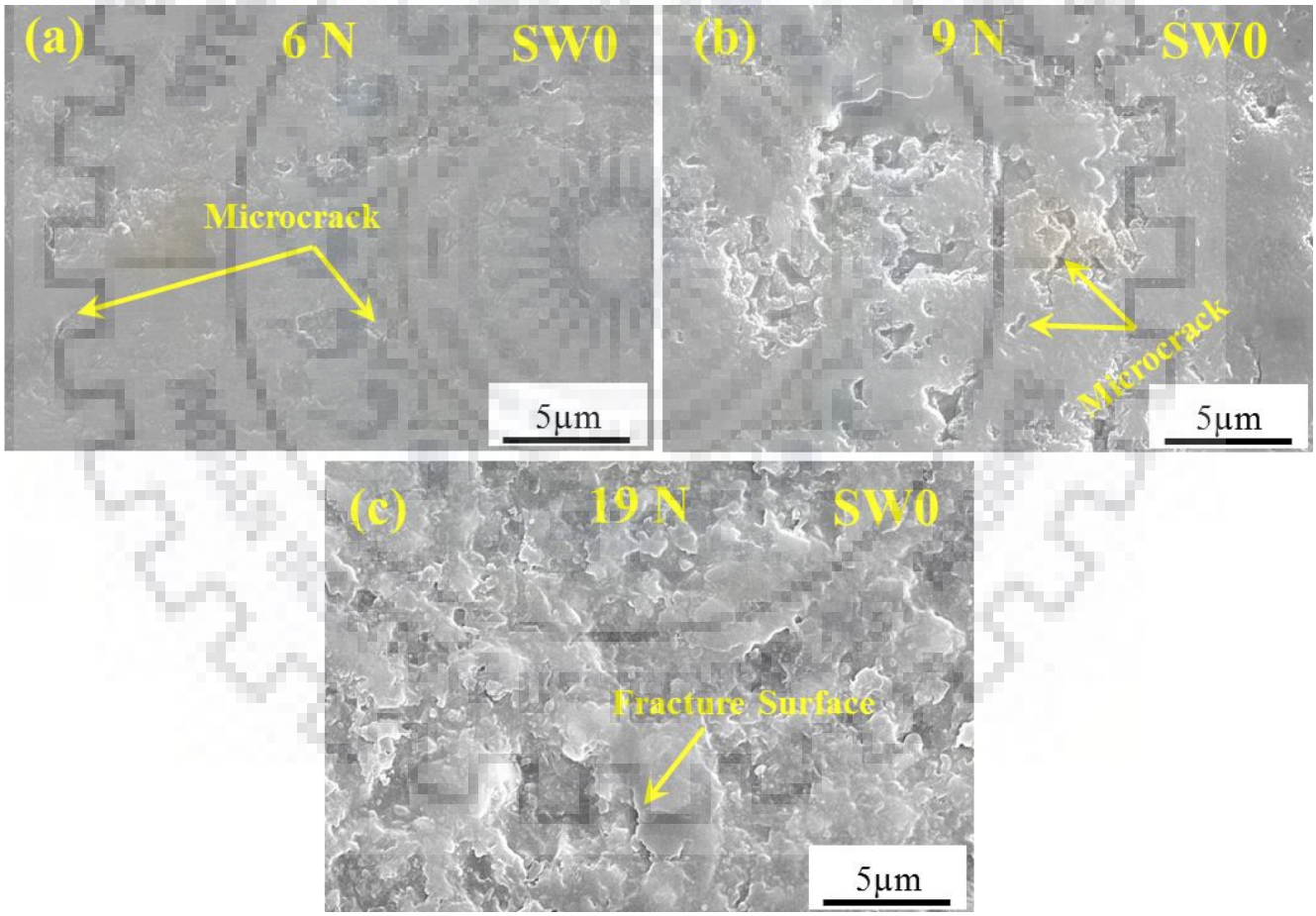

Figure 5.6. Worn surfaces of SiC ceramics after sliding in ambient conditions at (a) 6 N, (b) 9 N and (c) 19 N load.

The SiC-WC composite surfaces worn at 19 N load and ambient temperature are shown in **Figure 5.7.** SEM images of worn surfaces in the present study show shear fracture and compaction of fractured SiC grains. Also, WC particles are pulled-out from the top surface, and those beneath the surface are intact with the matrix. In general, extent of fracture is reduced due to the presence of WC particles in SiC ceramics. This indicates increased restriction of crack propagation. The wear volume data presented in **Figure 5.5b** is also in agreement with this observation. Thus, during reciprocated sliding in ambient conditions, SiC-50 wt% WC composite with the highest fracture toughness of 6.7 MPa.m$^{1/2}$ exhibited superior wear resistance. Similar observation was also made in previously reported worn surfaces of cemented carbide in sliding, where WC grains remained well bonded to the matrix during sliding and reduced grain fracture or particle pull-out [Pirso 2004, Bonny 2010; Muthuraja 2015].

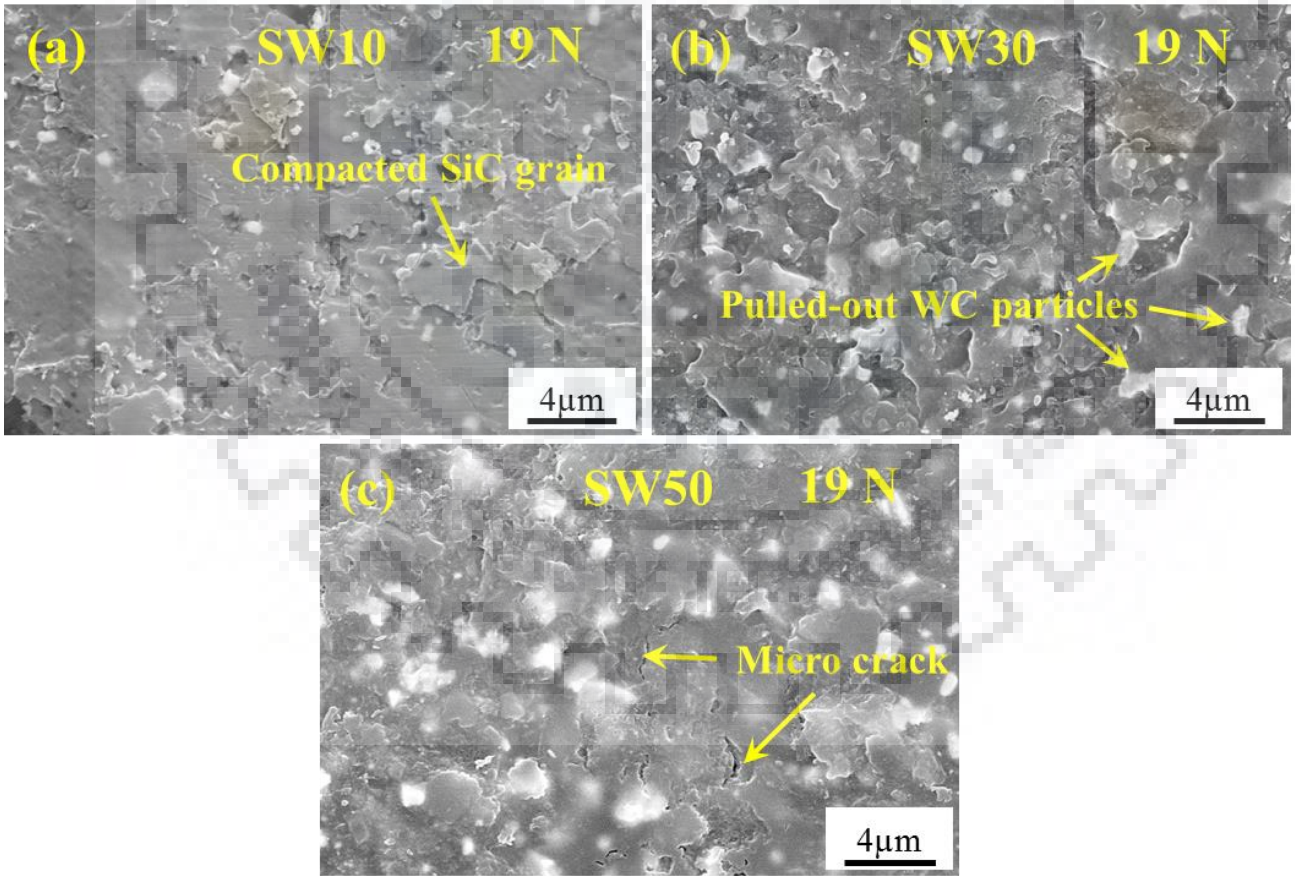

Figure 5.7. Worn surfaces of (a) SiC- 10wt% WC, (b) SiC- 30wt% WC and (c) SiC-50 wt% WC after sliding at 19 N at ambient temperature.

Figure 5.8 shows SEM images of SiC ceramics and SiC-WC composite surfaces worn at 500ºC. Compared with SiC ceramics worn at ambient temperature (***Figure 5.6c***), SiC ceramics worn at 500ºC (***Figure 5.8a***) show rough surface with increased number of fractured grains. This indicates dominant fracture of softened SiC grains worn at high temperature. With increase in WC content to 30 wt%, the worn surface exhibits decreased fracture compared to monolithic SiC ceramics.

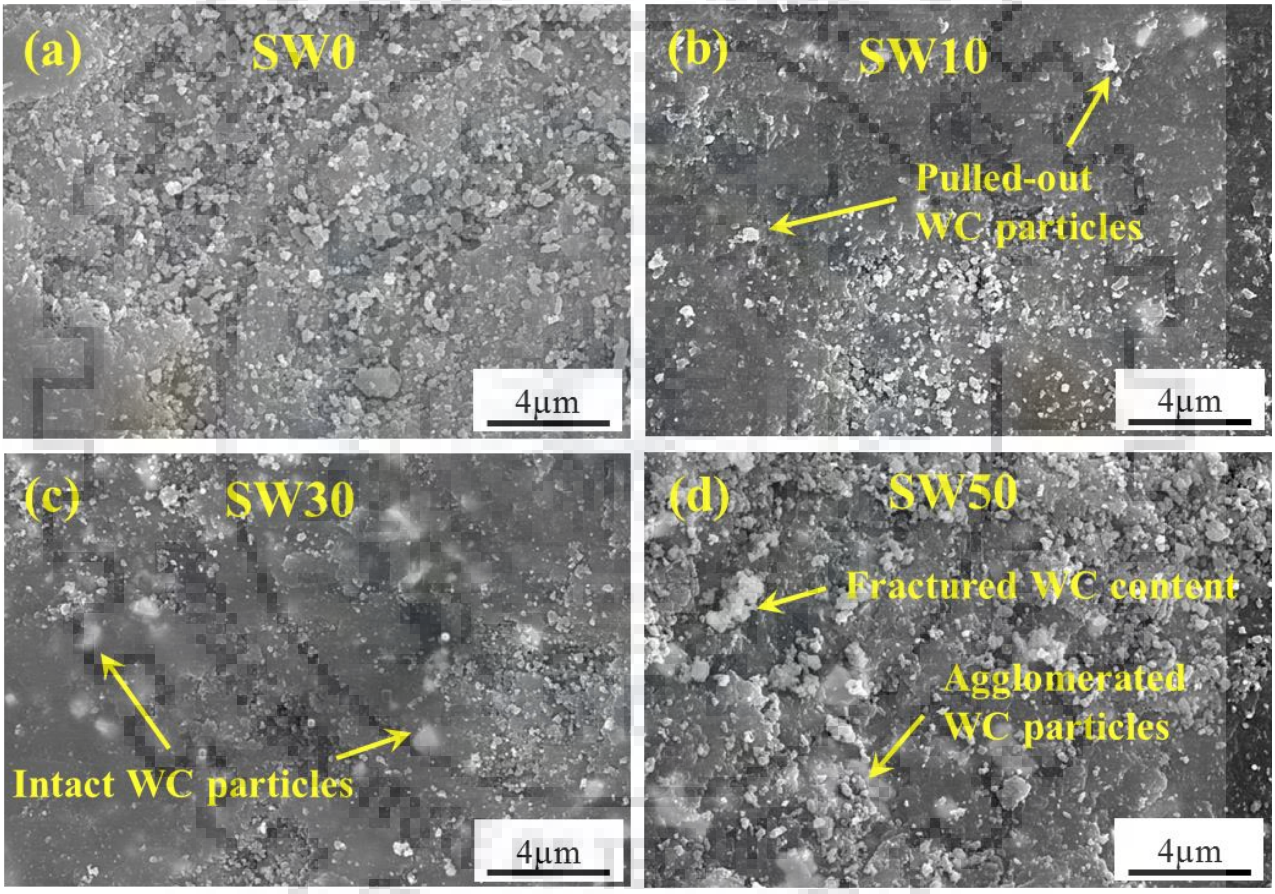

Figure 5.8. Worn surfaces of (a) SiC, (b) SiC- 10wt% WC, (c) SiC- 30wt% WC and (d) SiC-50 wt% WC after sliding at 19 N at 500ºC.

In case of SiC-50 wt% WC composites, the surface is severely fractured with increased pull-out of WC particles. Further, removed WC particles appear as clusters or agglomerates, as compared to pull-out of individual particles in ambient conditions. Close observation of **Figures 5.7c and 5.8d** suggests that WC particles are extensively pulled-out or fractured from the surface of the composites during wear at

500ºC. Large extent of WC particle removal further resulted in less constraint to fracture of SiC grains. Stress concentrations are reported to increase at higher temperature due to mismatch in coefficient of thermal expansion [Watts 2011]. It is believed that the stress concentrations at defect sites of agglomerates of WC particles in case of SiC-50wt% WC composites are further enhanced with thermal stresses generated at the matrix-particle interface, that result in large amount of material loss in high temperature sliding conditions. SiC-50 wt% WC composites also show highest wear loss after reciprocating wear at 500ºC in the present study (*see **Figure 5.5b***). Thus, addition of 30 wt% WC is optimum for the SiC ceramics for the less wear in the selected conditions of reciprocated sliding at 500ºC.

5.2.4. Debris analysis

Debris particles were carefully collected after each test and subjected to SEM-EDS analysis. Typical SEM images of debris collected after wear of SiC ceramics and SiC-WC composites at 19 N load in ambient conditions are shown in **Figure 5.9.** Debris particles generated from sliding of SiC ceramics are loose, irregular and small in size (*see **Figure 5.9a***). The debris particles generated from SiC-WC composites are larger in size with noticeable tendency for cylindrical shapes. The size and extent of cylindrical shape debris particles are found higher with increased WC content in SiC matrix. The formation of cylindrical debris is attributed to the combined effect of two facts: reduced grain size of SiC ceramics with WC reinforcements, and moderately humid atmosphere (55±5% RH) at the contact. The fine grains in SiC-WC composites are supposed to generate fine debris particles that are prone to connect with each other and form long cylindrical debris [Zhao 1997; Danyluk 1994; Murthy 2004]. Furthermore, oxygen peaks observed in EDS analysis suggests that cylindrical debris is rich with silica (*see insets in **Figure 5.9a and d***). Formation of cylindrical debris occurs for silicon-based materials with formation of hydrated silicon oxide as a result of following reactions with moisture in humid or moderately humid contacts of sliding [Tomizawa 1985; Zanoria 1991; Dong 1993; Wasche 2004; Zhao 1997]:

$$SiC + 2O_2 = SiO_2 + CO_2 \text{ ---------- } \textbf{(5.1)}$$

$$SiC + 2H_2O = SiO_2 + CH_4 \text{ ---------- } \textbf{(5.2)}$$

$$SiO_2 + 2H_2O = Si(OH)_4 \text{ ---------- } \mathbf{(5.3)}$$

In the present study, oxygen enrichment detected in EDS analysis of cylindrical debris of SiC-WC composites supports increased tendency for tribooxidation compared to SiC (*see inset* ***Figure 5.9a and d***). The formation of cylindrical debris is associated with the reduced friction and wear during sliding [Tomizawa 1985; Zanoria 1991; Dong 1993; Kumar 2005]. Combining results obtained from analyses of debris and worn surfaces, both tribochemistry and microcrack induced fracture are believed to play major roles in sliding wear behavior of SiC-WC composites at ambient reciprocated conditions.

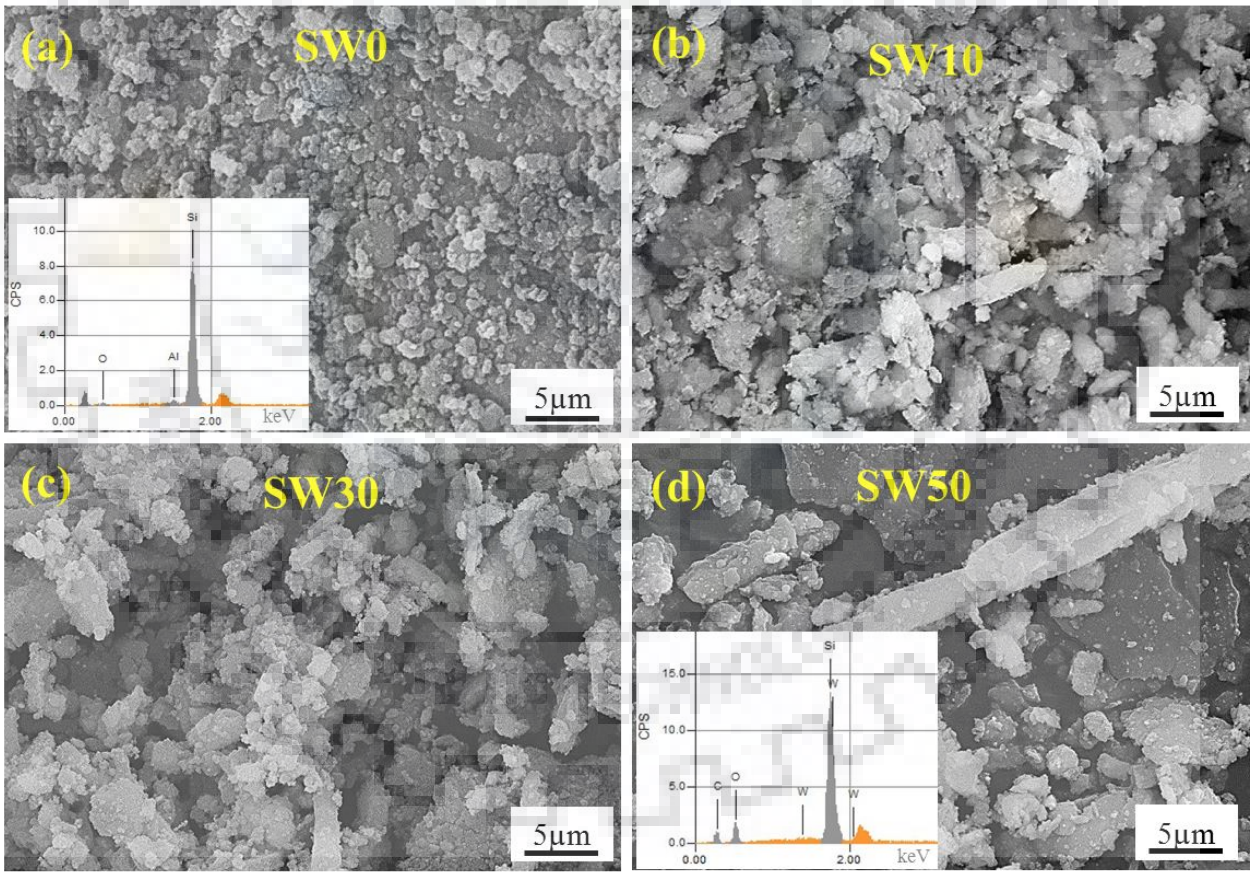

Figure 5.9. SEM images of debris collected after wear of (a) SiC, (b) SiC- 10wt% WC, (C) SiC-30wt% WC and (d) SiC-50 wt% WC. Sliding load: 19 N and temperature: ambient. EDS analysis for (a) and (d) are shown as insets in respective images.

Figure 5.10 shows SEM images of debris collected after sliding wear of SiC-WC composites at 500°C. These images show dry, loose and irregular size debris for all composites. The dry debris at the contact results in higher friction and wear in high temperature sliding of SiC-WC composites. Reduced size of debris with increased WC content advocates fracture of fine grains in composites (*see* ***5.10***). Further, EDS analysis (*inset in* ***Figure 5.10 d***) of collected debris does not show any notable change, as compared to room temperature. Thus, both debris analysis and worn surface analysis certainly suggests significant role of microcrack induced fracture in sliding wear behavior of SiC-WC composites in elevated temperature sliding conditions.

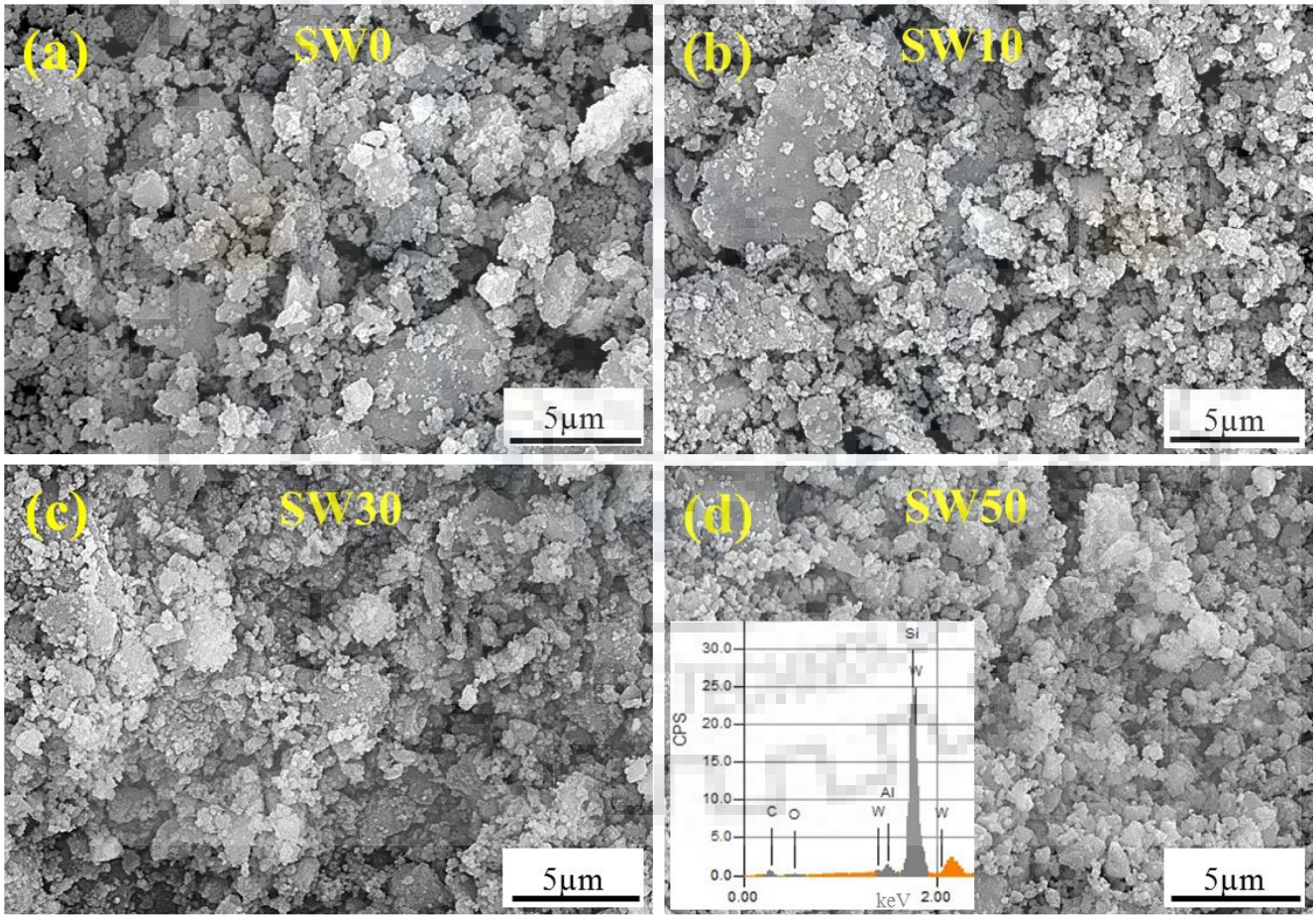

Figure 5.10. SEM images of debris collected after wear of (a) SiC, (b) SiC- 10wt% WC, (C) SiC-30wt% WC and (d) SiC-50 wt% WC. Sliding load: 19 N and temperature: 500°C.

5.2.5. Effect of temperature

Friction and wear results of SiC-WC composites in reciprocated sliding wear conditions proposed a considerable effect of temperature. Compared to room temperature, reciprocated sliding at high temperature resulted in a high initial friction value (0.7). The friction increased beyond 1.0 throughout the running-in-period for all the composites during 1000 reciprocating cycles. Dry and hard debris generated at 500^{o}C during wear led to high frictional values. Even being smaller in size, debris particles generated from wear of SiC-WC composites are not hydrated to connect with each other at high temperature; thus led to high friction. Softening of SiC grains at high temperature caused high wear for all the composites as compared to wear at room temperature. With increased WC content to 30 wt%, SiC ceramics exhibited reduced wear loss. Further increase of WC content to 50 wt% led to high wear loss. The increased tendency for agglomeration with large amount of WC content (indicated by arrow in ***Figure 5.8d***) offers increased defect sites and generation of severe stresses that led to large amount of material loss at high temperature.

5.2.6. Effect of WC content

The influence of WC content in wear of SiC ceramics in reciprocating sliding wear condition can be realized. The addition 50 wt% WC is beneficial in reducing wear of SiC ceramics in sliding at ambient temperature. This can be attributed to the higher fracture toughness with WC addition. WC particles do not allow the crack to propagate easily and restrict material loss. On the other hand, wear is found to increase in sliding at high temperature for SiC-WC composites. The softened matrix and the stresses generated at the interface of matrix and particles contributed for the increased materials loss in high temperature sliding. Results obtained in the high temperature sliding point to the fact that the non-uniformly dispersed WC particle agglomerates/clusters in SiC-50 wt% WC composites provide additional stress concentration sites to thermal stress sites at the interface and lead to increased tendency for pull-out or fracture of WC particles.

5.2.7. Effect of mechanical properties

Wear behavior of SiC ceramics is reported to influence by various mechanical properties like hardness, fracture toughness, elastic modulus etc. SiC ceramics showed variation in fracture toughness and hardness value with WC particle reinforcement. The SiC-30 wt% WC composite with

homogeneous dispersion of WC particles exhibits maximum hardness value (26.3 GPa), whereas SiC-50 wt% WC composite exhibits maximum fracture toughness (6.7 MPa.$m^{1/2}$) due to increased crack deflection or bridging by a large amount of WC particles. The fact that SiC-50 wt% WC composite in the present study resulted in minimum wear at ambient temperature campaigns dominant effect of fracture toughness. On the other hand, the maximum wear resistance for SiC-30 wt% WC composite at 500ºC indicates domination of hardness in high temperature sliding conditions.

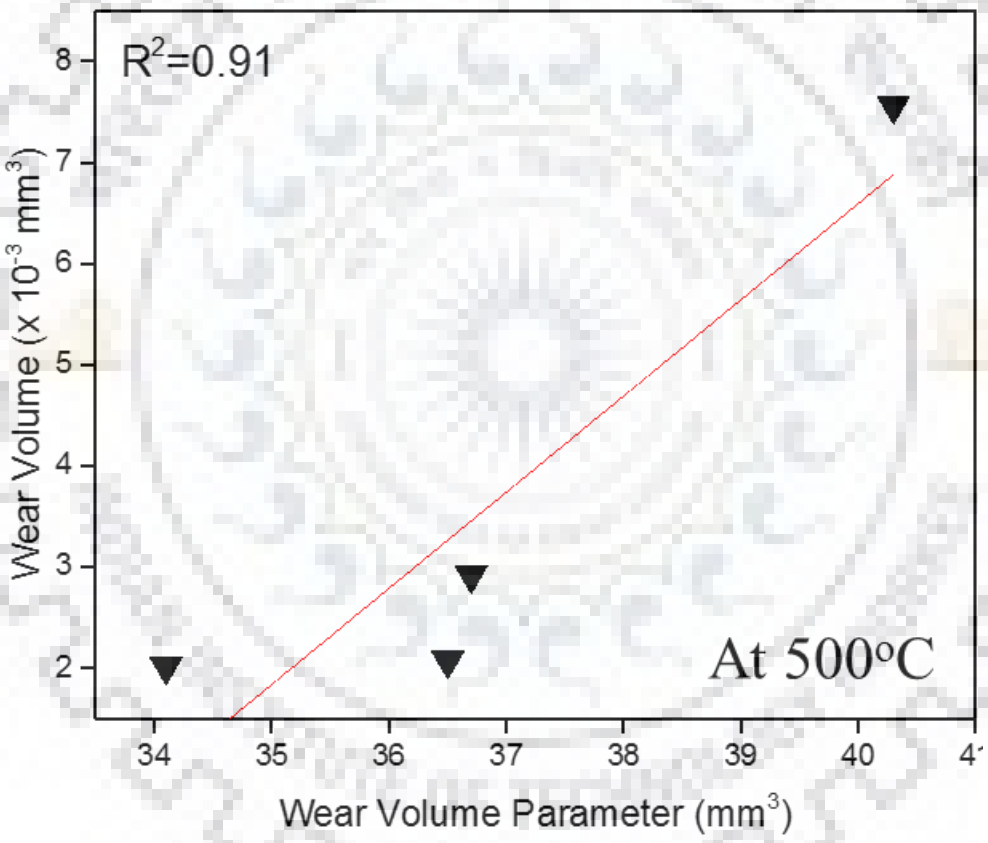

Figure 11. Experimentally measured wear volume for SiC-WC composites after sliding at 500ºC Vs. wear volume parameter using lateral fracture model (ref. ***equation 5.4***).

According to a model proposed by Evans and Marshall, the material removed by the formation and propagation of lateral cracks can be estimated as wear volume (*Vs*) using the following equation [Evans 1981]:

$$Vs = \alpha \frac{P^{9/8}}{K_{1c}^{1/2} H^{5/8}} \left(\frac{E}{H}\right)^{4/5} S \quad \text{---------- (5.4)}$$

where P is applied load, E is elastic modulus, H is hardness, K_{1c} is fracture toughness of composites and α is a material constant. However, experimentally measured wear volume at ambient temperature in the present study does not show a linear relation with estimated wear volume (using ***equation 5.4***) due to contribution from tribochemical wear. On the other side, a linear relation is observed with wear volume for the investigated ceramics when slid at 500^{o}C (*see* ***Figure 5.11***) indicating domination of fracture induced wear. SEM-EDS analysis, discussed in the previous section also indicates that the material is dominantly removed by fracture and pull-out of SiC-WC composites worn at 500^{o}C, whereas the analysis of debris generated from wear in ambient sliding conditions indicates significant contribution from tribo-oxidation. Thus, results obtained in the present investigation essentially indicate that the lateral fracture model is valid for the wear of SiC-WC composites obtained at high temperature where mechanical fracture dominates material removal.

5.3. Summary

Hot pressed SiC-WC composites with 0, 10, 30 or 50 wt% WC particle additions were analyzed for their frictional and wear behavior in reciprocated sliding conditions against SiC balls. The tribological behavior of SiC ceramics was estimated as function of load: 6, 9 or 19 N load at ambient temperature. Further effects of (10, 30 or 50 wt %) WC content and temperature (room temperature and 500^{o}C) on the friction and wear behavior of SiC-WC composites were systematically studied. The following are major conclusions:

a) With increase in load, reciprocated sliding of SiC ceramics in ambient conditions resulted in reduction in friction from 0.5 to 0.4, and increase in wear rate from 1.4 X 10^{-6} mm^3/N.m to 1.5 X 10^{-5} mm^3/N.m with increased microfracture on the worn surface.

b) With increase in WC content from 0 to 50 wt %, the friction in sliding at room temperature and 19 N load decreased from 0.4 to 0.3. The wear rate for SiC ceramics and SiC-WC composites varied from 1.5 X 10^{-6} mm^3/N.m to 4.2 X 10^{-5} mm^3/N.m with change in reciprocating temperature or WC content. SiC-30 wt% WC composites exhibited maximum wear resistance at high temperature.

c) SEM-EDS analysis of worn SiC-WC composts advocated the role of tribochemistry and microfracture in sliding at ambient temperature, whereas microfracture dominated for the wear at 500^{o}C. Softened SiC grains are responsible for easy fracture and removal of WC particles in sliding at high temperature. The wear results obtained from high temperature sliding of SiC-WC composites also validate the lateral fracture model.

d) The formation of cylindrical debris resulted in less friction and wear for the composites in ambient sliding conditions. Dry and loose debris generated from elevated temperature sliding exhibited high friction and wear.

CHAPTER 6

High Temperature Erosion Wear of SiC-WC Composites

In the present chapter, results obtained from solid particle erosion behaviour of SiC-WC composites against SiC erodent at high temperature (800°C) are discussed. Particularly, effect of WC content in SiC matrix and impingement angle of erodent on erosion behaviour of SiC-WC composites are analyzed. Change in major material degradation mechanisms with WC content or angle of erodent impingement are also elucidated.

6.1. Background:

Erosion in several structural components such as gas turbine parts, burner parts, cutting tools, and exhaust or fluidized bed combustion systems leads to heavy loss to industries [10]. Several material have been investigated for their high temperature strength for different applications [Neuman 2013; Murthy 2016; Fahrenholtz 2007; Kim 2017]. Erosion behavior of SiC ceramics and their composites at higher temperature is necessarily required to understand the potential of the ceramics for high temperature wear applications. Limited literature is available on high temperature erosion behavior of SiC ceramics and their composites. Generally, incorporation of second phase is made to achieve improved wear resistance of the SiC based composites compared to monolithic SiC ceramics [Colclough 1997; Wang 1990; Ding 2014]. Colclough and Yeomans [1997] studied the erosion behaviour of monolithic SiC and SiC-16 vol% titanium diboride against SiC erodent at elevated temperatures. They found less erosion rate at room temperature when compared to that at higher temperature (up to 1000°C) for both monolithic and composite materials. But, the composite exhibited less erosion rate compared to SiC ceramics in any conditions owing to superior fracture toughness of composites. Lateral fracture reported as responsible mechanism for material removal. Wang and Levy [1990] studied the erosion behavior of SiC fiber reinforced SiC composite at 25°C and 850°C and found an inverse relation of density and hardness to the erosion rate of the composite. The erosion rate reduced by one order of magnitude at 850°C (0.10 mg/g) compared to that at 25°C (2.20 mg/g), which attributed to increased ductility, less cracking and chipping of matrix and fibers from composite at 850°C. Similarly in a recent study [Li 2014], solid particle erosion rate of SiC-Si_3N_4 composite at

elevated temperature increased initially up to 800°C, and then decreased with increase in temperature to 1400°C. Wear occurred by brittle fracture where stripping of aggregates of composite resulted in loss of protection from the matrix in erosion at temperatures up to 800°C. On the other hand, plastic deformation and oxidation protection dominated above 800°C. Ham et al. [1997] found higher erosion rate for SiC fibers reinforced calcium aluminosilicate/silicon carbide glass-ceramic matrix composite at 200°C, when compared to erosion at room temperature. However, further rise in erosion temperature from 200°C to 726°C left no considerable change in erosion rate of composite. They further [Ham 1999] found strong dependency for the erosion rate on velocity of erodent particles (with an exponent of 2.6), irrespective of fiber orientation with respect to the erodent stream.

In the present part of the study, high temperature erosion behavior of SiC-WC composites is studied to assess the potential of SiC-WC composites for high temperature applications such as exhaust systems for the liquid rocket engine turbopumps, aerospace turbine blades, etc. The composites were subjected to solid particle erosion against SiC erodent at high temperature (800°C) and the effects of WC content (0 to 50 wt%) and impingement angle of erodent on the erosion wear behavior of SiC ceramics are studied, and the erosion mechanisms elucidated.

6.2. Results and discussion

6.2.1. Erosion results

Erosion behaviour of dense SiC-WC composites at 800°C is studied against stream of SiC erodent particles. **Figure 6.1** shows erosion rate of the sintered SiC composites as function of WC content and angle of impingement of erodent. Erosion rate of SiC ceramics varied from 210 mm^3/kg to 770 mm^3/kg with change in WC reinforcement (0, 10, 30 and 50 wt%) and the angle of impingement (30°, 60°, and 90°) at 800°C. Erosion rates for SiC ceramics are reported to vary in the range of 10 mm^3/kg - 10^3 mm^3/kg with varying experimental conditions [Routbort 1980, 1983; Wang 1990; Wang 1995; Kim 1998; Sharma 2014; Li 2014]. Erosion rate increased with higher impingement angle and resulted to a maximum at normal impact for all the SiC-WC composites. The increased fracture at normal impact leads to the highest erosion for brittle materials [Hutchings 1992; Basu 2011]. Owing to the highest hardness of 26 GPa, SiC-30 wt% WC composites exhibited lowest erosion rate at a given angle of impingement. Further, 50wt% WC reinforcement led to more erosion of SiC ceramics. A minimum erosion rate of 210 mm^3/kg is obtained for SiC-30 wt% WC composites at 30° impingement, while a

maximum of 700 mm^3/kg erosion rate obtained for SiC-50 wt% WC composites at 90º impingement. This can be attributed to the fact that the elimination of slow crack growth and absorption of energy in cracking glassy silica phase in dynamic loading conditions result in negligible change in hardness or fracture toughness of silicon carbide or silicon nitride based ceramics [Li 2014, Wiederhorn 1983; John 1975; Mendiratta 1977].

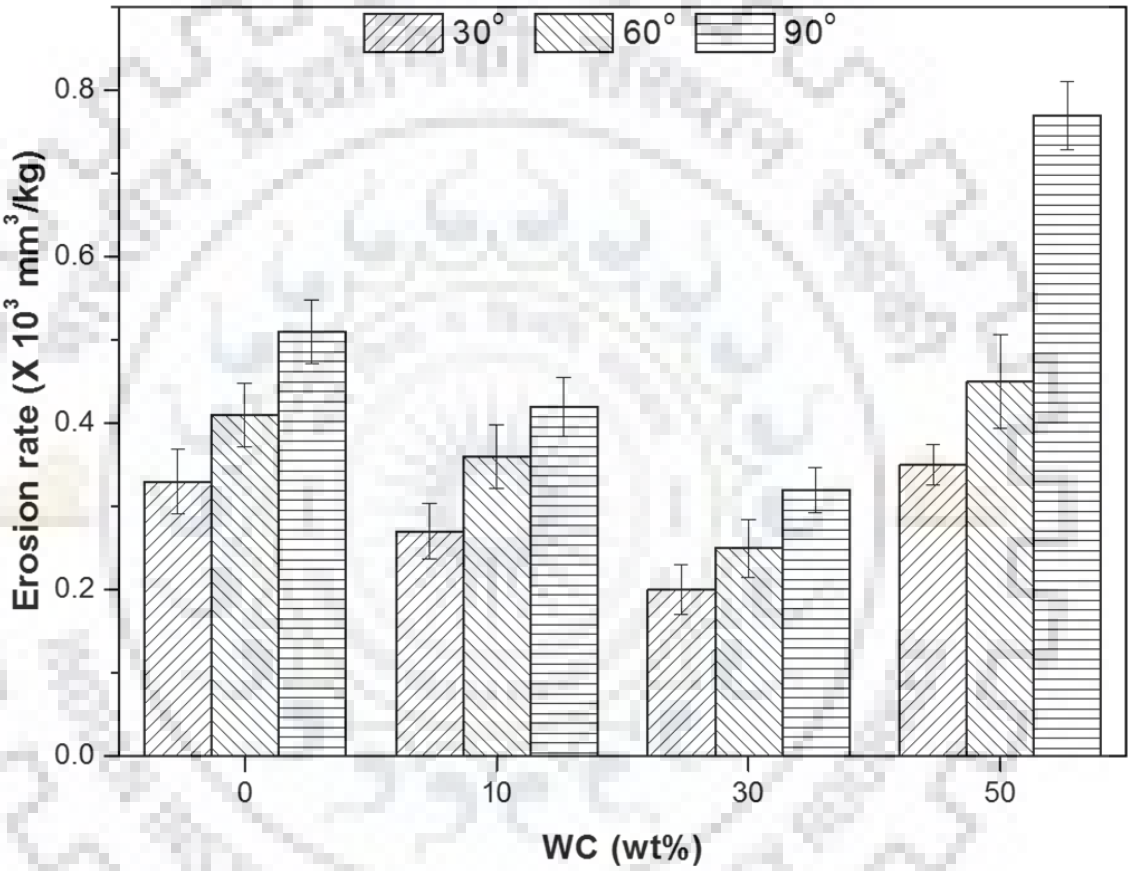

Figure 6.1. Erosion rate of SiC-WC composites as function of WC content and impingement angle at 800ºC

6.2.2. Worn surface analysis

Worn surfaces of the composites eroded at 800ºC and different angles of impingement (30º, 60º or 90º) of SiC erodent were studied in detail to elucidate dominant material removal mechanisms. Typical SEM images of eroded SiC ceramics after erosion at 30º, 60º and 90º show indentation-induced fracture and pull-out of grains at higher angles, while compaction of deformed surfaces is observed at lower angles of erodent impingement (***Figure 6.2***).

Fracture is attributed to the intersection of lateral cracks formed due to the multi-impacts and indentation of irregular shaped SiC particles on brittle SiC ceramics. Similar observations were reported earlier on high temperature erosion of SiC-Si_3N_4 ceramic composites [Li 2014]. When eroded by silicon carbide particles, extrusion of silicon nitride phase weaken the matrix and further fracture of silicon carbide grains were observed as dominant mechanisms of material removal in erosion of SiC-Si_3N_4 [Li 2014]. The smooth surfaces were attributed to compacted debris on multi-impacts and rolling of erodent at lower angles of impingement. EDS analysis of worn surfaces of monolithic SiC ceramics primarily indicates oxidation of silicon carbide at 800ºC (see ***Figure 6.2d***). Formation of glassy silica phase prevents the surface fracture during erosion at elevated temperatures [Li 2014, Wiederhorn 1983; John 1975; Mendiratta 1977; Huang 2012; Sharma 2017].

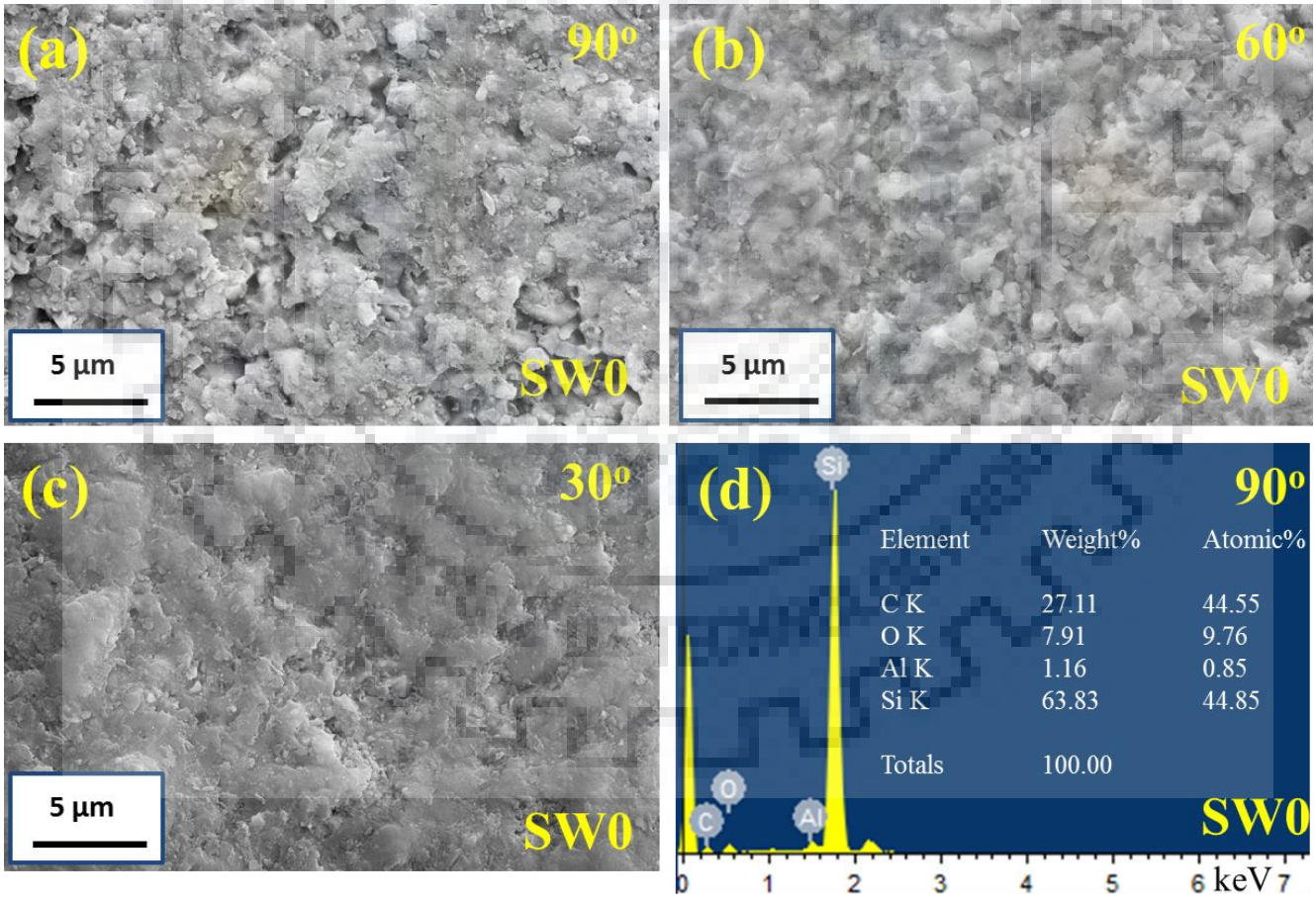

Figure 6.2. SEM images of monolithic SiC ceramics worn at 800ºC with an impingement angle of (a) 90º, (b) 60º and (c) 30º. EDS results of the surface worn at (d) 90º.

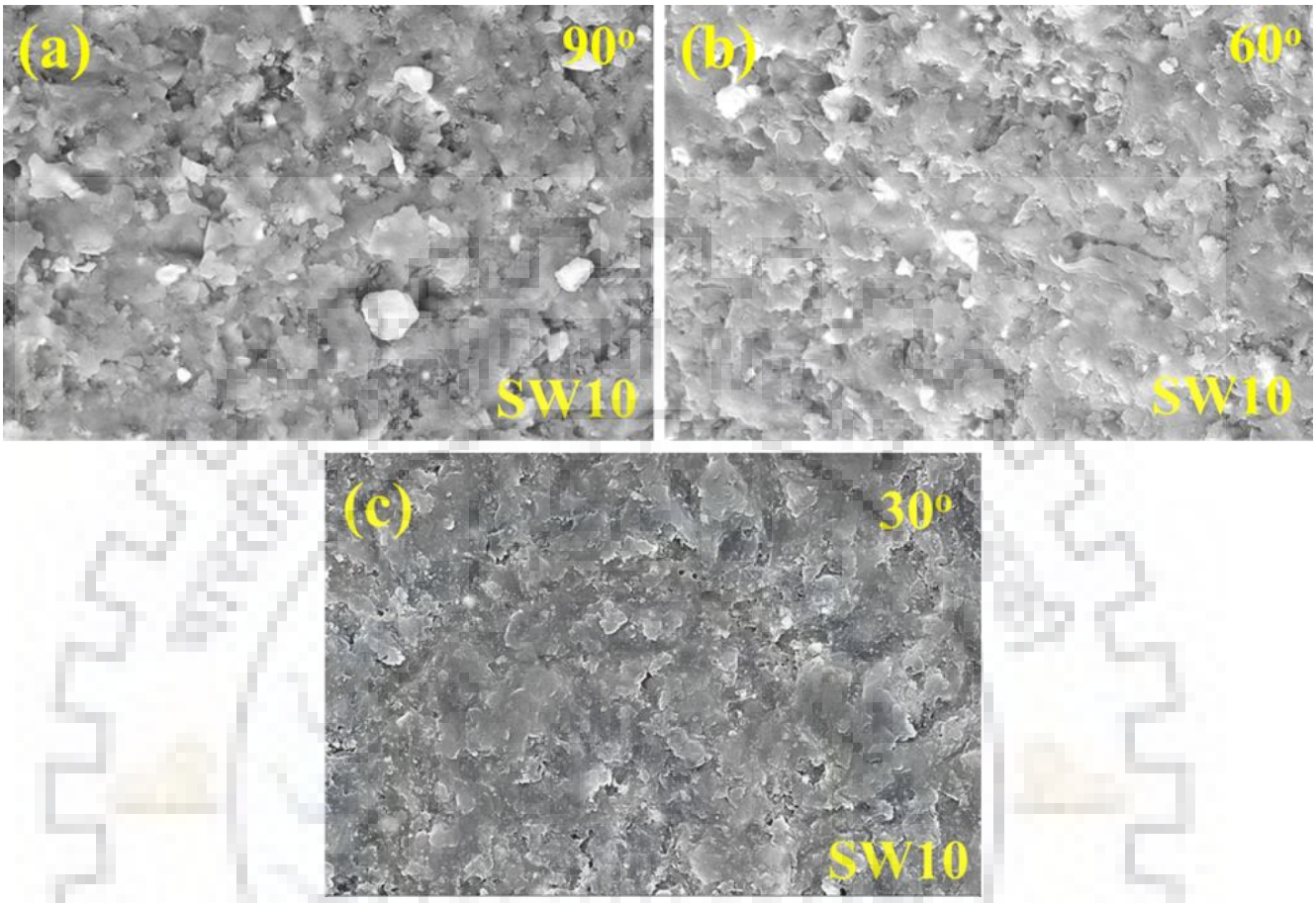

Figure 6.3. SEM images of SiC-10 wt% WC composites worn at 800°C with an impingement angle of (a) 90°, (b) 60° and (c) 30°.

Worn surfaces of SiC ceramics containing 10, 30 and 50 wt% WC are shown in **Figures 6.3-6.5**. The pull-out of WC particles (bright phase) from eroded surfaces is observed for different angles of impingement. It is interesting to observe less fracture for SiC-WC composites compared to SiC ceramics. Further, SiC-30 wt % WC composite showed mild pull-out of WC particles and SiC grain fracture on erosion at any impingement angle when compared to other composites (see ***Figure 6.4***). This indicates less damage for the SiC-30 wt% WC composite after erosion. But, with a further increase in WC content to 50 wt%, the worn surface reveals increased fracture and pull-out of WC particles from the SiC surface (see ***Figure 5***).

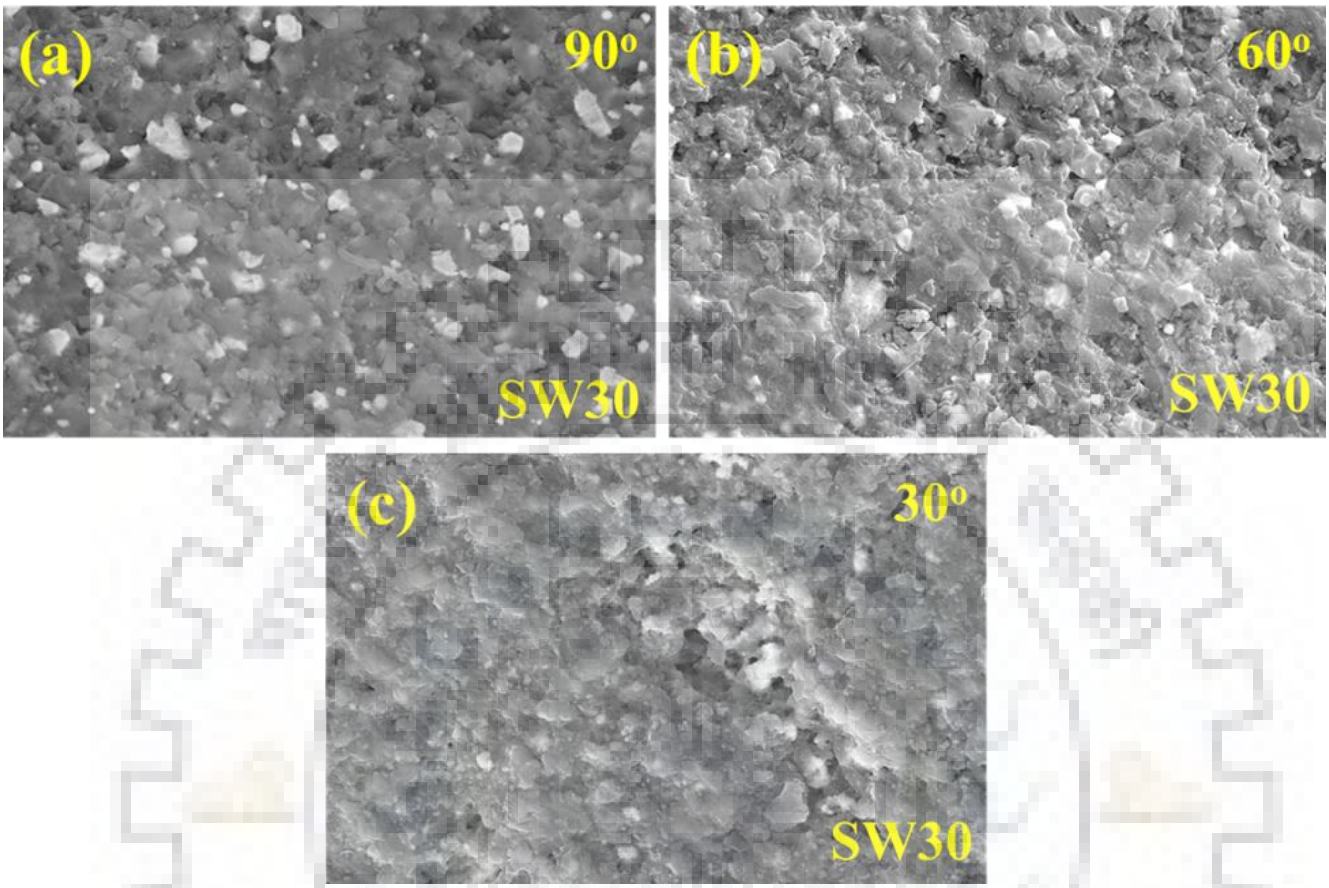

Figure 6.4. SEM images of SiC-30 wt% WC composites worn at 800°C with an impingement angle of (a) 90°, (b) 60° and (c) 30°.

High erosion loss in SiC-50 wt% WC composites attributed to easy removal of heavy WC particles and severe fracture of SiC grains. **Figure 6.5d** shows EDS analysis of worn surface of SiC-50 wt% WC composite after erosion at 90°. It indicates major presence of Si, W, C, and O. Presence of oxygen indicates the formation of silica, and/or tungsten oxide during erosion at 800°C. XRD analysis of eroded SiC-50 wt% WC composite also supports formation of silicon oxide and tungsten oxide (*see **Figure 6.6***). The less damage observed in the SiC-30 wt% WC composite is due to homogeneously distributed WC particles in its microstructure when compared to agglomerated WC particles in SiC-50 wt% WC composite. Superior hardness of the SiC-30 wt% WC composite compared to other SiC-WC composites is also responsible for the lowest wear of the composites.

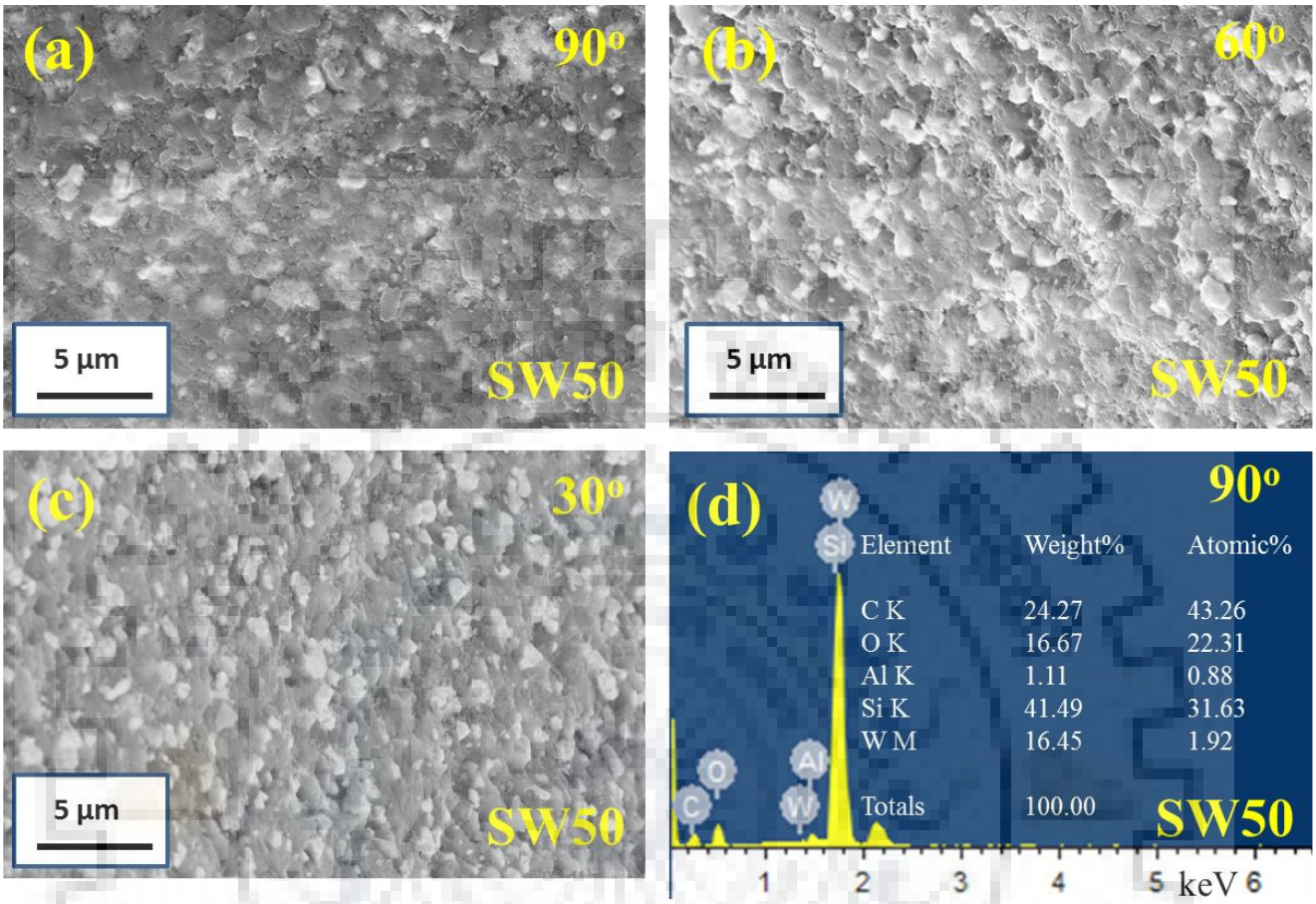

Figure 6.5. SEM images of SiC-50 wt% WC composite worn at 800°C with an impingement angle of (a) 90°, (b) 60° and (c) 30°. (d) EDS results of the surface eroded at 90°.

6.2.3. Influence of impingement angle on erosion behavior

The dominant mechanisms of material removal for the brittle ceramics in solid particle erosion wear conditions are elastic-plastic deformation based micro-fracture and crack formation below the plastic zone of subsurface [Colclough 1997; Li 2014; Kim 1998, Routbort 1980a,b; Evans 1977]. With an increase in the angle of particle impingement, material removal by lateral cracks increases and reaches a maximum at normal incidence for SiC based ceramics [Colclough 1997; Li 2014; Sharma 2014; Hutchings 1992]. Results in the present work show higher wear of SiC ceramics and SiC-WC composites at normal incidence (*see* ***Figure 6.1***). Highest erosion rate of 770 mm^3/kg is obtained for SiC-50 wt% WC composite at normal incidence. Lowest erosion rate of 210 mm^3/kg is obtained for SiC-30 wt% WC composites at 30° impingement angle. SEM images of eroded surfaces of the SiC-WC

composites also reveal increased fracture of SiC grains at high angle of impact of SiC erodent at 800ºC. WC particles are pulled-out in the case of SiC-WC composites. Less fracture and removal of SiC grains and WC particles are observed at shallow angles. This can be ascribed to the less contribution of kinetic energy of erodent particles in indentation fracture of the surface at lower angle. With increasing angle of impact, the increased normal force leads to increased cracking of grains and higher wear [Li 2014].

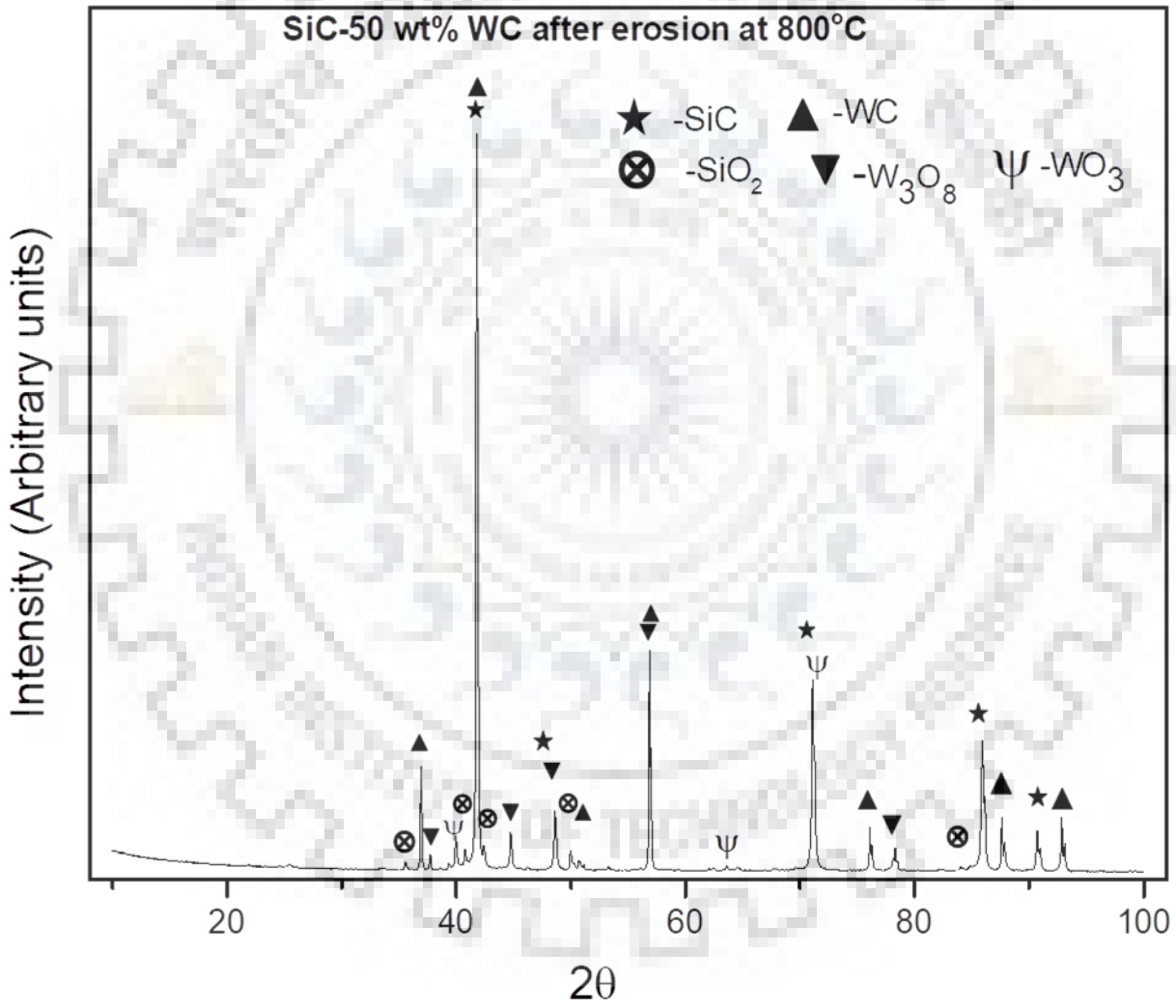

Figure 6.6. XRD analysis of surface of SiC-50 wt% WC composite after erosion at 800ºC.

6.2.4. Influence of WC content

In the present study, the influence of WC content on high temperature erosion behavior of SiC ceramics is observed. SiC-10 wt% WC composites showed reduced erosion rate compared to that for monolithic SiC ceramics at 800^{o}C. With increasing WC content from 0 to 30 wt%, SiC ceramics showed decrease in erosion rate with reduced fracture at any angle of impingement (comparing ***Figures 6.2 to 6.3 & 6.4***). SiC-30 wt% WC composites exhibited lowest fracture and wear among the materials investigated herein. Further, addition of WC upto 50 wt% resulted in agglomeration and easy fracture or removal of WC particles (see ***Figure 6.5a***). At elevated temperature, fracture of SiC grains and weak binder phase led to easy removal of weakly bonded agglomerates of WC particles. Easy removal of heavy WC particles caused high weight loss for the SiC-50 wt% WC composites. Since there was no restriction to fracture after removal of WC, SiC grains were subjected to easy fracture that led to the increased wear for SiC-50 wt% WC composites. This is also in agreement with the erosion rate data provided in **Figure 6.1**. The homogeneously distributed WC particles throughout the SiC microstructure are attributed to the reduced fracture of SiC grains in case of SiC-30 wt% WC composite.

6.2.5. Effect of Mechanical Properties

SiC based ceramics are reported to retain mechanical properties at high temperature upto 1400^{o}C-1600^{o}C [Kim 2007, 2017; Rixccker 2001]. In the present study, fracture toughness of the monolithic SiC and SiC-WC composites showed negligible effect on erosion behaviour at 800^{o}C in dynamic loading conditions. With regards to fracture toughness, SiC ceramics with the lowest fracture toughness of 5.8 MPa.m$^{1/2}$ showed higher erosion rate when compared to SiC-10 wt% WC composites with fracture toughness of 6.4 MPa.m$^{1/2}$. Furthermore, SiC-30 wt% WC composites possessing intermediate fracture toughness of 6.5 MPa.m$^{1/2}$ exhibited minimum erosion rate. But, SiC-50 wt% WC composites with the highest fracture toughness of 6.7 MPa.m$^{1/2}$ showed the highest erosion rate at any angle of impingement. On relating erosion rate with the hardness of composites, it is evident that the SiC-30 wt% WC composites with maximum hardness of 26 GPa exhibited the lowest erosion rate at any investigated angle of impingement, whereas SiC-50 wt% WC composites with lower hardness of 24 GPa, showed the highest erosion rate at any angle of impingements. Higher hardness of the composite

caused less fracture by indentation of erodent particles. Therefore it can be said that hardness of the SiC-WC composites is more influential than fracture toughness on erosion behavior at 800^{o}C.

The erosion loss (E) of brittle target materials against given erodent and testing parameters can generally be expressed as [Evans 1978]:

$$E = AK_{Ic}{}^{m} H^{n} \ldots\ldots\ldots\ldots\ldots\ldots\ldots\ldots\ldots\ldots\ldots\ldots\ldots\ldots \textbf{(6.1)}$$

In **Equation (6.1)**, *A* is proportionality constant; K_{Ic} and *H* are fracture toughness and hardness of the target material, respectively. The exponents given by the quasi-static model are $m = 0.11$ and $n = -1.3$, and by the dynamic model $m = -0.25$ and $n = -1.3$ [Routbort 1983]. Wiederhorn and Hockey [1983] used dimensional analysis to fit data obtained for a range of brittle solids with $m = 0.48$ and $n = -1.9$. However, erosion results obtained from the present experimental study are not in agreement with those obtained using Equation (6.11) for different *m* and *n* values. This observation clearly indicates the fact, which was also mentioned in other reported investigations [Routbort 1983; Wiederhorn 1983; Wang 1995; Gant 2015], that the important contribution from microstructural features like grain size, grain, shape, additional phases etc. must be also be considered in the modeling of erosion loss of ceramic composites.

6.3. Summary

Hot pressed SiC-WC composites with 0, 10, 30 or 50 wt% WC content were subjected to solid particle erosion at 800^{o}C against SiC erodent. The erosion behavior of SiC-WC composites as function of WC content and angle (30^o, 60^o or 90^o) of impingement is studied. Further, major material removal mechanisms in erosion at elevated temperature are elucidated. The following are major conclusions:

a) Erosion rate of SiC-WC composites ranged from 2.1 X 10^2 mm^3 /kg to 7.7 X 10^2 mm^3/kg with varying WC content or angle of impingement.

b) The erosion rate of the composites increased with extent of fracture at higher angles of impingement, and decreased with WC reinforcement up to 30 wt%. Minimum erosion wear rate

obtained for SiC-30 wt% WC composites at 30^{o} and maximum erosion rate for SiC-50 wt% WC composites at normal impact.

c) SEM-EDS analysis of worn surfaces revealed grain fracture as dominant material removal mechanism for SiC ceramics, whereas removal of WC particles from the SiC matrix and subsequent fracture of SiC grains observed for SiC-WC composites.

d) Extent of fracture reduced with WC content up to 30 wt% in SiC ceramics at lower impingement angles. Removal of heavy WC particles and severe fracture of SiC grains resulted in increased material loss for SiC-50 wt% WC composites.

CHAPTER 7

Subsurface Analysis of Worn SiC-WC Composites

To assess the origin of material removal mechanisms, subsurface beneath the worn region of SiC-WC composites after dry sliding wear against SiC ball was analyzed and major results are discussed in this chapter. Focused ion beam (FIB) cross sectioning of worn region of SiC and SiC-50wt% WC composite was made to investigate the deformation under the worn surface. HR-TEM analysis was used to explaine the stress induced dislocation and twins in the damaged region.

7.1. Background:

Generally, wear mechanisms of ceramics fall into two categories: wear due to mechanical processes, such as fracture and/or plastic deformation; and wear due to chemical reactions. In sliding wear under high contact stress, wear due to the mechanical processes dominates. Correlations between fracture and wear behavior has been explored in various ways. Earlier few studies were done to understand the deformation and crack generation/propagation underneath thermally or mechanically modified surfaces of the brittle ceramics [Elfallagh 2009; Kanematsu 2004; Desa 1999; Zarudi 1996; Wu 2001, 2003; Hockey 1975]. Elfallagh and Inkson [2009] studied the surface damage and induced cracks around Vickers indents in soda-lime-silicate glass in 3D by cross-sectioning the indents using a focused ion beam (FIB). They qualitatively analyzed the location and shape of the crack within a cluster around indentation and found significant increase in crack density and 3D interconnections with increase in applied indent load from 50 to 200 g. Kanematsu [2004] studied the sub-surface damage caused by scratch testing of silicon nitride; with groove like damaged zone and significant variations in the damage depths underneath the scratched surface being observed with increase in applied load. Zarudi et al. [1996] observed high dislocation density in large size grained alumina underneath single-point scratch. They also observed that rhombohedral twins or inhomogeneous distribution of dislocations led to cracking inside the plastic zone. Wu et al. [2001] studied the sub-surface deformation of machined Al_2O_3 and Al_2O_3-5 vol.% SiC nanocomposite. It was reported that increased depth of deformed surface underneath the damaged zone of the composites actually reduced the

dislocation density and/or the number of twins, which in turn resulted in suppression of fracture. In another comprehensive set of work, Wu et al. [2003] analyzed sub-surface deformation upon indentation scratch of ceramics and ceramic composites; in which deformation/damage and cracks were reported to originate in three stages, *viz.*, (i) crack-free compressed zone (up to ~3 μm depth), (ii) micro-crack zone below compressed zone, and (iii) lateral and median crack zone further deep beneath the micro-crack zone. These cracks/micro-cracks were observed to extend to the surface, causing material removal.

All such reports indicate that observation of the sub-surface damage is critical towards understanding the material removal mechanism taking place during wear of ceramics and ceramic composites. However, no report is available to-date on the observation/analysis of sub-surface damage of worn SiC-based ceramics and composites. Considering the superior wear resistance of SiC-based composites, especially for SiC-WC composites as observed in earlier chapters, the present study focuses for the first time on detailed observations of the sub-surfaces of monolithic SiC and SiC-50vol.%WC subjected to dry sliding wear against SiC counter-body at 20 N normal load. For the same, cross-section SEM observations have been carried out using dual-beam focused ion beam (FIB)/FEG-SEM, along with TEM (and HRTEM) observations with cross-section samples/lamellae prepared using dual-beam FIB/FEG-SEM from right below the worn surface (*i.e.*, wear track).

7.2. Results and discussion

7.2.1. Worn surface features

Typical morphologies of worn surfaces of monolithic SiC and SiC-50 wt% WC composite are shown in **Figure 7.1**. Overall, the worn surfaces show grooving, mechanical and abrasion as dominant wear mechanisms for both the materials. Macrocracks could also be observed on the worn surfaces (indicated by arrows in ***Figures 7.1c and d***), which appear to be relatively suppressed in the presence of WC. It is not unlikely that such cracking may have origin from sub-surface wear damages, as will be presented in the following.

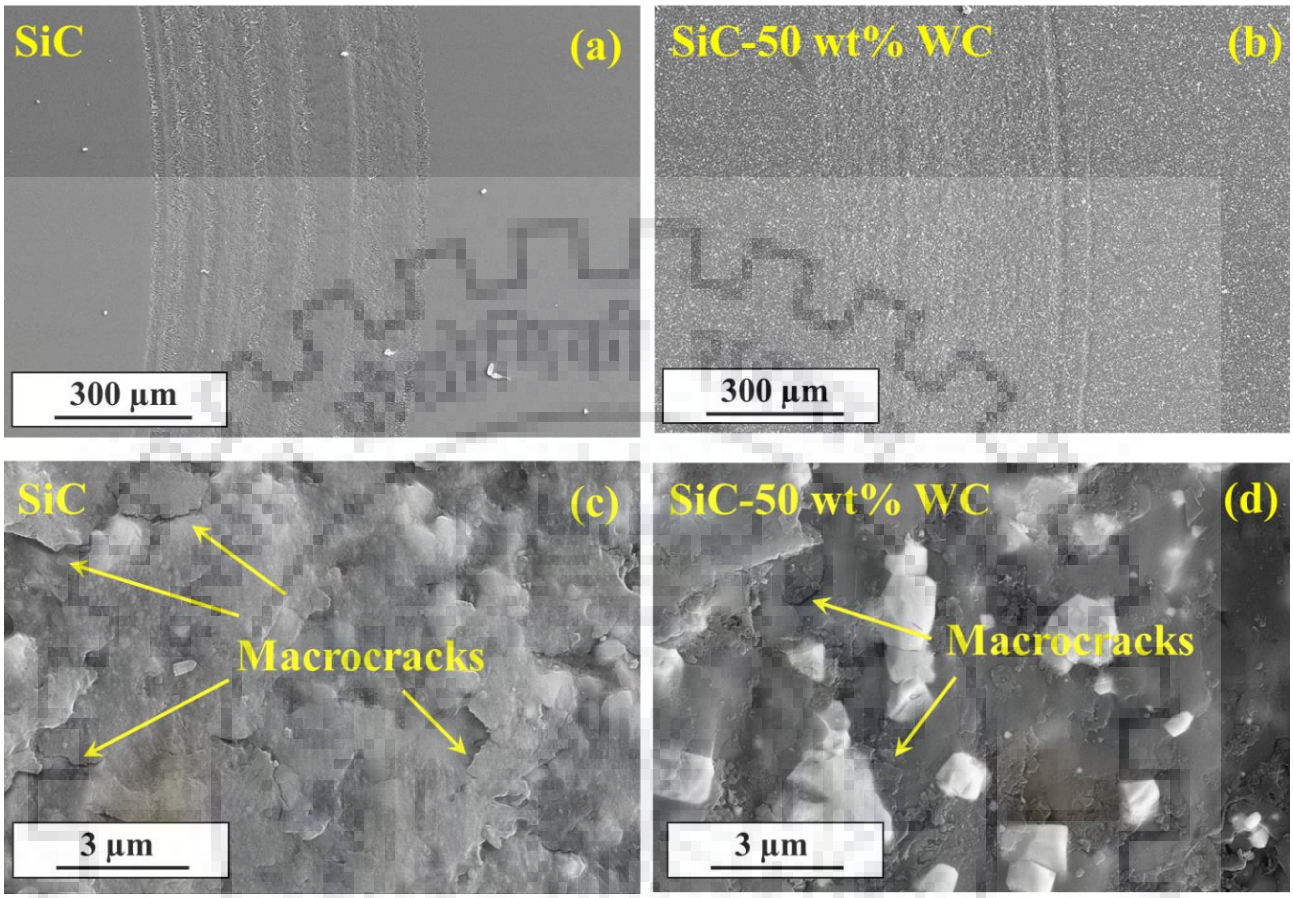

Figure 7.1. SEM images of worn surfaces of monolithic (a and c) SiC and (b and d) SiC-50 wt.% WC composite.

7.2.2. SEM observations of the sub-surface damages and inferences

Cross-section SEM micrographs (as obtained with the dual beam FIB/FEG-SEM) corresponding to the regions underneath the unworn (but polished) surfaces present no evidence for any deformation/damage for both the materials under consideration (*i.e.*, monolithic SiC and SiC-50 wt.% WC) (see ***Figure 7.2***). By contrast, considerable residual damage could be seen underneath the worn regions (*i.e.*, below the wear tracks), as presented in **Figure 7.3**. For both monolithic SiC and SiC-50 wt.% WC composites, two regions, at different depths from the worn surfaces could be demarcated in the cross-sectional SEM images; with them being more prominent for the SiC, sans WC.

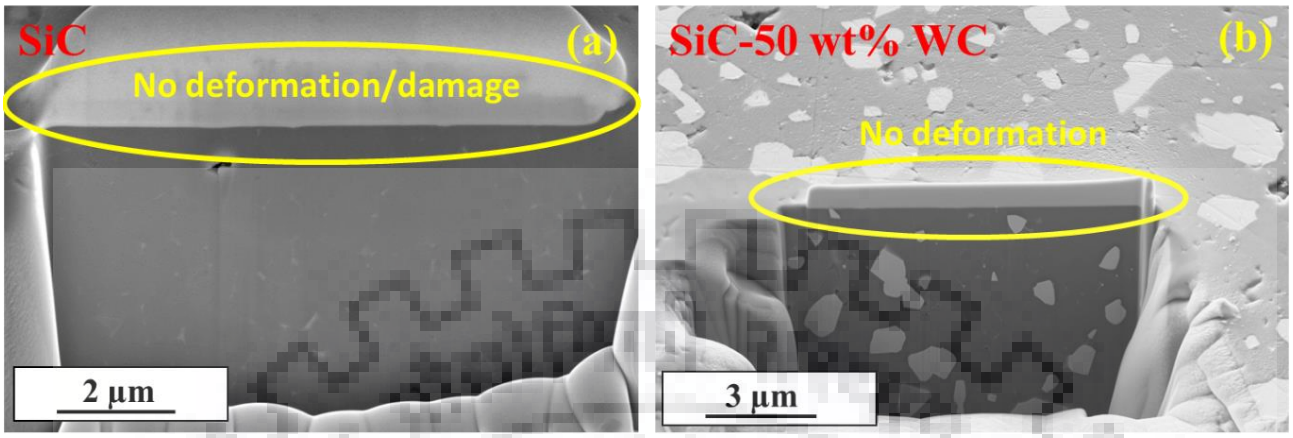

Figure 7.2. Cross-sectional SEM images obtained using dual-beam FIB/FEG-SEM from the unworn regions of (a) SiC, and (b) SiC-50 wt.% WC composite.

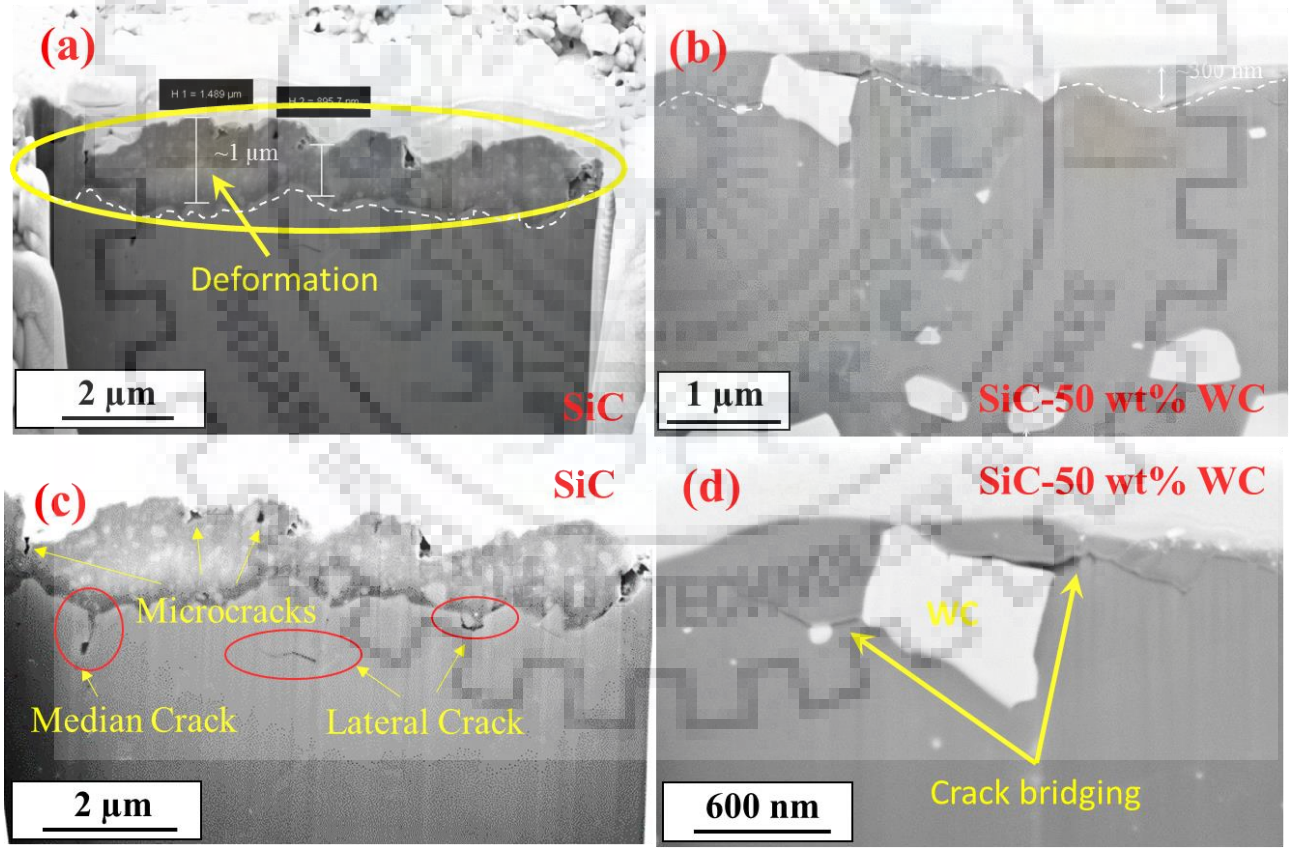

Figure 7.3. High magnification cross-section SEM images underneath the worn surfaces of (a and c) monolithic SiC and (b & d) SiC-50 wt.% WC composite.

Even though, it is not possible to state with certainty just based on SEM observations, the regions immediately below worn surfaces are possibly sub-surface deformation zones; more insights into which will be presented based on the TEM observations in the following sub-sections. In a point contact, stress field is known to result in sub-surface plastic deformation in ceramic materials [Lawn 1981; Hilton 2013; Bian 2015]; with such multiple (dynamic) point contacts taking place during the present dry sliding wear tests. More importantly, the observations indicate that the thickness of such deformed region is considerably greater in the case of monolithic SiC (~1 μm), compared to that in the SiC-50 wt% WC composite (~300 nm) (see ***Figure 7.3***). Below the deformed regions, the presence of median and lateral cracks could be observed (**Figures 7.3c and d**). Such cracks were observed to get bridged and deflected by the WC grains in the case of the composites; with nearly no crack being observed to penetrate considerably through the WC (see ***Figure 7.3d***). Such crack bridging was observed also on the fractured surfaces, as reported in ref. [Sharma 2014].

Closer observation of the cross-section images indicate the presence of microcracks below the worn surface (starting in the deformation zone itself) till up to ~2 μm depth in the case of monolithic SiC. Microcracking is expected where the stress field starts to be dominated by tensile components. Directional stress concentrations due to difficulties in initiation of enough independent slip systems and accommodating shape change primarily lead to the nucleation of cracks, even in the case of ceramic materials [Bajwa 2005, Mukhopadhyay 2011]. However, such sub-surface micro-cracking appeared to have been considerably suppressed in the presence of WC.

Accordingly, the sub-surface damage/features underneath the work surfaces of monolithic SiC and SiC-50 wt.% WC composite can be described in terms of two regions; *viz.*, a plastically deformed region immediately below the worn surface, also containing some micro-cracks (considerably suppressed in terms of layer thickness and micro-cracking in the presence of WC), followed by a zone comprising of extensive lateral and median cracking underneath (again, cracking suppressed by WC grains). Schematic illustration for the same is shown in **Figure 7.4**. Such observations suggest that the lateral cracks propagate and get connected to the surface (possibly via the micro-cracks), leading to the wear damage. WC particles in SiC-WC composite restricting the propagation of such cracks. The first region underneath the worn surface of SiC-50 wt.% WC composite has been

carefully observed in TEM in order to better understand the aspects related to deformation and micro-cracking.

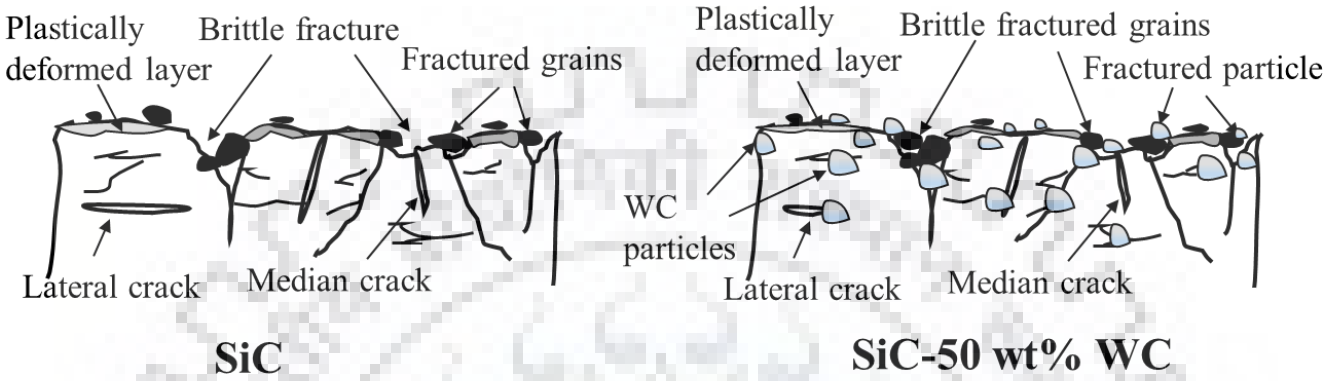

Figure 7.4. Schematic illustration of wear mechanisms during sliding wear of monolithic SiC ceramics and SiC-50 wt% WC composite.

7.2.3. Cross-sectional TEM observations

7.2.3.1. Microstructure and interfacial characteristics

Figure 7.5 shows the selected region of worn SiC-50 wt% WC composites from where lamella for the TEM sample was took-off and prepared TEM sample.

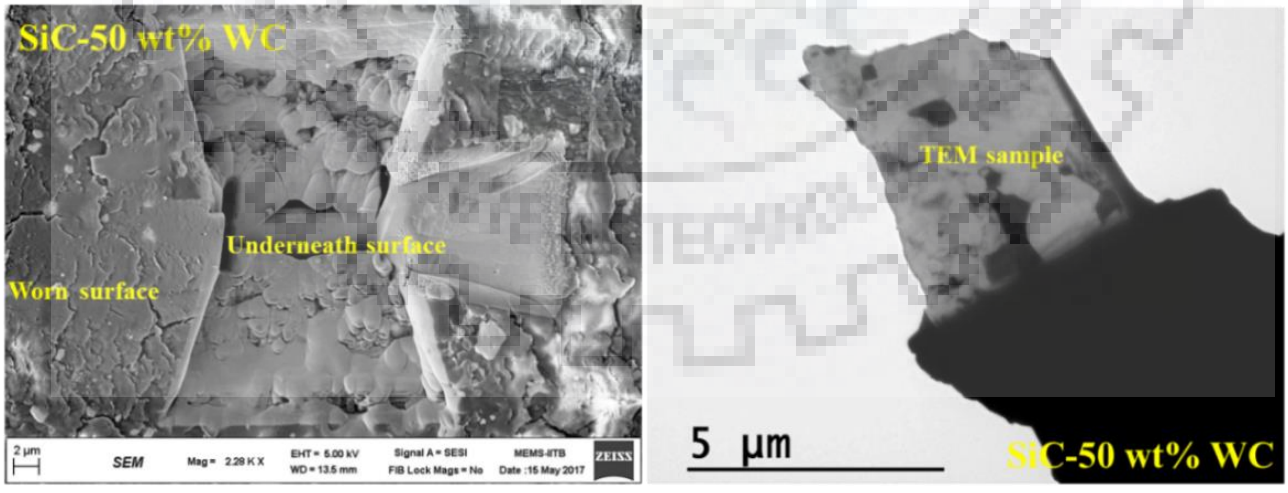

Figure 7.5. (a) Worn region of SiC-50 wt.% WC composite from where the cross-section TEM-lamella (as shown in b) has been prepared using the Omni probe nano-manipulator inside dual-beam FIB/FEG-SEM.

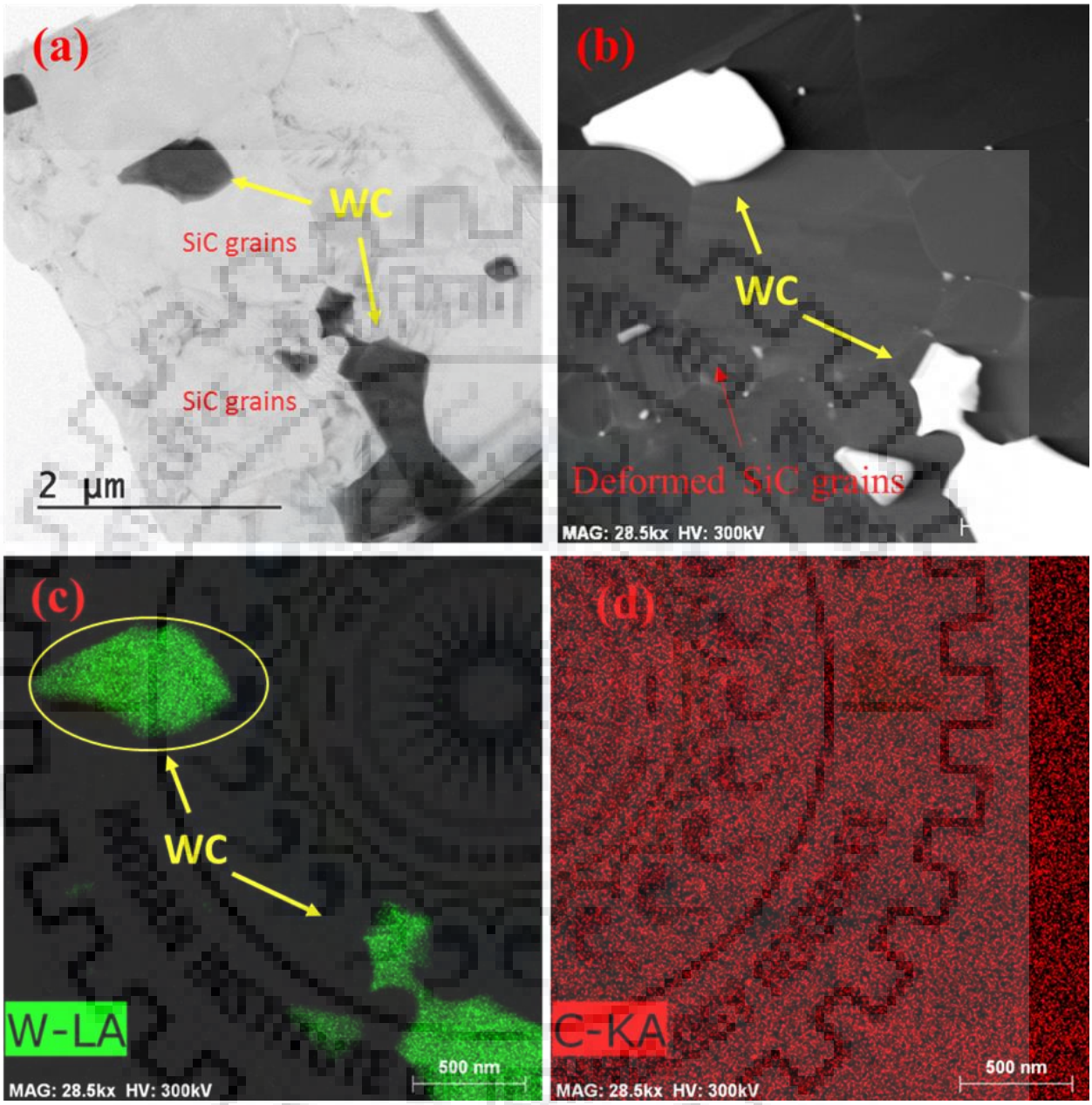

Figure 7.6. (a) BF and (b) STEM image of SiC-50 wt% WC composite. (c) & (d) EDS mapping indicating the presence of WC particle.

Representative bright field (BF) and STEM images, along with EDS mapping of SiC-50 wt% WC composite, are shown in **Figure 7.6**. EDS mapping confirms that the grains appearing brighter in contrast in **Figure 7.6b** are those of WC. HRTEM images obtained at the SiC/WC interfaces (***Figure 7.7a***) show the absence of any amorphous phase at the interfaces and indicates good

bonding at the atomic level between SiC and WC. This presumably forces most of the cracks to propagate through the SiC grain (rather than along the interface). This is likely to be one of the factors responsible for the dominant fracture mode being transgranular in case of the SiC-WC composites.

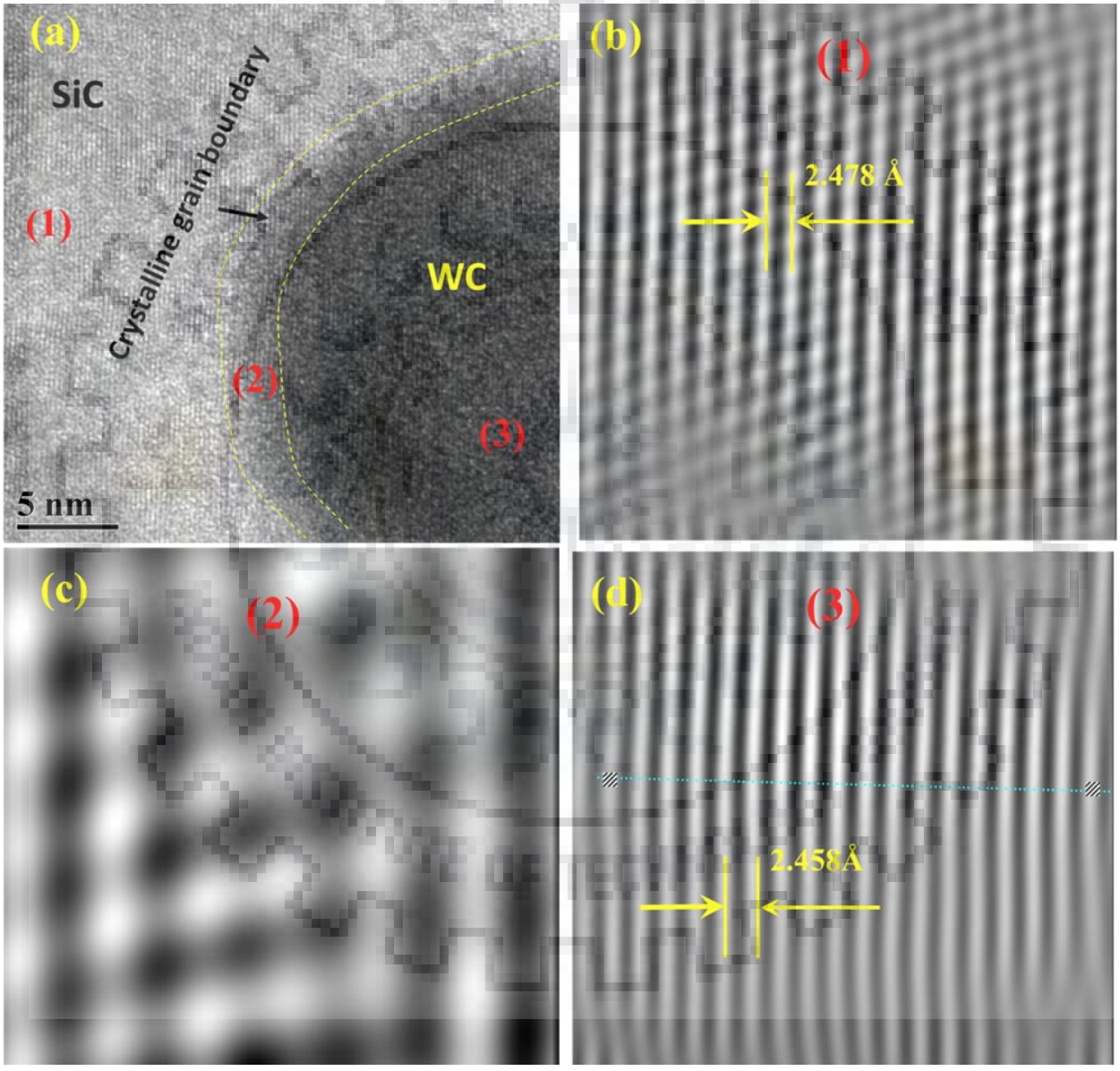

Figure 7.7. (a) BF-TEM images of SiC-50 wt% WC composite subsurface and (b) HR-TEM image of interface of SiC and WC. IFT images of zone (1), (2) and (3) are shown in (c), (d), and (e) respectively.

The atomic arrangements, as inferred based on the inverse Fourier transformed (IFT) images for SiC confirm the hexagonal structure with inter-planar spacing of 2.478 Å for the (103) plane (see **Figure 7.7b**). The IFT images for the interface also indicate crystalline nature (as mentioned above), but with distorted atomic arrangements (see **Figure 7.7c**). The IFT images corresponding to WC also indicate hexagonal structure with inter planar spacing of 2.458 Å for the (222) plane (see **Figure 7.7d**). The selected-are diffraction patterns (SADPs), as obtained from the respective phases (see ***Figures 7.8***), also re-confirm the above.

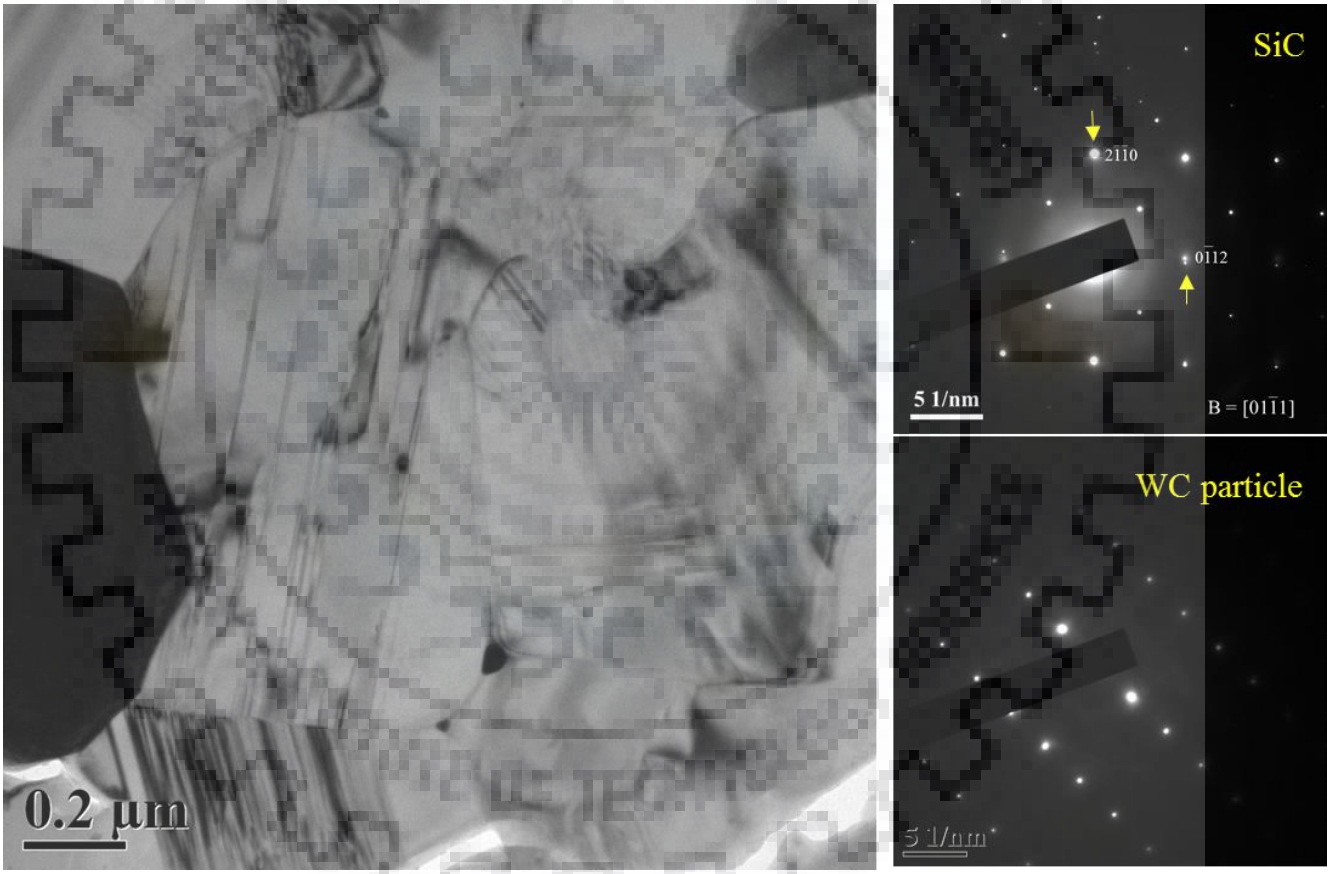

Figure 7.8. (a) High magnification BF-TEM image of subsurface of SiC-50 wt% WC composite after sliding wear. (b, c) diffraction patterns (SADPs) of SiC and WC particle respectively.

7.2.3.2. Observation of plastic deformation zone under the worn region

Typical BF-TEM images (in **Figure 7.9**), as obtained from the deformed regions underneath the worn surface of the SiC-50 wt.% WC composite, show deformed phases and interfaces. TEM images show extensive dislocation activity, twinning and also microcracking in the SiC phase.

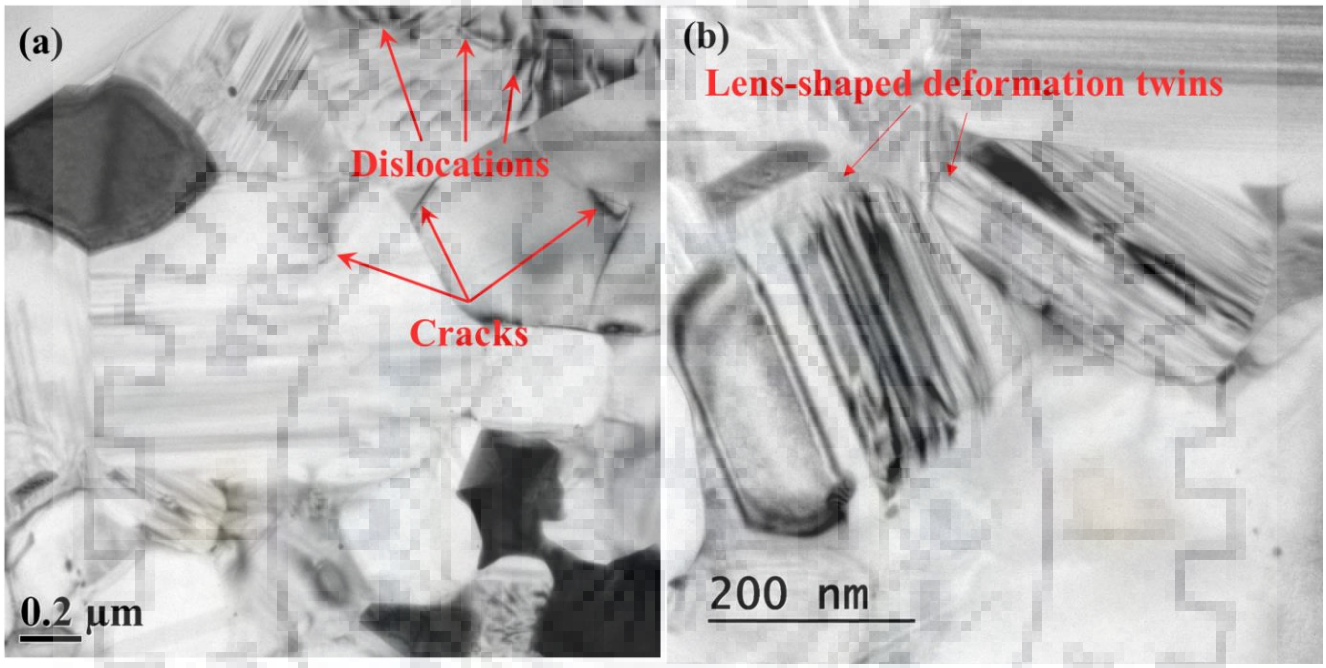

Figure 7.9. (a) High magnification BF-TEM image of subsurface of SiC-50 wt% WC composite after sliding wear. (b) Lens-shaped twins in SiC grains.

The residual dislocations observed in the SiC grains (with very low stacking fault energy [Maeda 1988; Hong 2000; Iwata 2003]) are likely to have been caused by the mechanical stresses associated with the interactive sliding under normal load. In addition to dislocation activity, TEM images indicate that more dominant deformation mode has been that of twinning, with the typical lens-shaped deformation twins being present in nearly all the SiC grains. The 'twin-spots' identified in the SADP corresponding to the SiC phase also indicate the presence of twins (see ***Figure 7.8***). This is not unexpected since less number of slip systems available in the typical hcp structure of SiC ceramics is known to promote twinning as the dominant mode of deformation. It must be mentioned here that presence of dislocations and deformation twins in sub-surfaces underneath indentations, scratches and worn surfaces of alumina, SiC and zirconia based ceramics was attributed to the

associated stress fields [Zarudi 1996; Wu 2001, 2003; Hockey 1975; Mukhopadhyay 2011; Hockey 1978; Canneto 2016], followed by median/radial cracking (as also observed in this case; see **Figures 7.4 and 7.5**).

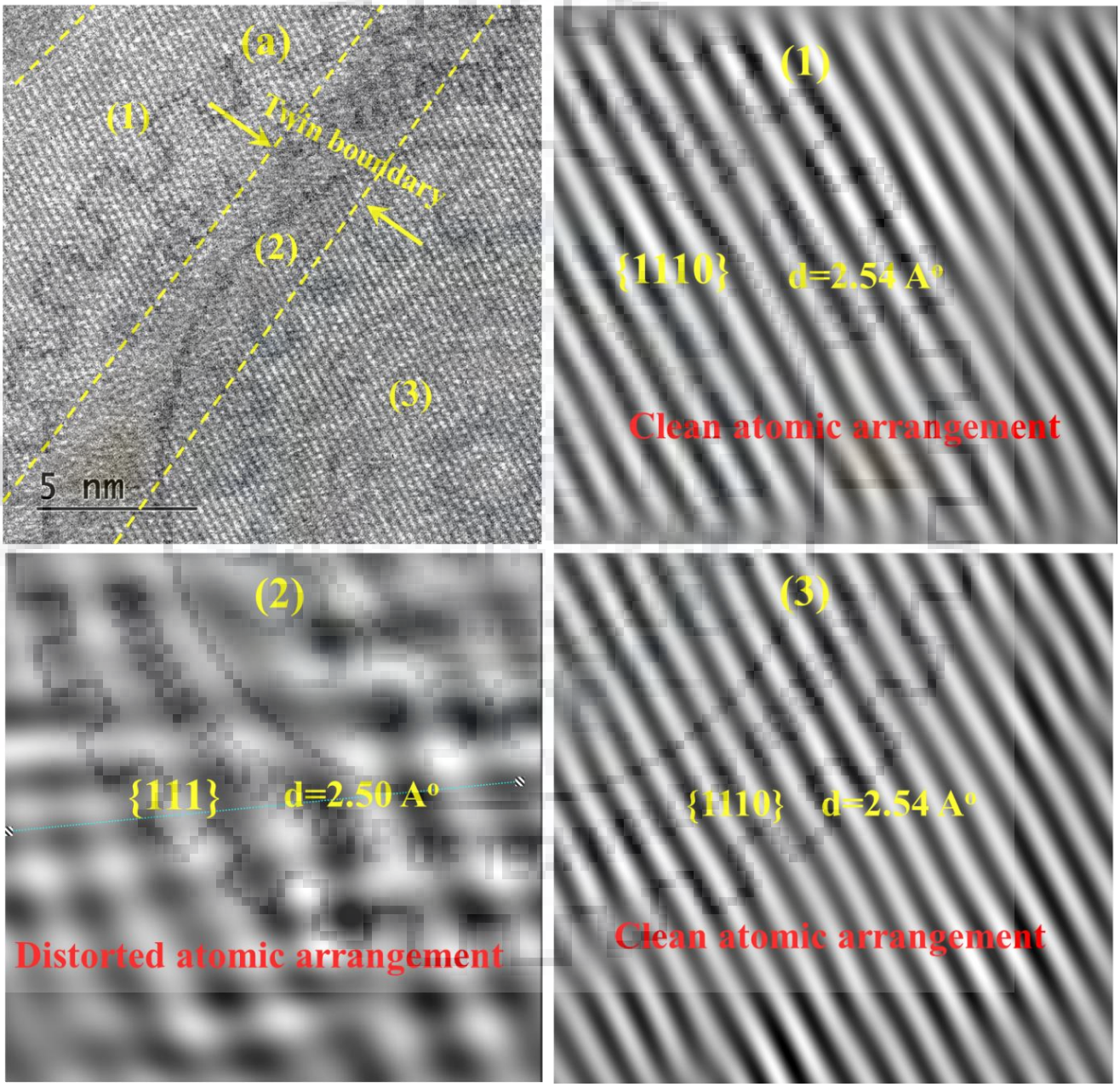

Figure 7.10. (a) HR-TEM image of twin, (b, c and d) IFT image of zone 1, 2 and 3 respectively.

In order to get more fundamental insights into the deformation twins in SiC, some of them were further analyzed by capturing HRTEM images, as shown in **Figure 7.10**. Zones (1) and (3) in **Figure 7.10a** are twinned zones, whereas zone (2) is the twin boundary. The atomic arrangements in the twinned zones (1) and (3) conform to rhombohedral structure with inter-planar spacing of 2.54 Å for the {1110} plane. The further zoomed-in IFT images of the twin boundary (zone (2)) show distorted atomic arrangements conforming to cubic structure and {111} plane. Such observations agree with the transformation of parent hexagonal structure to rhombohedral and cubic structures due to thermal or mechanical deformation [Kackell 1999; Pirouz 1993; Jayaseelan 2011]. Dislocation mechanism is responsible for the deformation induced polytypic transformation of SiC ceramics [Pirouz 1993]. Also, energy barriers for 6H→3C are reported to make the dislocation mechanism highly favorable for polytypic transformations in SiC ceramics [Pirouz 1993]. In the present study, dislocations induced polytypic transformation is believed to result from the compressive stresses generated during sliding. However, no such deformation sub-structure could be seen in the WC grains.

In this context, it is also not unlikely that the stresses at the tips of the piled-up dislocations and twins played some role towards the generation of the sub-surface cracks/micro-cracks in SiC and SiC/SiC interfaces, but which in turn got suppressed in the presence of the second phase particles (in the present case, WC) and accordingly contributed towards improving the wear resistance. Such phenomena was also reported earlier in the cases of Al_2O_3 (again, having hcp structure) and also MgO-based ceramics-composites/alloys [Zarudi 1996, Wu 2001, Mukhopadhyay 2011, Merino 2005, Gurnani 2006]. Such insights based on the TEM observations also agree very well with the observations based on the cross-section SEM images (as presented earlier in sub-section 3.2 and ***Figs. 7.2 and 7.3***).

The present study necessarily reveal the deformation and microcracking zones beneath the worn surfaces of SiC ceramics in sliding wear and beneficial role of WC in stopping crack propagation. Also, stress induced dislocation/twins networks are noted in SiC grains, whereas no such deformation signature found in WC grains.

7.3. Summary

The sub-surface regions underneath worn surfaces (after sliding wear under 20 N load) of monolithic SiC and SiC-50 wt.% WC composite were investigated in cross-section mode using dual-beam FIB/FEG-SEM and TEM (including HR-TEM). In more specific terms, the major observations and inferences can be summarized, as in the following.

(a) Cross-sectional FIB/SEM images indicate that the deformation zones underneath the worn surfaces are larger (~1 μm depth) for monolithic SiC, as compared to SiC-50 wt.% WC composite (~300 nm depth).

(b) Microcracks are observed in the deformation zone, that extend up to depth of ~2 μm downwards in the case of monolithic SiC, eventually connecting with the lateral and radial cracks, thus leading to material removal.

(c) The WC grains (atomically bonded to SiC grains, without any interfacial amorphous phase) are observed to suppress such crack propagation by bridging and deflection in the case of the SiC-WC composite; thus contributing partly in this way towards the considerably reduced rate of material removal during sliding wear.

(d) The deformation zone is observed to be comprised of extensive dislocation and twin networks, along with microcracks in the SiC grains. By contrast, no such deformation substructure could be seen in the WC grains, which also appeared to block the dislocations/twins at the interface from further propagation. This is also expected to have partly contributed towards suppression of microcrack formation (due to stress build-up at the tip of dislocations/twins) and accordingly the improvement in wear resistance upon incorporation of WC in SiC.

CHAPTER 8

Conclusions and future scope

8.1. Conclusions

The major aim of the present investigation is to investigate the tribological potential of SiC-WC composites in different tribological conditions. In particular, influence of composition (microstructure), mechanical properties on tribological behaviour of the SiC-WC composites is studied. Hot pressed SiC ceramic composites prepared with varying WC content (0 to 50 wt %) were investigated in continuous sliding, reciprocated sliding and solid particle erosion wear conditions. The major part of this thesis work is aimed to elucidate the material removal mechanisms of SiC-WC composites in the given wear conditions. In addition, surface beneath the worn region is analyzed for their post-wear morphology to understand the origin of contact surface fracture during sliding wear. The total research is broadly divided into four major parts. Salient results obtained from each experimental part is provided herewith.

In **Chapter 4**, the effect of load (5 N, 10 N and 20 N) on friction and wear behavior of SiC ceramics is discussed in unlubricated continuous sliding wear conditions. Further, effects of WC content in the composites and counterbody (SiC, WC and steel) materials on tribological behavior during sliding wear are particularly discussed. This is followed by the study of major material removal mechanisms in different sliding conditions. Results demonstrated that the COF is independent of the counterpart material hardness. Highest average steady state COF of 0.66 against WC-Co ball and lowest of 0.34 against steel are recorded. However, wear volume of SiC-WC composites is dependent on hardness of the counterbody ball. With increase in WC content from 0 to 50 wt%, wear volume decreased against any ball. SiC-WC composites exhibited maximum wear resistance with 50 wt% WC content. Change in dominant wear mechanisms observed with type of counterbody. Mechanical fracture was dominant on worn SiC-WC composites against SiC counterbody, while worn surfaces of composites revealed tribochemistry with increased WC content against WC-Co or steel counterbody.

Considering highest wear obtained against SiC ball in the previous chapter, tribological behaviour of the composites in reciprocated sliding wear conditions against SiC ball is studied in

Chapter 5. Tribological behaviour of the SiC-WC composites is discussed as function of (10-50 wt%) WC content and temperature (ambient and 500^{o}C). Results obtained from this study demonstrated that the coefficient of friction decreased from 0.4 to 0.3 with WC content at room temperature. SiC-50 wt% WC composites exhibited highest wear resistance during reciprocated sliding at ambient temperature. However, SiC-30 wt% WC composites exhibited maximum wear resistance at high temperature. Effect of high humidity (55±5% RH) (compare to (40 ±10% RH) in continuous sliding study) is also notable in domination of responsible mechanism of material removal. Worn surface analysis indicated tribochemistry as major material removal mechanism for sliding in ambient conditions, whereas microfracture dominated at 500^{o}C. Wear results obtained at high temperature are consistent with the lateral fracture model for wear volume estimation.

In the C**hapter 6,** high temperature (800^{o}C) erosion response of SiC-WC composites against SiC erodent particle is provided. Effects of WC content and angle of impingement of SiC erodent on erosion behaviour of SiC-WC composites are highlighted. Changes in material removal mechanisms with varying erosion test parameters and WC content in the composites are explained. Results obtained from this study demonstrated that the erosion rate of the composites increased with increasing the impingement angle from 30^{o} to 90^{o}, and decreased with WC content up to 30 wt%. Minimum and maximum erosion wear rates were respectively obtained for SiC-30 wt% WC composites at 30^{o} and for SiC-50 wt% WC composites at normal impact. Grain fracture and pull-out were found as major mechanisms of material removal for the composites. Decreased angle of impingement led to reduced grain fracture and pull-out and hence reduction in material removal. Owing to increased fracture toughness with incorporation of WC particles, the composites showed less fracture and removal of WC particles up to 30 wt%. Weak upholding of WC particles and severe fracture of SiC grains at normal impact led to large amount of material loss for SiC-50 wt% WC composites.

In **Chapter 7**, surface beneath the worn region is critically analyzed to evaluate the origin of material removal mechanisms after sliding wear. In monolithic SiC ceramics, significant damage of ~ 1 µm thickness is observed beneath the worn region, whereas plastically deformed region beneath the worn region limited to ~ 300 nm in the SiC-50 wt% WC composite. Beneath the damaged region, microcracks are initiated and extended up to ~2 µm downwards the worn surface for SiC ceramics; eventually leading to material removal. Deformation zones consisting of extensive dislocation and twin networks in SiC grains are observed immediately below the worn surface; followed by

lateral/radial/median cracks. WC grains not only stop the twins/dislocation networks at the SiC/WC interfaces, but also considerably restrict the crack propagation by deflection/bridging in the SiC-WC composites.

The outcome of the present research can be realized in terms of: (i) Optimum composition of SiC-WC composites for superior performance in given wear conditions. (ii) Physics of material degradation mechanisms of SiC-WC composites as function of composition and wear test parameters. Results obtained strongly indicate that SiC ceramics prepared with 50 wt% WC content is optimum for room temperature sliding wear applications, whereas SiC ceramics prepared with 30 wt% WC content is recommended for high temperature sliding wear and high temperature erosion wear applications. The major material degradation mechanism of SiC-WC composites in continuous sliding wear condition is changed from mechanical fracture against SiC ball to tribochemistry against WC-Co or steel ball. In reciprocated sliding, composites reveled tribochemistry as major material removal mechanism in ambient temperature, while mechanical fracture dominated during sliding at 500^{o}C. Pull-out of WC particle and subsequent SiC grains fracture dominated in wear for SiC-WC composites during high temperature solid particle erosion conditions. Extent of fracture and pull-out reduced at lower angle of SiC erodent impingements. Present thesis demonstrated the presence of stress induced dislocations and twins underneath the sliding wear surface of SiC-WC composite. WC particle restrict the propagation of surface or subsurface cracks and contributed towards wear of the materials.

8.2. Scope for future work

- In the present work, effects of load, WC content, counterbody and temperature on tribological behaviour are understood in unlubricated sliding wear conditions, while the study can be extended for the effect of other parameters like speed humidity etc.
- Similarly, effect of test parameters and materials (WC content) on friction and wear properties in water or oil lubricated sliding wear conditions can be studied.
- The erosion wear can be further studied to understand the effect of velocity of particle impingement and type of erodent particles in high temperature erosion conditions.
- The potential of the newly developed SiC-WC composites can be further assessed by the studying the behaviour in other wear modes like cavitation, fretting etc.
- Further, results obtained in experimental wear study can be used to propose analytical models for the estimation of material loss in given wear conditions.
- A study on the subsurface analysis and generation of stress induced dislocation and twins as function of WC content in SiC ceramics and test parameters in given wear conditions is strongly recommended.
- Also, dense SiC-WC composites can be prepared via different advanced technique like spark plasma sintering (SPS) to realize the difference in densification, and subsequent mechanical and wear properties.
- Results obtained in the present study demonstrate the effect of microstructure by the variations of WC contents on tribological behaviour. The composites can be subjected to carefully designed heat treatment in controlled atmospheres to provide significant change in microstructural features such as grain size, grain shape, size distribution etc. and the effect on tribology can be studied to find the optimum composition for the superior performance in given wear conditions.

References:

[1] A. A. Buchheit, Greg E. Hilmas, William G. Fahrenholtz, Douglas M. Deason, Thermal shock resistance of an AlN–BN–SiC ceramic, Journal of the American Ceramic Society 92, [6] (2009): 1358-1361.

[2] A. Anspoks, A. Kalinko, J. Timoshenko, A. Kuzmin, Local structure relaxation in nanosized tungstates. *Solid state communications* 183: 22-26 (2014).

[3] A. Cortes, C. Celedon, R. Zarate, CVD synthesis of graphene from acetylene catalyzed by a reduced CuO thin film deposited on SiO_2 substrates. *J Chilean Chem Soc* 60: 2911-2913 (2015).

[4] A. F. Colclough, J. A. Yeomans, Hard particle erosion of silicon carbide and silicon carbide-titanium diboride from room temperature to 1000°C, Wear 209 (1997) 229-236.

[5] A. G. Evans, M. E. Gulden, M. Rosenblatt, Impact Damage in Brittle Materials in the Elastic-Plastic Response Regime, Proc. of the Royal Society of London **361** 343-365 (1978).

[6] A. G. Evans, M. E. Gulden, M. Rosenblatt, Impact damage in brittle materials in the elastic-plastic response regime, In Proceedings of the Royal Society of London A: Mathematical, Physical and Engineering Sciences- The Royal Society, 361 [1706] (1978) 343-365.

[7] A. G. Evans, T. R. Wilshaw, Dynamic Solid Particle Damage in Brittle Materials, An Appraisal, *J. Mater. Sci*. **12** (1977) 97-116.

[8] A. J. Gant, M. G. Gee, Wear modes in slurry jet erosion of tungsten carbide hardmetals: their relationship with microstructure and mechanical properties, International Journal of Refractory Metals and Hard Materials 49 (2015) 192-202.

[9] A. Kovalcikova, J. Balko, J. Dusza, Influence of Microstructure on Tribological Properties and Nanohardness of Silicon Carbide Ceramics. *Key Eng Mater* 662 (2015) 55-58.

[10] A. Kovalcikova, P. Kurek, J. Balko, J. Dusza, P. Sajgalik, and M. Mihalikova, Effect of the Counterpart Material on Wear Characteristics of Silicon Carbide Ceramics, *Int. J. Refract. Met Hard Mater*., **44** (2014) 12-18.

[11] A. L. Ham, J. A. Yeomans, J. F. Watts, Elevated temperature solid particle erosion of silicon carbide continuous fibre reinforced calcium aluminosilicate glass-ceramic matrix composite, Wear 203 (1997) 387-392.

[12] A. L. Ham, J. A. Yeomans, J. F. Watts, Effect of temperature and particle velocity on the erosion of a silicon carbide continuous fiber reinforced calcium aluminosilicate glass–ceramic matrix composite, Wear 233 (1999) 237-245.

[13] A. L. Ortiz, O. B. Lopez, M. Z. Quadir, F. Guiberteau, A Route for the Pressureless Liquid-Phase Sintering of SiC with Low Additive Content for Improved Sliding-Wear Resistance, J. Eur. Ceram. Soc., 32 [4] (2012) 965-973.

[14] A. Mukhopadhyay, R. I. Todd, Relationship between microstructure and abrasive wear resistance of Al_2O_3–$FeAl_2O_4$ nanocomposites produced via solid-state precipitation, Journal of the European Ceramic Society 31 (2011) 339-350.

[15] A. Muthuraja, S. Senthilvelan, Adhesive wear performance of tungsten carbide based solid lubricant material, Int. J. Refra. Met. & Hard Mater. 52 (2015) 235-244.

[16] A. R. de A. Lopez, J. M. Fernandez, F. M. V. Feria, T. S . Orlova, K. C. Goretta, F. G. Mora, Nan Chen, and J. L. Routbort, Erosion and Strength Degradation of Biomorphic SiC, *J. Eur. Ceram. Soc*., **24** (2004) 861–870.

[17] A. Skopp, M. Woydt, Ceramic-ceramic composite materials with improved friction and wear properties. *Tribol Int* 25 (1992) 61-70.

[18] A. Tewari, B. Basu, and R. K. Bordia, Model for Fretting Wear of Brittle Ceramics, *Acta Mater*., **57 (**2009) 2080-2087.

[19] A. Udayakumar, M. Balasubramanian, H. B. Gopala, P. Sampathkumaran, S. Seetharamu, R. Babu, D. Sathiyamoorthy, and G. R. Reddy, Influence of the Type of Interface on the Tribological Characteristics of ICVI Generated SiC_f/SiC Composites, *Wear*, **271** (2011) 859-865.

[20] A.F. Colclough, J.A. Yeomans, Hard particle erosion of silicon carbide and silicon carbide-titanium diboride from room temperature to 1000˚C, Wear 209 (1997) 229-236.

[21] A.G. Evans, D.B. Marshall, Wear mechanisms in ceramics, in: D.A. Rigney (Ed.), Fundamentals of friction and wear of materials, ASM, Metals Park, Ohio (1981) 439-452.

[22] B. Basu and M. Kalin, Tribology of Ceramics and Composites, John Wiley & Sons, Inc., New Jersy, 2011.

[23] B. Basu, and Kantesh Balani, Advanced structural ceramics, John Wiley & Sons, 2011.

[24] B. Basu, and Kantesh Balani, Sintering of ceramics, Advanced Structural Ceramics (2011): 76-104.

[25] B. Frisch, W. R. Thiele, R. Drumm, and B. Muennich, On the Oxidation Mechanism of Silicon Carbide in the 300ºC to 1300ºC Temperature Range, *Ceram. Forum Int*., **65** (1988) [8-9] 277-284.

[26] B. Wang and A.V. Levy, Erosion Behavior of SiC Fiber-SiC Matrix Composites, Wear, 138 (1990) 125-136.

[27] B.J. Hockey and B. R. Lawn, Electron Microscopy of Microcracking about Indentations in Aluminium Oxide and Silicon Carbide, *J. Mater. Sci*., **10** [8] (1975) 1275-1284.

[28] B.J. Hockey, S. M. Wiederhorn, and H. Johnson, Erosion of brittle materials by solid particle impact, In Flaws and Testing, 379-402. Springer US, (1978).

[29] B.Q. Wang and A. V. Levy, Erosion Behavior of SiC Fiber-SiC Matrix Composites, Wear 138 (1990) 125-136.

[30] B.R. Lawn, and V.R. Howes, "Elastic recovery at hardness indentations," Journal of Materials Science, 16(10), (1981) 2745-2752.

[31] B.R. Lawn, B. J. Hockey, and S. M. Wiederhorn, Atomically Sharp Cracks in Brittle Solids: An Electron Microscopy Study, *J. Mater. Sci*., **15** (1980) 1207-1223.

[32] B.R. Lawn, N. P. Padture, F. Guiberteau, and H. Cai, A Model for Microcrack Initiation and Propagation Beneath Hertzian Contacts in Polycrystalline Ceramics, *Acta Metall. Mater*., **42** [5] (1994) 1683-1693.

[33] B.R. Zhang, F. Marino, M. Ferraris, Liquid-phase hot-pressing and WC particle reinforcement of SiC-Si composites, J. Eur. Ceram. Soc. 14 (6) (1994) 549-555.

[34] B.V.M. Kumar, B. Basu, J. Vizintin, M. Kalin, Tribochemistry in sliding wear of TiCN-Ni-based cermets, J. Mater. Research. 23 (5) (2008) 1214-1227.

[35] B.V.M. Kumar, B. Basu, M. Kalin, J. Vizintin, Load-Dependent Transition in Sliding Wear Properties of TiCN-WC-Ni Cermets, J. Am. Ceram. Soc. 90 (5) (2007) 1534-1540.

[36] B.V.M. Kumar, B. Basu, S. Kang, and J. Ramkumar, Erosion wear behavior of TiCN–Ni cermets containing secondary carbides (WC/NbC/TaC), Journal of the American Ceramic Society 89, no. 12 (2006): 3827-3831.

[37] B.V.M. Kumar, B. Basu, V.S.R. Murthy, Manoj Gupta, The role of tribochemistry on fretting wear of Mg-SiC particulate composites, Composites: Part A 36 (2005) 13-23.

[38] B.V.M. Kumar, Y.W. Kim, D.S. Lim, W.S. Seo, Influence of small amount of sintering additives on unlubricated sliding wear properties of SiC ceramics, Ceram. Int. 37 (2011) 3599-3608.

[39] C.D. Hilton, James W. McCauley, Jeffrey J. Swab, Eugene R. Shanholtz, and Ming W. Chen, "Using hardness tests to quantify bulk plasticity and predict transition velocities in SiC materials," International Journal of Applied Ceramic Technology 10 (2013) 114-122.

[40] C.G. Knight, M. V. Swain, and M. M. Chaudhri, "Impact of Small Steel Spheres on Glass Surfaces," *J. Mater. Sci.*, **12** [8] (1977) 1573-1586.

[41] C.S. John, The brittle-to-ductile transition in pre-cleaved silicon single crystals, Philosophical Magazine 32 (1975) 1193-1212.

[42] D. B. Marshall, B. R. Lawn, A. G. Evans, "Elastic/plastic indentation damage in ceramics: the lateral crack system," *J. Am. Ceram. Soc.*, **65** [11] (1982) 561-566.

[43] D. Jianxin, L. Lili, D. Mingwei, Erosion wear behaviours of SiC/(W,Ti)C laminated ceramic nozzles in dry sand blasting processes, Mater. Sci. Eng. A444 (2007) 120–129.

[44] D. K. Shetty, I. G. Wright, and A. H. Clauer, Coal Slurry Erosion of Reaction-Bonded SiC, *Wear*, **79** 275-279 (1982).

[45] D. Sciti, A. Bellosi, Effects of Additives on Densification, Microstructure and Properties of Liquid-Phase Sintered Silicon Carbide J. Mater. Sci., 35 3849-3855 (2000).

[46] D. W. Gebretsadik, J. Hardell, I. Efeoglu, B. Prakash, Tribological properties of composite multilayer coating, Tribology-Materials, Surfaces & Interfaces 5, no. 3 (2011): 100-106.

[47] D. Wang and Z. Mao, Microscopic Observations of Wear of Heat-Resistant Ceramics, *Wear*, **167** [1] (1993) 87-89.

[48] D.C. Cranmer, Friction and wear properties of monolithic silicon-based ceramics, J. Mater. Sci. 20 (1985) 2029-2037.

[49] D.C. Evans, J. K. Lancaster, The Wear of Polymers, pp. 85-139 in Treatise on Materials Science and Technology: Wear, Vol. 13, Academic Press, New York and London, 1979.

[50] D.D. Jayaseelan, Y. Wang, G. E. Hilmas, W. Fahrenholtz, P. Brown, W. E. Lee, TEM investigation of hot pressed-10 vol.% SiC–ZrB_2 composite, Advances in Applied Ceramics 110 (2011) 1-7.

[51] D.F. Wang, J. H. She, Z. Y. Ma, Effect of Microstructure on Erosive Wear Behavior of SiC Ceramics, Wear, 180 35-41 (1995).

[52] D.F. Wang, J.H. She, Z.Y. Ma, Effect of microstructure on erosive wear behavior of SiC ceramics, Wear 180 (1995) 35-41.

[53] E. Ciudad, O. B. Lopez, F. Rodriguez-Rojas, A. L. Ortiz, F. Guiberteau, Effect of Intergranular Phase Chemistry on the Sliding-Wear Resistance of Pressureless Liquid-Phase-Sintered α-SiC, J. Eur. Ceram. Soc., 32 [2] (2012) 511-516.

[54] E. Ciudad, O.B. Lopez, A.L. Ortiz, F. Guiberteau, Microstructural effects on the sliding-wear resistance of pressureless liquid-phase-sintered SiC under diesel fuel. *J Eur Ceram Soc* 33 (2013) 879-885.

[55] E. Medvedovski, Ballistic Performance of Armour Ceramics: Part 1. Influence of Design and Structure, *Ceram. Int*., **36** (2010) 2103-2115.

[56] E. W. Neuman, Gregory E. Hilmas, W. G. Fahrenholtz, "Mechanical behavior of zirconium diboride–silicon carbide ceramics at elevated temperature in air," Journal of the European Ceramic Society 33 [15] (2013) 2889-2899.

[57] E. Zanoria, S. Danyluk, M. McNallan, Effects of load and temperature on the formation of rolls by reciprocal sliding of silicon-on-silicon at 34% humidity, in: D. Dowson Ed., Proceedings of the 18th Leeds–Lyon Symposium on Tribology, Elsevier, Amsterdam (1991) 501-506.

[58] F. Elfallagh, B. J. Inkson, 3D analysis of crack morphologies in silicate glass using FIB tomography, Journal of the European Ceramic Society 29 (2009) 47-52.

[59] G. Amirthan, M. Balasubramanian, Reciprocating sliding wear studies on Si/SiC ceramic composites, Wear 271 [7] (2011) 1039-1049.

[60] G. Amirthana, A. Udaya Kumar, V.V. Bhanu Prasad, M. Balasubramanian, Solid Particle Erosion Studies on Biomorphic Si/SiC Ceramic Composites, *Wear*, **268** (2010) 145–152.

[61] G. Bian, Houzheng Wu, Friction and surface fracture of a silicon carbide ceramic brake disc tested against a steel pad, Journal of the European Ceramic Society 35 (2015) 3797-3807.

[62] G. Rixccker, I. Wiedmann, A. Rosinus, F. Aldinger, High-temperature effects in the fracture mechanical behavior of silicon carbide liquid-phase sintered with AlN-Y_2O_3 additives, J. Eur. Ceram. Soc. 21 (2001) 1013-1019.

[63] H. J. Choi, J. G. Lee, Y.-W. Kim, Oxidation Behavior of Liquid-Phase Sintered Silicon Carbide with Aluminum Nitride and Rare-Earth Oxides (Re_2O_3, where Re =Y, Er, Yb), J. Am. Ceram. Soc., 85 [9] (2002) 2281-2286.

[64] H. J. Choi, Y.-W. Kim, M. Mitomo, T. Nishimura, J. H. Lee, D. Y. Kim, Intergranular Glassy Phase Free SiC Ceramics Retains Strength at 1500ºC, Scripta Mater., 50 (2004) 1203-1207.

[65] H. J. Yeom, Y.W. Kim, K. J. Kim, Electrical, Thermal and Mechanical Properties of Silicon Carbide-Silicon Nitride Composites Sintered with Yttria and Scandia, *J. Eur. Ceram. Soc*., **35** (2015) 77-86.

[66] H. Miyazaki, H. Hyuga, Y. I. Yoshizawa, K. Hirao, T. Ohji, Correlation of wear behavior and indentation fracture resistance in silicon nitride ceramics hot-pressed with alumina and yttria. *J Eur Ceram Soc* 29 [8] (2009) 1535-1542.

[67] H. P. Iwata, U. Lindefelt, S. Oberg, and P.R. Briddon, Stacking Faults in Silicon Crabides, Phys. B., 340-342, (2003) 165-170.

[68] H. Tomizawa and T. E. Fischer, Friction and Wear of Silicon Nitride and Silicon Carbide in Water: Hydrodynamic Lubrication at Low Sliding Speed Obtained by Tribochemical Wear, *ASLE Trans*., **30** [1] (1987) 41-46.

[69] H. Tomizawa, T.E. Fisher, Friction and wear of silicon nitride at 150ºC to 800ºC, ASLE Trans. 29 (4) (1985) 481-488.

[70] H. Xia, G. Qiao, S. Zhou, J. Wang, Reciprocating friction and wear behavior of reaction-formed SiC ceramic against bearing steel ball, Wear 303 (2013) 276-285.

[71] H. Y. Liu and M. E. Fine, Modeling of Grain-Size Dependent Microfracture-Controlled Sliding Wear in Polycrystalline Alumina, *J. Am. Ceram. Soc*., **76 [9]** (1993) 2393-2396 .

[72] H. Z. Wu, B. J. Inkson, S. G. Roberts, Subsurface deformation of machined Al_2O_3 and Al_2O_3/5vol% SiC nanocomposite, Journal of microscopy 201 (2001) 212-220.

[73] H. Z. Wu, S. G. Roberts, G. Mobus, B. J. Inkson, Subsurface damage analysis by TEM and 3D FIB crack mapping in alumina and alumina/5vol.% SiC nanocomposites, Acta Materialia 51, (2003) 149-163.

[74] I. Finnie, J. Wolak, and Y. H. Kabil, Erosion of Metals by Solid Particles, *J. Mater*., **2** [3] (1967) 682-700.

[75] I. Zarudi, L. Zhang, and Y-W. Mai, Subsurface damage in alumina induced by single-point scratching, Journal of Materials Science 31 (1996) 905-914.

[76] I.M. Hutchings, Tribology: Friction and Wear of Engineering Materials, Edward Arnold, London, 1992.

[77] J. Bijwe, Composites as friction materials: Recent developments in non-asbestos fiber reinforced friction materials-a review, Polymer composites 18 [3] (1997) 378-396.

[78] J. D. O. B. Sanchez and W. M. Rainforth, 'On the Role of Plastic Deformation during the Mild Wear of Alumina, *Acta Mater*., **46** [18] (1998) 6475-83.

[79] J. F. Bell, and P. S. Rogers, Laboratory Scale Erosion Testing of a Wear Resistant Glass-Ceramic, *Mater. Sci. Tech*., **3** (1987) 807-813.

[80] J. F. Li, J. Q. Huang, S. H. Tan, Z. M. Cheng, and C. X. Ding, Tribological Properties of Silicon Carbide under Water-Lubricated Sliding, *Wear*, **218** (1998) 167-171.

[81] J. G. C. Nava, F. H. Stott, S. D. de la Torre, and A. Martinez-Villafane, Erosion of Al_2O_3 and SiC at Low Impact Velocities, *Mater. Lett*., **55** (2002) 269–273.

[82] J. J. Kim and S. K. Park, Solid-Particle Erosion of Hot-Pressed Silicon Carbide and SiC-TiB_2 Composite, *J. Mater. Sci. Lett*., **16** (1997) 821–823.

[83] J. J. Kim, and S. K. Park, Solid particle erosion of SiC and SiC–TiB_2 composite hot-pressed with Y_2O_3, Wear 222, (1998) 114-119.

[84] J. K. Sonber, T. SR Ch Murthy, K. Sairam, A. Nagraj, Kulwant Singh, R. D. Bedse, Sanjib Majumdar, and Vivekanand Kain, "Development and tribological properties of SiC fibre reinforced CrB2 composite," Journal of the Australian Ceramic Society (2017): 1-9.

[85] J. L. O. Merino, R. I. Todd, Relationship between wear rate, surface pullout and microstructure during abrasive wear of alumina and alumina/SiC nanocomposites, Acta Materialia 53 (2005) 3345-3357.

[86] J. L. Routbort and A. P. L. Turner, The Erosion Rate of Reaction-Bonded SiC Containing Various Amounts of Free Silicon, *Wear*, **84** (1983)a 381-385.

[87] J. L. Routbort and H. Matzke, "On the Correlation Between Erosion and Fracture Parameters in SiC Ceramics," *J. Mater. Sci*., **18** (1983)b 1491-1496.

[88] J. L. Routbort and R. O. Scattergood, Anomalous Solid-Particle Erosion Rate of Hot Pressed Silicon Carbide, *J. Am. Ceram. Soc*., **63** (1980)a 593–595.

[89] J. L. Routbort, H. Matzke, On the correlation between solid-particle erosion and fracture parameters in SiC, Journal of Materials Science 18 [5] (1983) 1491-1496.

[90] J. L. Routbort, R. O. Scattergood and A. P. L. Turner, The erosion of reaction-bonded SiC, Wear 59 (1980)b 363-375.

[91] J. L. Routbort, R. O. Scattergood, and A. P. L. Turner, The Erosion of Reaction-Bonded SiC, *Wear*, **59** (1980)c 363-375.

[92] J. Llorente, B. R. Manso, P. Miranzo, and M. Belmonte, "Tribological Performance Under Dry Sliding Conditions of Graphene/Silicon Carbide Composites," *J. Eur. Ceram. Soc*., **36** 429-435 (2016).

[93] J. Lundmark, E. Kassfeldt, J. Hardell, and B. Prakash, The influence of initial surface topography on tribological performance of the wheel/rail interface during rolling/sliding conditions, Proceedings of the Institution of Mechanical Engineers, Part F: Journal of Rail and Rapid Transit 223, no. 2 (2009): 181-187.

[94] J. Pang, J. Li, Low thermal expansion porous SiC-WC composite ceramics, Ceram. Int. 35 (2009) 3517-3520.

[95] J. Pirso, S. Letunovits, M. Viljus, Friction and wear behaviour of cemented carbides, Wear 257 (2004) 257-265.

[96] J. Qian, Z. Peng, D. Wu, X. Fu, $FeWO_4$/FeS core/shell nanorods fabricated by thermal evaporation. *Mater Letters* 122 (2014) 86-89.

[97] J. Takadoum, Z. Zsiga, and C. Roques-Carmes, Wear Mechanism of Silicon Carbide: New Observations, *Wear*, **174** (1994) 239-242.

[98] J. Watts, G. Hilmas, W. G. Fahrenholtz, Don Brown, and Bjorn Clausen, Measurement of thermal residual stresses in ZrB_2–SiC composites, Journal of the European Ceramic Society 31 [9] (2011) 1811-1820.

[99] J.K. Lancaster, A review of the influence of environmental humidity and water on friction, lubrication and wear, Tribology Int., **23 [6]** (1990) 371-389.

[100] J.Y. Luo, X.X. Chen, W.D. Li, W. Y. Deng, W. Li, H. Y. Wu, L. F. Zhu, Q. G. Zeng, Variable-temperature Raman spectroscopic study of the hydrogen sensing mechanism in Pt-WO_3 nanowire film. *Appl Phy Lett* 102 (2013) 104-113.

[101] J-J. Canneto, Maria Cattani-Lorente, Stephane Durual, Anselm HW Wiskott, and Susanne S. Scherrer, Grinding damage assessment on four high-strength ceramics, Dental Materials 32, (2016) 171-182.

[102] K. Bonny, P. D. Baets, Y. Perez, J. Vleugels, B. Lauwers, Friction and wear characteristics of WC–Co cemented carbides in dry reciprocating sliding contact, Wear 268 (2010) 1504-1517.

[103] K. H. Z. Gahr, R. Blattner, D. H. Hwang, and K. Pohlmann, "Micro- and Macro-Tribological Properties of SiC Ceramics in Sliding Contact," Wear 250 (2001) 299-310.

[104] K. Kato and K. Adachi, "Wear of Advanced Ceramics," Wear 253 [11–12] (2002) 1097-1104.

[105] K. Kato, "Tribology of Ceramics," *Wear*, **136** (1990) 117-133.

[106] K. Maeda, K. Suzuki, S. Fujita, Mi Ichihara, and S. Hyodo, "Defects in plastically deformed 6H SiC single crystals studied by transmission electron microscopy," Philosophical Magazine A 57 (1988) 573-592.

[107] K. Negita, "Effective Sintering Aids for Silicon Carbide Ceramics: Reactivities of Silicon Carbide with Various Additives," J. Am. Ceram. Soc., 69 [12] C308-C310 (1986).

[108] K. Sang, Z. Jin, Non-lubricated friction of reaction-sintered silicon carbide and its composite with nickel, Wear 246 (2000) 34–39.

[109] K. Umeda, Y. Enomto, Friction and wear of boride ceramics in air and water, Wear 169 (1993) 63–68.

[110] K. Y. Lim, Y.-W. Kim, and K. J. Kim, Mechanical Properties of Electrically Conductive Silicon Carbide Ceramics, Ceram. Int., 40 (2014) 10577-10582.

[111] K.-H.Z. Gahr, R. Blattner, D.H. Hwang, K. Pohlmann, Micro and micro-tribological properties of SiC ceramics in sliding contact, Wear 250 (2001) 299-310.

[112] K.H.Z. Gahr, Sliding wear of ceramic-ceramic, ceramic-steel and steel-steel pairs in lubricated and unlubricated contact, *Wear* 133 (1989) 1-22.

[113] K.H.Z. Gahr, W. Bundschuh, B. Zimmerlin, Effect of grain size on friction and sliding wear of oxide ceramics. *Wear* 162 (1993) 269-279.

[114] L. C. Erickson, A. Blomberg, S. Hogmark, and J. Bratthall, Tribological Characterization of Alumina and Silicon Carbide under Lubricated Sliding, *Tribology Int*., **26** [2] (1993) 83-92.

[115] L. Gurnani, R. Kathuria, A. Mukhopadhyay, Wear Behavior of Bulk Polycrystalline MgO–MgFe2O4 "Age-Hardened Alloys", Journal of the American Ceramic Society 99 (2016) 5-8.

[116] L. Jordi, C. Iliev, and T. E. Fischer, Lubrication of Silicon Nitride and Silicon Carbide by Water: Running in, Wear and Operation of Sliding Bearings, Tribol. Lett., 17 [3] (2004) 367-376.

[117] L. Rama Krishna, A. Sudha Purnima, and G. Sundararajan, A comparative study of tribological behavior of microarc oxidation and hard-anodized coatings, Wear 261, no. 10 (2006) 1095-1101.

[118] L. Rama Krishna, K. R. C. Somaraju, and G. Sundararajan, The tribological performance of ultra-hard ceramic composite coatings obtained through microarc oxidation, Surface and Coatings Technology 163 (2003) 484-490.

[119] L. Rama Krishna, P. S. V. N. B. Gupta, and G. Sundararajan, The influence of phase gradient within the micro arc oxidation (MAO) coatings on mechanical and tribological behaviors, Surface and Coatings Technology 269 (2015) 54-63.

[120] M. G. Jeong, Seo Hyun Yoon, Yoon Soo Chun, Eung Seok Lee, and Dae-Soon Lim, Effect of lattice structure of silicon carbide on crystal formation of carbide-derived carbon, Carbon 79 (2014) 19-27.

[121] M. G. Mendiratta, J. Wimmer, and I. Bransky, Dynamic K_{1C} and dynamic flexural strength in HS-130 Si_3N_4, Journal of Materials Science 12 (1977) 212-214.

[122] M. H. Hong, A. V. Samant, and P. Pirouz, Stacking fault energy of 6H-SiC and 4H-SiC single crystals, Philosophical Magazine A 80, (2000) 919-935.

[123] M. Herrmann, G. Standke, S. Hohn, G. Himpel, and T. Gestrich, High-Temperature Corrosion of Silicon Carbide Ceramics by Coal Ashes, Ceram. Int., 40 (2014) 1471-1479.

[124] M. Keppeler, H.G. Reichert, J. M. Broadley, G. Thurn, I. Wiedmann, F. Aldinger, High temperature mechanical behaviour of liquid phase sintered silicon carbide, J. Euro. Ceram. Soc. 18 (1998) 521-526.

[125] M. M. Chaudhri and S. M. Walley, Damage to Glass Surfaces by the Impact of Small Glass and Steel Spheres, *Phil. Mag. A*, **37** [2] (1978) 153-165.

[126] M. S. Suh, T. Hinoki, and A. Kohyama, Erosive Wear Mechanism of New SiC/SiC Composites by Solid Particles, *Tribol. Lett*., **41** (2011) 503-513.

[127] M. Woydt, J. Schenzien, Dry and water-lubricated slip-rolling of Si and SiC-based ceramics, Tribol. Int. 26 (3) (1993) 165-173.

[128] O. B. Lopez, A. L. Ortiz, F. Guiberteau, and N. P. Padture, Effect of Microstructure on Sliding-Wear Properties of Liquid-Phase-Sintered α-SiC, *J. Am. Ceram. Soc*., **88 [8]** (2005)a 2159-2163.

[129] O. B. Lopez, A. L. Ortiz, F. Guiberteau, and N. P. Padture, Effect of the Nature of the Intergranular Phase on Sliding-Wear Resistance of Liquid-Phase-Sintered α-SiC, *Scripta Mater*., **57** [6] (2007)a 505-508.

[130] O. B. Lopez, A. L. Ortiz, F. Guiberteau, and N. P. Padture, Improved Sliding-Wear Resistance in In-situ Toughened Silicon Carbide, *J. Am. Ceram. Soc*., **88** [12] (2005)b 3531-3534.

[131] O. B. Lopez, A. L. Ortiz, F. Guiberteau, and N. P. Padture, Microstructural Design of Sliding-Wear-Resistant Liquid-Phase-Sintered SiC: An Overview, *J. Eur. Ceram. Soc*., **27** (2007)b 3351-3357.

[132] O. B. Lopez, A. L. Ortiz, F. Guiberteau, and N. P. Padture, Sliding-Wear-Resistant Liquid-Phase-Sintered SiC Processed Using α-SiC Starting Powders, *J. Am. Ceram. Soc*., **90** [2] (2007)c 541-545.

[133] O. Desa, and S. Bahadur, Material removal and subsurface damage studies in dry and lubricated single-point scratch tests on alumina and silicon nitride, Wear 225 (1999) 1264-1275.

[134] O.O. Adewoye and T. F. Page, Frictional Deformation and Fracture in Polycrystalline SiC and Si_3N_4, *Wear*, **70** (1981) 37-45.

[135] P. Anderson, A. Blomberg, Instability in the tribochemical wear of silicon carbide in unlubricated sliding contacts, Wear 174 (1994) 1-7.

[136] P. Blau, J. ASM Handbook, Volume 18-Friction, Lubrication, and Wear Technology. ASM international, 1992.

[137] P. C. Kong and E. Pfender, Formation of Ultrafine β-Silicon Crabide Powders in an Agron Thermal Plasma Jet, *Langmuir*, **3** [2] (1987) 259-265.

[138] P. F. Becher, Microstructural Design of Toughened Ceramics, J. Am. Ceram. Soc., 74 (1991) 255-269.

[139] P. Gautier and K. Kato, Wear Mechanisms of Silicon Nitride Partially Stabilized Zirconia and Alumina in Unlubricated Sliding against Steel, *Wear*, **162-164** (1993) 305-313.

[140] P. Kackell, J. Furthmuller and F. Bechstedt, Polytypic transformations in SiC: an ab initio study, Phys. Rev. B, 60B (19), (1999) 13261–13264.

[141] P. Pirouz, and J. W. Yang, Polytypic transformations in SiC: the role of TEM, Ultramicroscopy 51 (1993) 189-214.

[142] P. T. B. Shaffer, A Review of the Structure of Silicon Carbide, Acta Cryst., B 25, (1969) 477-488.

[143] P. Tatarko, M. Kasiarova, J. Dusza, J. Morgiel, P. Sajgalik, P. Hvizdos, Wear resistance of hot-pressed Si_3N_4/SiC micro/nanocomposites sintered with rare-earth oxide additives. *Wear* 269 [11] (2010) 867-874.

[144] P. V. Gurunath, and J. Bijwe, Friction and wear studies on brake-pad materials based on newly developed resin, Wear 263 [7] (2007) 1212-1219.

[145] R. Rattan, and Jayashree Bijwe, Influence of impingement angle on solid particle erosion of carbon fabric reinforced polyetherimide composite, Wear 262 [5] (2007) 568-574.

[146] R. S. Gates and S. M. Hsu, Tribochemistry between Water and Si3N4 and SiC: Induction Time Analysis, Tribol. Lett., 17 [3] (2004) 399-407.

[147] R. Ward, A comparison of reciprocating and continuous sliding wear, Wear 15 [6] (1970) 423-434.

[148] R. Wasche and D. Klaffke, Ceramic Particulate Composites in the System SiC-TiC-TiB_2 Sliding against SiC and Al_2O_3 Under Water, *Tribology Int.*, **32** (1999) 197-206.

[149] R. Wasche, D. Klaffke, and T. Troczynski, Tribological Performance of SiC and TiB_2 against SiC and Al_2O_3 at Low Sliding Speeds, *Wear*, **256** (2004) 695-704.

[150] R. Wasche, D. Klaffke, In situ formation of tribologically effective oxide interfaces in SiC-based ceramics during dry oscillating sliding. *Tribo Lett* 5 (1998) 173-190.

[151] R. Yuan, J. J. Kruzic, X. F. Zhang, L. C. De Jonghe, and R. O. Ritchie, Ambient to High Temperature Fracture Toughness and Cyclic Fatigue Behavior in Al Containing Silicon Carbide Ceramics, Acta Mater., 51 (2003) 6477-6491.

[152] R.K. Iier, The Chemistry of Silica, pp. 40-60, Wiley Inc., New York, USA, 1979.

[153] R.W. Rice, Micromechanics of microstructural aspects of ceramic wear, In Proceedings of the 9th Annual Conference on Composites and Advanced Ceramic Materials: *Ceram Eng and Scie Procee, John Wiley & Sons* 6 (1985) 940-958.

References:

[154] S. Bajwa, W. M. Rainforth, W. E. Lee, Sliding wear behaviour of SiC–Al 2 O 3 nanocomposites, Wear 259, (2005) 553-561.

[155] S. C. Singhal, Thermodynamical Analysis of the High-Temperature Stability of Silicon Nitride and Silicon Carbide, *Ceram. Int*., **2** [3] (1976) 123-130.

[156] S. Danyluk, M. McNallan, D.S. Park, Friction and wear of silicon nitride exposed to moisture at high temperatures, in: S. Jahanmir Ed., Friction and Wear of Ceramics, Marcel Dekker, New York (1994) 61-77.

[157] S. G. Lee, Y.-W. Kim, M. Mitomo, Relationship between Microstructure and Fracture Toughness of Toughened Silicon Carbide Ceramics, J. Am. Ceram. Soc., 84 (2001) 1347-1353.

[158] S. Gochnour, J. D. Bright, D. K. Shett, Solid Particle Erosion of SiC-Al_2OC Ceramics, *J. Mater. Sci*., **25** (1990) 3229-3235.

[159] S. Grasso, T. Saunders, H. Porwal, and M. Reece, "Ultra-High Temperature Spark Plasma Sintering of α-SiC," Ceram. Int., 41 225-230 (2015).

[160] S. Gupta, S.K. Sharma, B.V.M. Kumar, Y.-W. Kim, Tribological characteristics of SiC ceramics sintered with a small amount of yttria, Ceram. Int. 41 (2015) 14780-14789.

[161] S. Hotta and Y. Mizutani, Effect of Water and Organic Solvents on the Friction of SiC, pp. 1-4 in Proc. 32nd JSLE Conf. Tokyo, Japan (1988).

[162] S. I. Youn, Gyung Sun Cho, Mi Rae Youm, Dae Soon Lim, and Sang Whan Park, Mechanical and electrical properties of Si-SiC fabricated using SiC-C composite powders synthesized by sol-gel process, Journal of the Korean Ceramic Society 51 [5] (2014) 459-465.

[163] S. J. Cho, B. J. Hockey, B. R. Lawn, S. J. Bennison, Grain-Size and R-Curve Effects in the Abrasive Wear of Alumina, *J. Am. Ceram. Soc*., **72** [7] (1989) 1249-1252.

[164] S. J. Cho, C. D. Um, and S. S. Kim, Wear and Wear Transition in Silicon Carbide Ceramics During Sliding, *J. Am. Ceram. Soc*., **79** (1996) 1247-1251.

[165] S. J. Cho, C. D. Um, S. S. Kim, Wear and Wear Transition Mechanism in Silicon Carbide during Sliding, *J. Am. Ceram. Soc*., **78** [4] (1995) 1076-1078.

[166] S. Lafon-Placette, K. Delbe, J. Denape, M. Ferrato, Tribological Characterization of Silicon Carbide and Carbon Materials, J. Eur. Ceram. Soc., 35 (2015) 1147-1159.

[167] S. M. Hsu and M. Sheng, Wear Prediction of Ceramics, Wear 256 (2004) 867-878.

[168] S. M. Hsu, M. C. Shen, Ceramic wear maps. *Wear* 200 (1996) 154-175.

[169] S. M. Wiederhorn and B. J. Hockey, Effect of material parameters on the erosion resistance of brittle materials, Journal of Materials Science 18 (1983) 766-780.

[170] S. M. Wiederhorn, B. J. Hockey, Effect of material parameters on the erosion resistance of brittle materials, Journal of Materials Science 18 [3] (1983) 766-780.

[171] S. Sasaki, The Effects of Water on Friction and Wear of Ceramics, *J. Jpn. Soc. Lubr. Eng*., **10** (1988) 10-26.

[172] S. Wada and N. Watanabe, Solid Particle Erosion of Brittle Materials. III. The Interaction with Material Properties of Target and That of Impingement Particle on Erosive Wear mechanism, *J. Ceram. Soc. Jpn*., **95** [6] (1987) 573-578.

[173] S.J. Cho, C.D. Um, S.S. Kim, Wear and wear transition in silicon carbide-titanium boride ceramic matrix composites, J. Am. Ceram. Soc. 79 [5] (1996) 1247–1251.

[174] S.J. Cho, H. Moon, B. J. Hockey, and S. M. Hsu, The Transition from Mild to Severe Wear in Alumina During Sliding, *Acta Metall*., **40** [1] (1992) 185-192.

[175] S.K. Sharma, A.W. Selokar, B.V.M. Kumar, T. Venkateswaran, High temperature erosion behavior of spark plasma sintered ZrB_2-SiC composites, Ceram. Int. 43 (2017) 8982–8988.

[176] S.K. Sharma, B.V.M. Kumar, K. Y. Lim, Y.W. Kim, S. K. Nath, Erosion Behavior of SiC-WC Composites, Ceram. Int., 40 (2014) 6829-6839.

[177] T. H. Kosel, Solid particle erosion, ASM handbook 18 (1992) 199-213.

[178] T. Hase, Boron Transport and Change of Lattice Parameter During Sintering of β-SiC, J. Am. Ceram. Soc., 63 [5-6] (1980) 349-350.

[179] T. S. R. Ch Murthy, J. K. Sonber, K. Sairam, R. D. Bedse, and J. K. Chakarvartty, Development of Refractory and Rare Earth Metal Borides & Carbides for High Temperature Applications, Materials Today: Proceedings 3 (2016) 3104-3113.

[180] U. Dulias, K. H. Zum Gahr, Investigation of Al_2O_3-and SSiC-ceramic under lubricated, reciprocating sliding contact and cavitation erosion, Materialwissenschaft und Werkstofftechnik 36 (3-4) (2005) 140-147.

[181] V. A. Izhevskyi, L. A. Genova, J. C. Bressiani, and A. H. A. Bressiani, "Silicon Carbide. Structure, Properties and Processing,"Ceramica, 46, (2000) 4-13.

[182] V. S. R. Murthy, H. Kobayashi, N. Tamari, S. Tsurekawa, T. Watanabe, and K. Kato, "Effect of Doping Elements on the Friction and Wear Properties of SiC in Unlubricated Sliding Condition," *Wear*, **257** (2004) 89-96.

[183] V.M. Candelario, O.B. Lopez, F. Guiberteau, R. Morenob, and A.L. Ortiz, Sliding-Wear Resistance of Liquid-Phase-Sintered SiC Containing Graphite Nanodispersoids, *J. Eur. Ceram. Soc*., **34** (2014) 2597-2602.

[184] V.S.R. Murthy, H. Kobayashi, S. Tsurekawa, N. Tamari, T. Watanabe, K. Kato, Influence of humidity and doping elements on the friction and wear of SiC in unlubricated sliding, Tribol. Int. 37 (2004) 353–364.

[185] W. G. Fahrenholtz, and G. E. Hilmas, Ultra-high temperature ceramics: Materials for extreme environments, Scripta Materialia 129 (2017) 94-99.

[186] W. G. Fahrenholtz, Thermodynamic Analysis of ZrB_2-SiC Oxidation: Formation of a SiC-Depleted Region, Journal of the American Ceramic Society 90 [1] (2007) 143-148.

[187] W. Kanematsu, Subsurface damage in scratch testing of silicon nitride, Wear 256, (2004) 100-107.

[188] W. M. Rainforth, The Wear Behavior of Oxide Ceramics-A Review, *J. Mater. Sci*., **39** [2] (2004) 6705–6721.

[189] X. Dong, S. Jahanmir, and L. K. Ives, Wear Transition Diagram for Silicon Carbide, Tribo. Int., 28 (1995) 559-572.

[190] X. Dong, S. Jahanmir, Wear transition diagram for silicon nitride, Wear 165 (1993) 169-180.

[191] X. F. Chen, X. G. Xu, X. B. Hu, J. Li, S. Z. Jiang, L. N. Ning, Y. M. Wang, M. H. Jiang, Anisotropy of Chemical Mechanical Polishing in Silicon Carbide Substrates, *Mater. Sci. Eng. B*, **142** 28-30 (2007).

[192] X. Guo, H. Yang, L. Zhang, and X. Zhu, Sintering Behavior, Microstructure and Mechanical Properties of Silicon Carbide Ceramics Containing Different Nano-TiN Additive, *Ceram. Int*., **36** (2010) 161-165.

[193] X. Li, H. Ding, Z. Huang, M. Fang, B. Liu, Y. Liu, X. Wu, S. Chen, Solid Particle Erosion-Wear Behavior of SiC–Si_3N_4 Composite Ceramic at Elevated Temperature, Ceram. Int. 40 (2014) 16201-16207.

[194] X. Li, H. Ding, Z. Huang, M. Fang, B. Liu, Y. Liu, X. Wu, S. Chen, Solid Particle Erosion-Wear Behavior of SiC–Si_3N_4 Composite Ceramic at Elevated Temperature, Ceram. Int. 40 (2014) 16201-16207.

[195] X. Wang, N. P. Padture, H. Tanaka, A. L. Ortiz, Wear-Resistant Ultra-Fine-Grained Ceramics, *Acta Mater*., **53** [2] (2005) 271-277 .

[196] X. Yang, X. Liu, L. Wang, H. Zhang, X. Yao, and Z. Huang, R-Curve Analysis of Solid-Phase-Sintered and Liquid-Phase-Sintered Silicon Carbide Ceramics by Indentation Fracture and Indentation-Strength-in-Bending Methods, *Ceram. Int*., **42** (2016) 4011-4018.

[197] X. Zhang, Y. Niu, X. Meng, Y. Li, J. Zhao, Structural evolution and characteristics of the phase transformations between α-Fe_2O_3, Fe_3O_4 and γ-Fe_2O_3 nanoparticles under reducing and oxidizing atmospheres. *Cryst Eng Comm* 15 (2013) 8166-8172.

[198] X. Zhao, J. Liu, B. Zhu, H. Miao, Z. Luo, Tribological characteristics of Si_3N_4 ceramic sliding on stainless steel, Wear 206 (1) (1997) 76-82.

[199] Y. S. Kim, Won Tae Kwon, Moonsu Seo, Shinhoo Kang, Tool performance of new wear-resistant cermets, International Journal of Precision Engineering and Manufacturing 13 [6] (2012) 941-946.

[200] Y. W. Kim, K. Y. Lim, and W. S. Seo, Microstructure and Thermal Conductivity of Silicon Carbide with Yttria and Scandia, J. Am. Ceram. Soc., 97 (2014) 923-928.

[201] Y. W. Kim, S. H. Jang, T. Nishimura, S. Y. Choi, S. D. Kim, Microstructure and high-temperature strength of silicon carbide with 2000ppm yttria, J. Eur. Ceram. Soc. (2017).

[202] Y. Wang and S.M. Hsu, Wear and Wear Transition Mechanisms of Ceramics, *Wear* **195** (1996) 112-122.

[203] Y. Wang, L. Wang, Q. Xue, Improvement in the tribological performances of Si_3N_4, SiC and WC by graphite-like carbon films under dry and water-lubricated sliding conditions. *Surf and Coat Tech* 205 (2011) 2770-2777.

[204] Y. Zhou, K. Hirao, Y. Yamauchi, S. Kanzaki, Tribological Properties of Silicon Carbide and Silicon Carbide–Graphite Composite Ceramics in Sliding Contact, *J. Am. Ceram. Soc*., **8**6 [6] (2003) 991-1002.

[205] Y.W. Kim, Y.S. Chun, T. Nishimura, M. Mitomo, Y.H. Lee, High-temperature strength of silicon carbide ceramics sintered with rare-earth oxide and aluminum nitride, Acta Mater. 55 (2007) 727-736.

[206] Z. H. Huang, J. L. Sun, J. X. Wang and Y. R. Hong, α-sialon-Al-SiC composite refractories, Key Eng. Mater. 224 (2012) 275-280.

[207] Z. Zhu, V. Muratov, T. E. Fischer, Tribochemical Polishing of Silicon Carbide in Oxidant Solution, *Wear*, **225-229** (1999) 848-856.